Cilium length regulation in *Caenorhabditis elegans*

by

Kwangjin Park

M.Sc., Seoul National University, 2014

B.Sc., Yonsei University, 2011

Thesis Submitted in Partial Fulfillment of the
Requirements for the Degree of
Doctor of Philosophy

in the
Department of Molecular Biology and Biochemistry
Faculty of Science

SIMON FRASER UNIVERSITY

Fall 2019

Approval

Name:	**Kwangjin Park**
Degree:	**Doctor of Philosophy** **(Molecular Biology and Biochemistry)**
Title:	**Cilium length regulation in *Caenorhabditis elegans***
Examining Committee:	**Chair:** **Mani Larijani** Associate Professor
	Michel Leroux Senior Supervisor Professor
	Lynne Quarmby Supervisor Professor
	Nancy Hawkins Supervisor Associate Professor
	Sherryl Bisgrove Internal Examiner Associate Professor Department of Biological Sciences
	Moe Mahjoub External Examiner Assistant Professor Nephrology Division Washington University School of Medicine
Date Defended/Approved:	September 26th, 2019

Abstract

Nearly all vertebrate cells possess a primary cilium, akin to a cellular antenna, that plays essential roles in various physiological and developmental processes. Cilium length is tightly regulated to provide the optimal functions for each type of cell and tissue, such as the eye and kidney. Impairment of this regulation can result in cilium-associated disorders, collectively termed ciliopathies. The intraflagellar transport (IFT) system, involved in cilium assembly, and microtubule depolymerizing kinesins, which participate in cilium disassembly, play key roles in cilium length regulation. Additionally, several classes of kinases, including CDKL5, modify IFT components and/or depolymerizing kinesins to modulate ciliary length. We therefore hypothesized that the entire family of cyclin-dependent kinase-like (CDKL) proteins (CDKL1-5) may have similar ciliary functions.

To test this hypothesis, we undertook studies in *C. elegans*. This nematode has one CDKL protein (CDKL-1) closely related to CDKL1-4 and more distantly related to CDKL5. We find that CDKL-1 localizes to cilia, including the transition zone (TZ), and negatively regulates cilium length by controlling IFT flux. Cilium length regulation by CDKL-1 is distinct from that of other kinases, namely DYF-18 (mammalian CCRK ortholog), DYF-5 (MAK) and NEKL-1 (NEK8/9). It also occurs independently from the depolymerizing kinesin-13 family, KLP-7 (KIF2A), which positively controls cilium length at the TZ.

To query the molecular etiologies of human diseases caused by mutations in CDKL5 (epilepsy and atypical Rett syndrome) or KIF2A (brain malformations), we introduced corresponding patient mutations in *C. elegans* CDKL-1 and KLP-7, respectively. The mutations cause mislocalization and ciliary length defects. In addition, we find that disrupting *C. elegans cdkl-1* results in sensory (CO_2 avoidance) and developmental (body size) phenotypes, possibly resulting from anomalies in signaling pathway(s), including cGMP signaling. These data suggest that human ailments such as Rett syndrome and brain anomalies may arise from cilium length misregulation, and consequently, disruption of signaling pathways.

In summary, our findings provide evidence that CDKL-1 works cooperatively with other kinases, and independently from a depolymerizing kinesin, to maintain correct ciliary length. Our work also suggests links between ciliary length control and potential ciliopathies, which provides potentially useful experimental avenues of exploration.

Keywords: protein kinases; cyclin-dependent kinase-like(CDKL); cilium length regulation; intraflagellar transport (IFT); depolymerizing kinesins; ciliopathy

Dedication

To my family

for your unconditional love and support

Acknowledgements

I would like to express my deepest gratitude to my supervisor, Dr. Michel Leroux, who has given me the opportunity to study and pursue my PhD in his group. He has great knowledge and attitude towards science and his huge support allowed to me achieve many goals, such as publishing research articles and completing this thesis. I thank him for his kindness, patience, and encouragement throughout my PhD.

I also feel honored to have had Dr. Lynne Quarmby and Dr. Nancy Hawkins as my committee members. I would like to thank them for their guidance, motivation, and valuable advice. I would not have completed this dissertation without their support.

I extend my appreciation to all of the collaborators I worked with. I thank them for sharing their knowledge and for all their dedication to my projects.

Lastly, I would like to thank the people who have helped me during my 5 years at the Department of Molecular Biology and Biochemistry (MBB): all members of the Leroux lab, who have provided immense support and help, including Dr. Tiffany Timbers, Dr. Victor Jensen, Dr. Catrina Loucks, Dr. Marine Barbelanne, Dr. Adam Warner, Dr. Nils Lambacher, Jerry Cai and Hannah Domnic. I especially thank Chunmei Li and Christine Kondratev, who were heavily involved in my research projects, for their hard work. I also thank MBB staff members, Nancy Suda, Mimi Fourie, Nagisa Inoue, and Christine Beauchamp, for their help, support, and patience. Furthermore, I feel very grateful to have been able to work alongside Deidre de Jong-Wong, Dr. Daniel Chiang, Chuanyun Luo and Dr. Jaeyong Lee. I truly appreciate all their support in the lab and outside.

Table of Contents

List of Figures

List of Acronyms

APC	Adenomatous polyposis coli
APX	Ascorbate peroxidase
BB	Basal body
BBS	Bardet-biedl syndrome
BioID	Proximity dependent biotin identification
CALK	*Chlamydomonas* aurora/Ipl1p-like protein kinase
CCRK	Cell cycle related kinase
CDK	Cyclin-dependent kinase
CDKL	Cyclin-dependent kinase-like
CIZE	Ciliary zone of exclusion
CLK	CDC-like kinases
CRMP-2	Collapsin response mediator protein 2
DC	Doublecortin
DS	Distal segment
FLS1	Flagellar shortening 1
FRAP	Fluorescence recovery after photobleaching
GCY	Guanylate cyclase
GFP	Green fluorescent protein
GPCR	G protein-coupled receptor

GSK	Glycogen synthase kinases
Hh	Hedgehog
HSD	Honestly significant difference
ICK	Intestinal cell kinase
IFT	Intraflagellar transport
IFT-A	IFT subcomplex A
IFT-B	IFT subcomplex B
INV	Inversin
JATD	Jeune asphyxiating thoracic dystrophy
JBTS	Joubert syndrome
jck	*juvenile cystic kidneys*
KAP	Kinesin-associated protein
KD	Kinase-dead
LCA	Leber Congenital Amaurosis
LECA	Last eukaryotic common ancestor
LF	Long flagella
LRC	Length regulatory complex
MAK	Male germ cell associated kinase
MAP1B	Microtubule-associated protein 1B
MAPK	Mitogen-activated protein kinases

MBP	Microtubule binding protein
MCHR1	Melanin-concentrating hormone receptor 1
MKS	Meckel-gruber syndrome
MOK	MAPK/MAK/MRK overlapping kinase
MS	Middle segment
MSS	Mainzer–saldino syndrome
MWT	Multi-worm tracker
NIMA	Never in mitosis A
NPHP	Nephronophthisis
NRK	NIMA-related kinase
OFD	Oral-facial-digital
PCD	Primary ciliary dyskinesia
PCMC	Periciliary membrane compartment
PKD	Polycystic kidney disease
PLK1	Polo-like kinase 1
RCK	*Ros-cross* hybridizing kinase
RID	Rpgr interaction domain
RPE-1	Retinal pigment epithelium
SSTR3	Somatostatin receptor type 3
STED	Stimulated emission depletion

SLNS	Senior løken syndrome
TEM	Transmission electron microscopy
TF	Transition fiber
ts	*temperature sensitive*
TZ	Transition zone

1 Introduction

1.1 Cilia

The cilium is a hair-like organelle with a microtubule-base backbone that protrudes from the plasma membranes of cells into the extracellular environment. Dating back to the Last Eukaryotic Common Ancestor (LECA), this organelle is present in most eukaryotic cells (Carvalho-Santos et al., 2011). During the resting phase of the cell cycle, a mature mother centriole from the centrosome (microtubule organizing center) relocates and docks to the cellular membrane to form a basal body (Garcia-Gonzalo and Reiter, 2017). A ciliary axoneme then extends from the basal body by a process which relies on a bidirectional intraflagellar transport (IFT) machinery, which delivers microtubule building blocks (heterodimer α/β tubulins) to the growing cilium (Hao et al., 2011b; Marshall and Rosenbaum, 2001). The basic ciliary axoneme contains nine doublet microtubules whose plus (+) ends are oriented toward the tip of the cilium (**Figure 1.1**).

Cilia are divided into two major types based on their motility. The first type is the motile cilium (also known as flagellum) found in many unicellular eukaryotes, and a subset of metazoan cell types. These cilia have an additional central pair of singlet microtubules (9+2 axoneme), inner and outer dynein arms, and radial spokes, which enable cell locomotion and the generation of fluid flow (Mitchison and Valente, 2017). For example, sea urchin sperm cilia create a helical motion, allowing the cell to swim, while *Chlamydomonas* moves using the breaststroke motions of its two cilia (Ishijima, 2013; Ringo, 1967). In the mammalian brain, beating cilia contribute to the circulation of cerebrospinal fluid (Goetz and Anderson, 2010). Defects in motile cilia can cause primary ciliary dyskinesia (PCD), which in male PCD patients present itself as infertility, due to loss of sperm motility, chronic bronchitis, caused by lack of respiratory airway cleaning, *situs inversus*, a left-right patterning defect arising from dysfunction at the embryonic node, and head enlargement, caused by the resultant accumulation of cerebrospinal fluid (Reiter and Leroux, 2017).

The second type of cilia are the non-motile or primary cilia, which lack the central pair of microtubules (9+0 axoneme) (**Figure 1.1**). This group of cilia transduces

environmental cues to regulate signaling pathways essential for a variety of physiological and developmental processes (Oh and Katsanis, 2012). One example of a primary cilium is the photoreceptor sensory cilium, which captures and relays light signals (Goetz and Anderson, 2010). In vertebrates, primary cilia play a crucial role in the Hedgehog (Hh) and Wnt signaling pathways, both of which are essential for correct developmental patterning (May-Simera and Kelley, 2012; Mukhopadhyay and Rohatgi, 2014). Unlike motile cilia, primary cilia are present in most human cells (Jensen and Leroux, 2017). Because of their critical roles in regulating signal pathways and their omnipresence, dysfunction of primary cilia is known to underlie a growing number of human diseases, known as ciliopathies (Waters and Beales, 2011). Common ciliopathy-associated disorders include retinal degeneration, polycystic kidney disease (PKD), multi-syndromic Meckel-Gruber syndrome (MKS), Bardet-Biedl syndrome, and Joubert syndrome (JBTS) (Reiter and Leroux, 2017). Ciliopathies are discussed in more detail in section **1.1.3**.

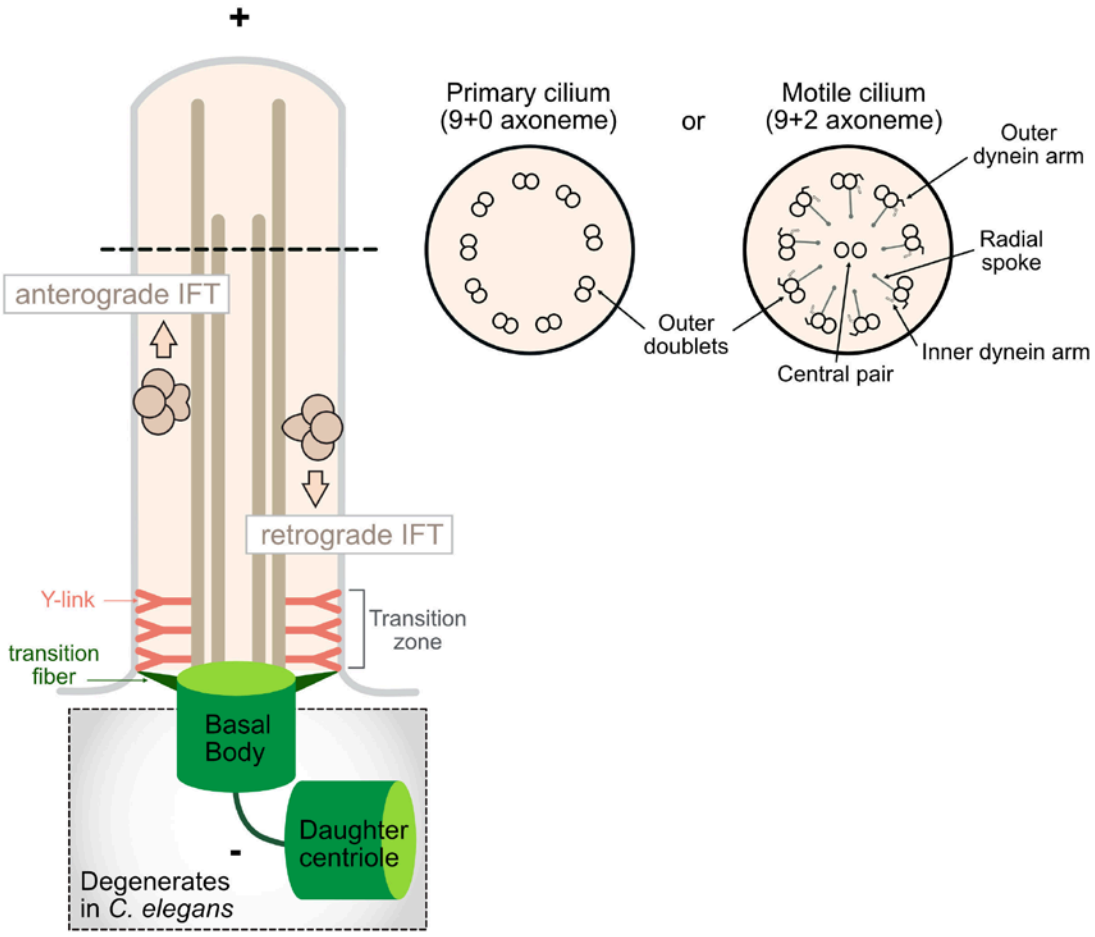

Figure 1.1 Basic structures of primary and motile cilia and intraflagellar transport (IFT) system required for ciliogenesis. After a mother centriole anchors to the cellular membrane via its transition fibers (TFs), it forms the basal body at the base of the cilium. In *C. elegans*, the basal body almost completely degenerates after ciliogenesis, likely retaining only distal end microtubules connected to TFs. The minus ends of microtubules are anchored at the basal body and the plus ends extend towards the ciliary tip. Extension (formation) of the ciliary axoneme depends on the multi-protein IFT machinery, which is powered by plus-end anterograde (kinesin) motors and a minus-end retrograde (dynein) motor. While the axoneme of motile cilia has a central pair and thus a “9+2” arrangement of microtubules, primary cilia lack this central pair and have “9+0” axonemes. Motile cilia also contain inner and outer dynein arms, and radial spoke which are important for force generation (Reiter et al., 2012).

1.1.1 Ciliary subcompartments

1.1.1.1 Basal body

The basal body, almost invariably consisting of triplet microtubules, is present at the base of all known cilia. It is derived from the mature mother centriole and is firmly anchored to the plasma membrane through specialized distal appendages termed transition fibers (TFs) (Garcia-Gonzalo and Reiter, 2017; Reiter et al., 2012) (**Figure 1.1**). The importance of basal bodies and the TFs is highlighted by the finding that their dysfunction results in loss of ciliogenesis. The basal body is important not only for cilium formation but also in the assembly and docking of IFT particles, and sorting of ciliary proteins. Vesicles containing ciliary proteins are delivered to the ciliary base via the trans-Golgi network and fuse to the periciliary membrane in a SNARE-dependent manner (Sung and Leroux, 2013). Other ciliary proteins, including smoothened and polycystin-2, are transported to the periciliary membrane via the recycling endosome and lateral diffusion (Sung and Leroux, 2013). The IFT machinery which assembles at the base of cilia are thought to specifically recognize one or more proteins and dock at the TFs prior to entry into the ciliary compartment (Garcia-Gonzalo and Reiter, 2017). Interestingly, in contrast to other ciliated organisms, the sensory neurons of adult *C. elegans* remodel their basal bodies such that only the distal end, including what are presumed to be TFs, are retained—suggesting that this IFT-docking region of the basal body is sufficient for the biogenesis and maintenance of cilia (Reiter et al., 2012) (**Figure 1.1**).

1.1.1.2 Transition zone (TZ)

Immediately distal to the basal body is a region called the transition zone (TZ). The TZ is composed of doublet microtubules. An apical ring is present beneath these doublet microtubules, and structures which are typically Y-shaped connect the doublet microtubules to the ciliary membrane (Reiter et al., 2012) (**Figure 1.2**). This ciliary membrane is decorated with bead-like particles that form a so-called ‘ciliary necklace’, which appear as concentric rings but may also be a spiral (Heller and Gordon, 1986). It is likely that the necklace is formed from the tips of the Y-links. Although the compositions of both the Y-link and ciliary necklace structures are largely unknown,

there is mounting evidence that they are essential for correct cilium formation and the function of the TZ as a ciliary gate (Garcia-Gonzalo and Reiter, 2017; Reiter et al., 2012; Williams et al., 2011).

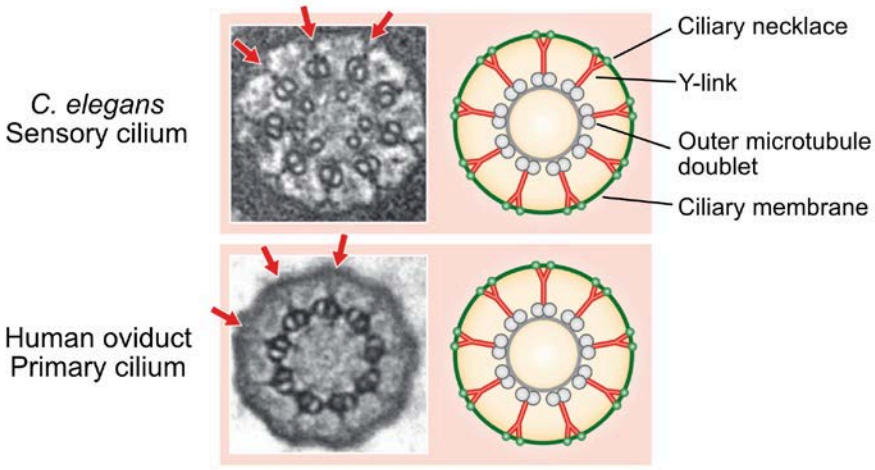

Figure 1.2 The evolutionarily conserved structure of the transition zone. The transition zone is depicted schematically in cross-section together with representative transmission electron microscopes from a *C. elegans* sensory cilium and human oviduct primary cilium. Y-link (red in schematic; arrows in TEM images) structures organize, or make up, the ciliary necklace present on the ciliary surface (shown as green beads). Figure adapted from (Reiter et al., 2012).

Although the ciliary membrane is continuous with the cellular membrane, the cilium maintains a distinctly different composition, designed to capture and relay environmental signals (Garcia-Gonzalo et al., 2011; Reiter et al., 2012; Williams et al., 2011). It is generally accepted that the TZ acts as the ciliary gate for membrane proteins, and it may form part of a gate for soluble proteins as well (Jensen and Leroux, 2017). The TZ establishes a selective diffusion barrier for membrane and membrane-associated proteins to control their distribution within the cilium and it prevents non-ciliary membrane proteins from entering. The plasma membrane protein CEACAM1 (carcinoembryonic antigen-related cell adhesion molecule 1) has been observed to leak into the cilium upon disruption of the TZ (Chih et al., 2011; Wei et al., 2015; Williams et al., 2011). In *C. elegans*, the periciliary membrane-associated proteins TRAM-1a (ortholog of mammalian TRAM) and RPI-2 (retinitis pigmentosa 2), which are absent

from the cilium in wild-type animals, accumulate abnormally inside the cilia of TZ-disrupted mutants (Canning et al., 2018; Li et al., 2016; Williams et al., 2011). The TZ also concentrates ciliary proteins within, and prevents them from inappropriately leaking out of, ciliary compartments. In mammals, membrane associated proteins— including ARL13B (ADP ribosylation factor like GTPase 13B), ADCY3 (adenylate cyclase 3), INPP5E (inositol polyphosphate-5-phosphatase E), and PKD2 (polycystic kidney disease 2)—are concentrated within cilia (Cevik et al., 2013; Garcia-Gonzalo et al., 2011; Roberson et al., 2015; Yee et al., 2015). However, they fail to accumulate within cilium when the TZ is abolished. In *C. elegans*, ARL-13 (orthologue of ARL13B) and other membrane-associated signaling proteins such as ODR-10, SRBC-66, NPHP-2, and TAX-4 localize to the cilium, but not within the TZ subcompartment (Jensen et al., 2015; Li et al., 2016). Upon disruption of the TZ, these proteins appear to fill the region, leading to the notion that the TZ acts as a ciliary zone of exclusion (CIZE). Notably, some proteins, including ARL-13, appear to leak outside of the cilium upon loss of TZ function. Lastly, loss of the TZ in *Chlamydomonas* leads to changes of ciliary protein composition, including of some membrane-associated proteins (Craige et al., 2010). Together, these findings suggest a role for the TZ as a selective membrane diffusion barrier. The majority of the proteins linked to TZ function, discussed below, are membrane-associated, potentially consistent with their roles in supporting a membrane diffusion barrier.

A seemingly separate function of the ciliary base is to regulate the diffusion of soluble membrane proteins into and potentially out of the organelle (Awata et al., 2014; Breslow et al., 2013; Garcia-Gonzalo and Reiter, 2017; Jensen and Leroux, 2017; Kee et al., 2012; Verhey and Yang, 2016). A size-selective mesh-like structure of unknown composition may be responsible for such gating. Lin et al. have suggested the average of the mesh radius is ~8 nm, as proteins ranging from 40-650 kDa and with Stoke radii of less than 8 nm pass through the mesh-like barrier and enter primary cilia in mouse kidney (IMCD3) and fibroblast (NIH 3T3) cells. However, increasing protein size leads to a decreased efficiency of diffusion into the cilium (Lin et al., 2013b). Another study also demonstrated the green fluorescent protein (GFP) trimer (81 kDa) which has a 5.5 nm Stoke radius, cross the barrier and diffuse into the outer segments in frog rod cells (Najafi et al., 2012). The nature of the proteins associated with soluble protein gate functionality, and their precise positions at the ciliary based (*e.g.*, at TFs and/or Y-links?)

remains uncertain, although there is evidence implicating nucleoporins, which have known gating functions at nuclear pores (Endicott and Brueckner, 2018).

To date, there are at least 20 proteins that have been localized to the TZ in a variety of different organisms, including *Chlamydomonas*, *Trypanosoma*, *C. elegans*, *Drosophila*, and vertebrates (Garcia-Gonzalo and Reiter, 2012; Reiter et al., 2012). The majority of these have been disrupted and found to support the function of the TZ as a membrane diffusion barrier (Garcia-Gonzalo and Reiter, 2017; Jensen and Leroux, 2017; Reiter et al., 2012). Furthermore, most have been associated with one or more different ciliopathies, indicating their importance in human health and disease (Reiter and Leroux, 2017).

TZ-associated ciliopathies include Meckel Syndrome (MKS), Joubert syndrome (JBTS), Nephronophthisis (NPHP), Leber Congenital Amaurosis (LCA), Oral-Facial-Digital type (OFD), and Senior Løken syndrome (SLNS) (Hurd and Hildebrandt, 2011; Reiter and Leroux, 2017; Valente et al., 2013). Notably, most TZ genes are linked to MKS and/or NPHP. Furthermore, both protein-protein interaction studies in mammalian cells and genetic analyses in *C. elegans* and mice support the notion of at least two functional modules which include, are collectively termed “MKS module” and “NPHP module” (Diener et al., 2015; Li et al., 2016; Sang et al., 2011; Williams et al., 2011; Yee et al., 2015). Each module appears to have a hierarchical organization, in which ‘peripheral’ proteins require ‘core’ proteins for TZ localization (**Figure 1.3**). Of the ‘core’ TZ proteins, at least two, namely RPGRIP1/RPGRIP1L (MKS-5 in *C. elegans*) and CEP290 (CEP-290) are thought to play important roles as assembly factors or scaffolds for all or a large subset of TZ proteins.

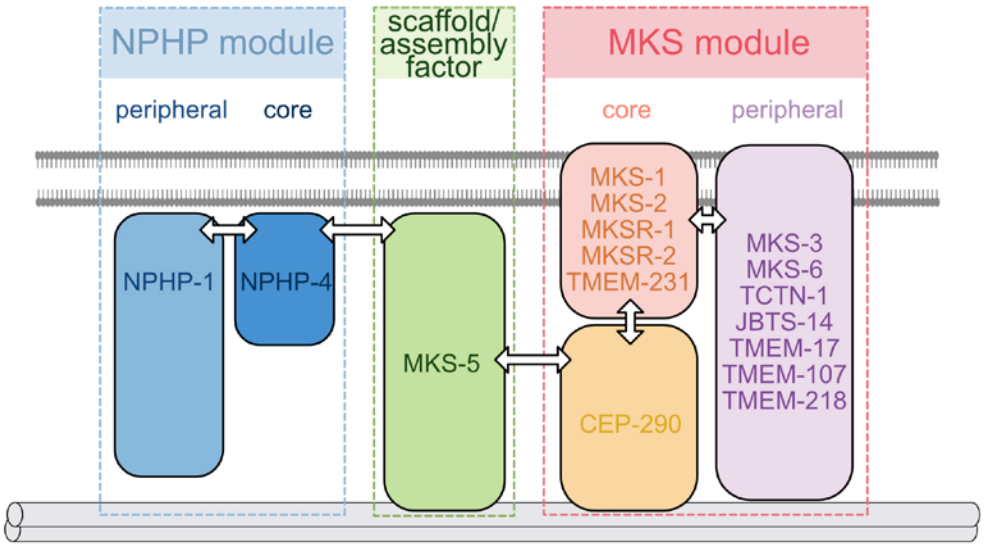

Figure 1.3 Hierarchical organization of *C. elegans* transition zone proteins. MKS-5, the NPHP module, and the MKS module all combine to form a functional transition zone (TZ). A detailed spatial/topological/hierarchical map of TZ proteins, relative to the microtubule axoneme (double cylinders at bottom) and ciliary membrane (bilayer shown), is suggested, but their positioning within a Y-link framework is unclear and other components are likely missing. Major connections (potentially direct or indirect) between different modules or proteins are depicted with double-headed arrows, and are based on a combination of data from *C. elegans* and other organisms. Figure adapted from (Li et al., 2016).

The *C. elegans* MKS module comprises several transmembrane proteins (MKS-2/TMEM216, MKS-3/TMEM67, JBTS-14/TMEM237, TMEM-17/TMEM17, TMEM-107/TMEM107, TMEM-218/TMEM218, TMEM-231/TMEM231), proteins containing B9 domains which are structurally related to lipid-binding C2 domains (MKS-1/MKS1, MKSR-1/B9D1, MKSR-2/B9D2), a coiled-coil protein with a C2 domain (MKS-6/CC2D2A), tectonic protein (TCTN-1/TCTN1) and CEP-290/CEP290 (Lambacher et al., 2016; Li et al., 2016; Roberson et al., 2015; Williams et al., 2011; Yee et al., 2015). Two of the transmembrane proteins (MKS-2 and TMEM-231) and the three B9 domain proteins form the core MKS components (Li et al., 2016). Importantly, CEP-290 is a central assembly factor for all other MKS module proteins; in the absence of CEP-290, the other MKS proteins fail to localize to the TZ (Li et al., 2016).

The *C. elegans* NPHP module contains two nephronophthisis-associated proteins, NPHP-1 and NPHP-4, which are also predicted to harbor lipid-binding C2 domains (Zhang and Aravind, 2012). NPHP-4 is hierarchically positioned as a core

component while NPHP-1 is peripheral (Williams et al., 2011). In mammals, one major proteomic study has linked RPGRIP1L (MKS-5) to the NPHP module, while in *C. elegans*, MKS-5 appears to have a central function relevant to both the MKS and NPHP modules (Arts et al., 2007; Jensen et al., 2015; Roepman et al., 2005; Sang et al., 2011; Williams et al., 2011; Winkelbauer et al., 2005).

Proteins from either the NPHP or MKS modules do not influence each others' TZ localizations. For instance, loss of *C. elegans* NPHP-4 causes the mislocalization of NPHP-1, but none of the MKS module proteins (Li et al., 2016; Williams et al., 2011). Similarly, depletion of CEP-290 results in abnormal localization of MKS module proteins, but NPHP module proteins properly assemble at the TZ. As alluded to above, *C. elegans* MKS-5 functionally interacts with both modules, acting as the most 'central' TZ assembly factor. In *C. elegans*, NPHP-4 and CEP-290 fail to localize to the TZ in the *mks-5* mutant and consequently all NPHP and MKS module proteins are absent from the TZ (Li et al., 2016). MKS-5 interacts with both module proteins through its N-terminal and C-terminal domains. MKS-5 consists of 8 tandem coiled-coils, two C2 domains (C2-N and C2-C) and a Rpgr interaction domain (RID) (Jensen et al., 2015). The truncated MKS-5 harboring only N-terminal coiled-coils rescues the TZ localization of MKS module proteins, whereas NPHP module proteins additionally require the C2 domains for their proper TZ localization.

Further support for the notion of two major modules (MKS and NPHP) and MKS5 as an assembly factor responsible for the functions of these modules comes from ciliopathy associations. On one hand, the two NPHP module proteins NPHP1 and NPHP4 are associated with NPHP, but not MKS. On the other hand, MKS module proteins, namely MKS1, B9D1 (MKSR1), B9D2 (MKSR2), MKS2 (TMEM216), MKS3 (TMEM67), MKS6 (CC2D2A), TMEM107 (MKS13), TCTN2 (MKS8) and TMEM231 (MKS11) have all been linked to MKS, but not NPHP. Similarly, CEP290, known to be important for the correct TZ localization of MKS module proteins but not NPHP module proteins in *C. elegans*, is implicated in MKS and other ciliopathies but not NPHP. In contrast, mutations in MKS5 cause not only NPHP (it is also known as NPHP8), but also MKS (Arts et al., 2007; Delous et al., 2007; Garcia-Gonzalo and Reiter, 2017; Wolf et al., 2007). Some 'peripheral' TZ proteins, including TCTN1, TCTN3 and JBTS14 are not associated either MKS or NPHP. Together, these observations provide strong support for the modular organization shown in **Figure 1.3**, although there may be differences in

the composition and potentially, specific physical/functional relationships between the TZ proteins in different organisms.

Studies using stimulated emission depletion (STED) super-resolution microscopy, NPHP and MKS module proteins appear to form rings with arrays of puncta on the surface of the ciliary membrane, presumably representing the ciliary necklace (Yang et al., 2015b). Meanwhile, the human RPGRIP1L ring has a smaller radial width compared to rings of other TZ proteins, suggesting a potentially role in anchoring to the TZ microtubules (Lambacher et al., 2016; Yang et al., 2015b), a role ascribed to the coiled coils for *C. elegans* MKS-5 (Jensen et al., 2015). Notably, in human retinal pigment epithelium (RPE-1) cilium, CEP290 localizes to a more proximal region of the TZ (closer to the basal body) compared to other TZ proteins, and the CEP290 ring has a size similar to that of the RPGRIP1L ring (Yang et al., 2015b). Moreover, transmission electron microscopy (TEM) studies reveal that *Chlamydomonas* CEP290 resides between the TZ membrane and the microtubules, specifically at the connectors of the Y-links. Consistent with this localization pattern, loss of CEP-290 leads to abrogation of the assembly of the apical ring and Y-links in *C. elegans* (Craige et al., 2010; Li et al., 2016; Schouteden et al., 2015). These findings suggest that CEP290 has a more central assembly function, similar to that of MKS5.

The two TZ modules, MKS and NPHP, are essential and functionally interact during ciliogenesis. Disrupting either the NPHP or MKS module components results in ciliogenesis defects in mice, although this depends on the cell type (Dowdle et al., 2011; Garcia-Gonzalo et al., 2011; Jiang et al., 2008; Sang et al., 2011). When both MKS and NPHP are disrupted, ciliogenesis is synergically perturbed, and polydactyly is increased in limbs (Yee et al., 2015). In *C. elegans*, ciliary and TZ ultrastructures are largely intact in single *nphp* or *mks* mutant animals, but the TZ is mostly missing in a variety of *mks;nphp* double mutants (*e.g.*, *mks-6;nphp-4*) concomitant with cilium ultrastructure defects (Williams et al., 2011).

1.1.1.3 Proximal and distal segments

Moving beyond the TZ towards the ciliary tip, the axoneme is divided into at least two separate regions based on microtubule ultrastructure: the proximal and distal segments. The proximal segment consists of doublet microtubules similar to those in the TZ, but the distal segment typically contains singlet microtubules (Lee and Chung, 2015). The length of each segment appears may vary according to cell types. Each segment can also contain a different assortment of proteins. Most *C. elegans* sensory cilia exhibit the canonical arrangement of having two distinct segments (termed middle and distal segments) with doublet and singlet microtubules, respectively. Mammalian primary cilia have a proximal segment with doublet microtubules that contains a protein, Inversin (INV), and is thus referred to as the Inversin compartment (Shiba et al., 2009; Warburton-Pitt et al., 2014) (**Figure 1.4**). Different mammalian cilia may have short (renal cilia) or long (olfactory cilia) singlet microtubule-containing distal segments (Falk et al., 2015; Sun et al., 2019). Proteins such as NPHP2 (inversin) and ARL13B, and their *C. elegans* orthologs, similarly localize to the Inversin compartment and middle segment, respectively (Cevik et al., 2013; Warburton-Pitt et al., 2014). A relatively small number of proteins are known to localize at the tip of mammalian cilia. Of interest are three Glioma transcription factors (Gli1, Gli2, and Gli3) which are targets of Sonic hedgehog signaling, and Suppressor of fused (Sufu) which interacts with Gli proteins (Haycraft et al., 2005).

It remains an open question how, mechanistically, the length and composition of each ciliary segment is defined. One possibility is that a barrier exists at the boundaries of the segments established with yet-to-be-discovered protein(s). Each ciliary subcompartment may also have a different lipid environment that facilitates retention of proteins with different membrane associations (transmembrane proteins, lipid-modified proteins, *etc.*). One study in *C. elegans* is consistent with the middle and distal segments having different lipid compositions (Jensen et al., 2015), and myristoylated NPHP3 and palmitoylated ARL13B are restricted to the Inversin compartment (Li et al., 2010; Nakata et al., 2012).

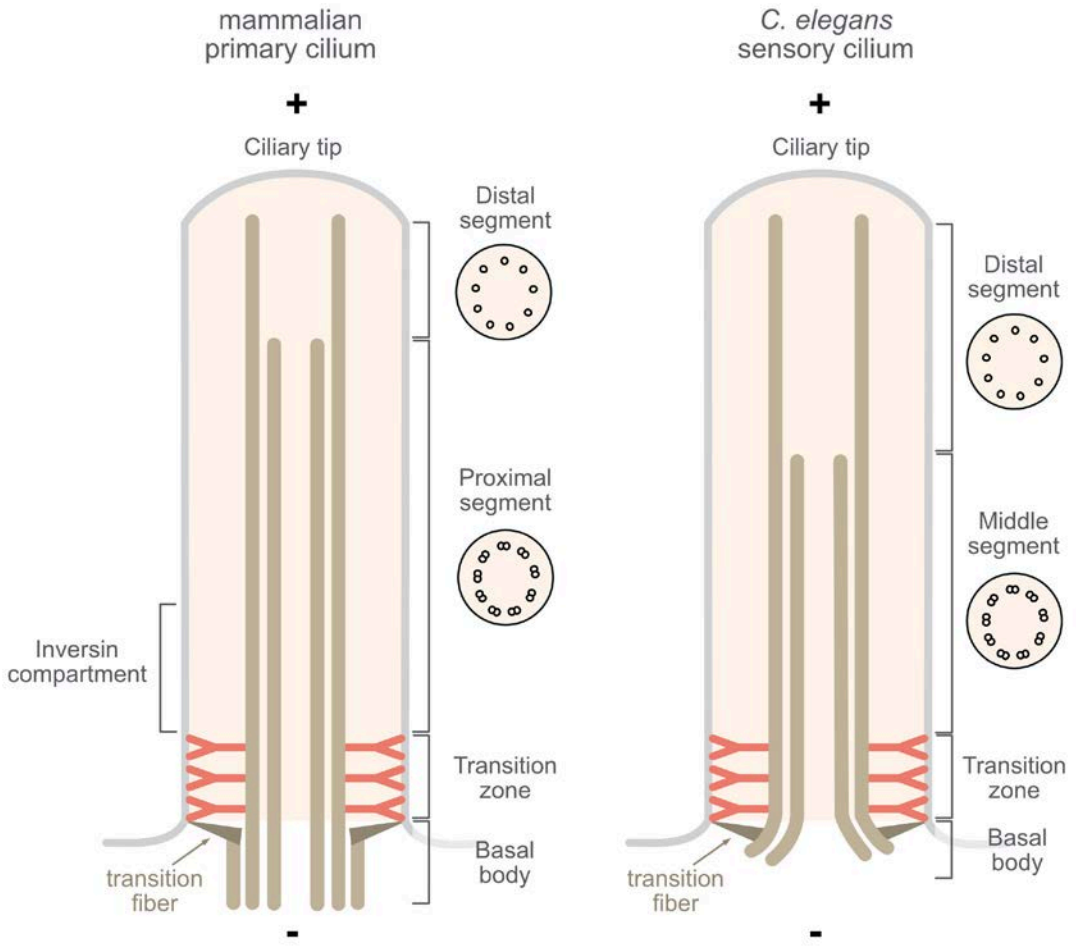

Figure 1.4 Ciliary subcompartments. Vertical (left) and cross (right) sections of the mammalian primary cilia and *C. elegans* sensory cilia. The ciliary base consists of the basal body (BB) and the Y-link-containing transition zone (TZ). In *C. elegans*, the BB mostly remodels after ciliogenesis, leaving the distal end, which contains transition fiber-associated proteins. The TZ functions as a 'ciliary gate' or 'membrane diffusion barrier' which helps to establish the distinct composition of proteins and lipids within a cilium. Most *C. elegans* sensory cilia possess a distinct middle segment containing doublet microtubules and a distal segment with singlet microtubules. Mammalian primary cilia also contain a proximal region which consists of microtubule doublets and contains the so-called 'inversin compartment' given the presence of the protein NPHP2/Inversin. In *C. elegans*, NPHP-2 (Inversin ortholog) occupies a similar region (middle segment; not shown). The distal region of most if not all primary cilia also contain singlet microtubules. Microtubule minus (-) and plus (+) ends are indicated.

1.1.2 Intraflagellar transport

Ciliary proteins are synthesized in the cell body and transported to the base of the cilium. Some of these proteins require the help of IFT machinery to enter the cilium. Evolutionarily conserved in most ciliated organisms, the IFT machinery—first discovered in *Chlamydomonas* by the Rosenbaum lab in 1993 (Kozminski et al., 1993)—operates from the base of the cilium at TFs to the tip, and back, moving bidirectionally along the axonemal microtubules in association with the ciliary membrane (Johnson and Rosenbaum, 1992). It delivers ciliary proteins, such as heterodimer alpha/beta-tubulin and signaling receptors, to the inside of the ciliary compartment (Kozminski et al., 1995; Kozminski et al., 1993; Pigino et al., 2009); for example, IFT has been demonstrated to transport tubulin building blocks to the tip of the cilium to support axonemal assembly and maintenance (Hao et al., 2011b; Marshall and Rosenbaum, 2001). IFT also transports signaling proteins out of the cilium to modulate signal transduction cascades. An example of this is patched1 (PTCH1) exiting from the cilium in an IFT-dependent manner in mouse embryonic fibroblasts upon activation of sonic Hh pathway (Keady et al., 2012). Hence, defects in anterograde or retrograde IFT causes abnormal ciliary formation and abrogates ciliary functions, leading to ciliopathies such as BBS, Mainzer–Saldino syndrome (MSS), and Jeune asphyxiating thoracic dystrophy (JATD) (Huber and Cormier-Daire, 2012; Perrault et al., 2012; Reiter and Leroux, 2017). Ciliopathies are discussed in more detail in section **1.1.3**. Below, I describe the different functional modules of the IFT system, namely the kinesin and dynein molecular motors as well as the core multi-subunit IFT subcomplexes (IFT-A and IFT-B) and BBS protein complex, which work together to transport cargo into and out of cilia.

1.1.2.1 IFT motors

The IFT machinery comprises two types of microtubule-based motors: kinesins, which are drive anterograde transport towards the plus ends of the microtubules, and dynein, which powers retrograde movement from the tip to the base of the cilium (**Figure 1.5**). Both motors play crucial roles in the ciliary assembly and maintenance.

Heterotrimeric kinesin-2 is a canonical anterograde motor (**Figure 1.5**). It includes two motor subunits (KIF3A and KIF3B), and a kinesin-associated protein (KAP)

(Rosenbaum and Witman, 2002). Disruption of the KIF3B motor subunit results in the loss of cilia in mouse nodal cells (Nonaka et al., 1998). The involvement of motors in ciliary assembly is also highlighted by the *fla10* (*Chlamydomonas* kinesin-2) temperature-sensitive (*ts*) mutant, which develops defects in ciliary assembly at the non-permissive temperature (Walther et al., 1994). Moreover, shifting the *fla10 ts* mutant from a permissive to a restrictive temperature rapidly leads to the resorption of the already-assembled cilium (Kozminski et al., 1995). Some types of cells contain an additional anterograde motor, homodimeric kinesin-2, which helps to build the correct ciliary structure. In *C. elegans*, the homodimeric kinsesin-2 (OSM-3) is responsible for constructing most of the distal segments of sensory cilia. Similarly, the homodimeric kinesin KIF17 is essential for the assembly of the ciliary outer segments in zebrafish photoreceptors (Insinna et al., 2008).

Retrograde IFT depends on the cytoplasmic dynein-2 complex, which is composed of heavy, intermediate, light, and light intermediate chains (Grissom et al., 2002; Ishikawa and Marshall, 2017; Jensen et al., 2018; Patel-King et al., 2013; Pazour et al., 1999; Pazour et al., 1998; Perrone et al., 2003; Porter et al., 1999; Rompolas et al., 2007; Schafer et al., 2003). In various model organisms, *dynein-2* mutants possess short, often bulbous cilia with large accumulations of IFT particles at the tips (Engel et al., 2012; Hou et al., 2004; May et al., 2005; Pazour et al., 1999; Signor et al., 1999). Defects in retrograde IFT cause the IFT machinery transported by anterograde motors to be unable to return to the ciliary base, where IFT components are remodeled in preparation for another round of IFT. As a result, both the assembly and maintenance of the cilia are impaired (Jensen et al., 2018; Pazour et al., 1999). For instance, after cell division, *dhc1b-3* (*Chlamydomonas* dynein-2) *ts* mutant cells assemble new cilia at a permissive temperature, but not at a restrictive temperature. Another *Chlamydomonas* dynein-2 *ts* mutant, *fla24,* shows rapid cilia shortening at the restrictive temperature (Lin et al., 2013a). In *C. elegans*, CHE-3 is the ortholog of human cytoplasmic dynein-2 heavy chain 1. *che-3 ts* mutant animals are also unable to maintain the proper length of sensory cilia at the non-permissive temperature (Jensen et al., 2018).

Since anterograde and retrograde IFT depend on different types of motors, IFT travels at different velocities along the ciliary axoneme. Interestingly, anterograde and retrograde IFT speeds also vary in different organisms (Dentler, 2005; He et al., 2014; Ishikawa et al., 2014; Kozminski et al., 1993). In *Chlamydomonas*, anterograde and

retrograde IFT speeds are 2 μm/s and 3.5 μm/s, respectively (Dentler, 2005; Kozminski et al., 1993). In *C. elegans*, heterotrimeric kinesin-2 (Kinesin-II) and OSM-3 motors move at velocities of 0.5 μm/s and 1.3 μm/s, respectively. The two anterograde motors function cooperatively, such that they share the task of transporting IFT particles, in the middle (proximal) segment of the cilium. The contribution of the kinesin-II motor to transport is greater in the proximal region of the middle segment and decreases towards the end of the middle segment. Conversely, the contribution of OSM-3 is less in the proximal region, and greater in the distal region. The speed of the IFT machinery in the middle segment therefore reflects the proportion of slower-moving Kinesin-II and faster-moving OSM-3 that transport the IFT particles, from slower to faster, with the average being ~0.7 μm/s (**Figure 1.5**). However, in the distal segment, the transport rate is faster (1.3 μm/s) than in the middle segment since IFT is powered solely by the OSM-3 motor (Kinesin-II does not enter the distal segment) (**Figure 1.5**). The speed of dynein-driven retrograde IFT movement is 1.5 μm/s (Hao et al., 2011a; Jensen et al., 2018).

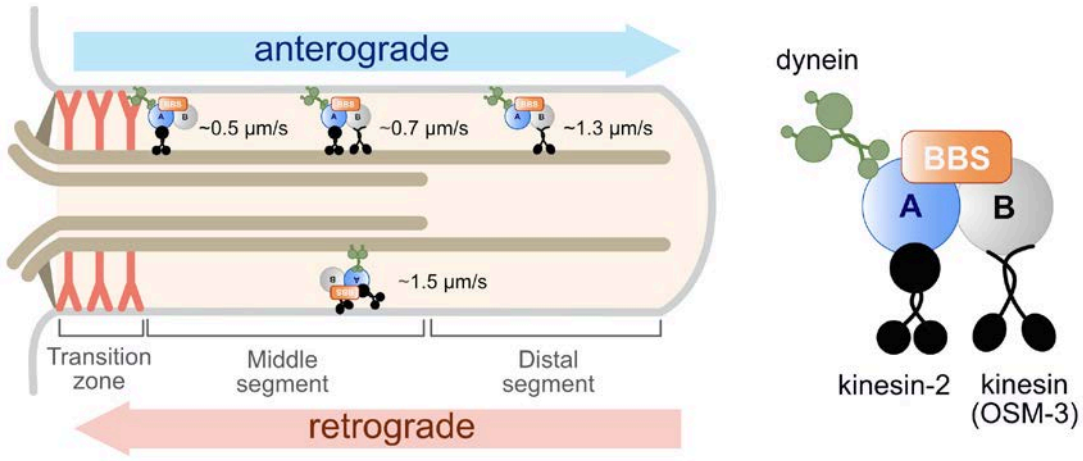

Figure 1.5 Intraflagellar transport (IFT) in *C. elegans*. The IFT machinery is composed of kinesin and dynein motors, two IFT subcomplexes (IFT-A and IFT-B) and a Bardet-Biedl syndrome (BBS) complex. Cargo loading, transport and unloading is omitted for clarity. IFT particles move bidirectionally along axonemal microtubules within a cilium. Heterotrimeric kinesin-2 and homodimeric OSM-3 are responsible for anterograde IFT. The slower-moving kinesin-2 is initially the predominant motor employed in the proximal-most region of the middle segment, and a gradual hand-over to the faster-moving OSM-3 occurs, leading to OSM-3 being the predominant motor used towards the end of the middle segment. IFT velocities therefore increase gradually in the middle segment, with the average being ~0.7 μm/s. Kinesin-II disengages and does not enter the distal segment, and OSM-3 becomes the only motor to operate in the distal segment, at the fast speed of ~1.3 μm/s. IFT-Dynein, after being transported in an inactive form by the anterograde motors, becomes active at the ciliary tip and returns the IFT machinery to the base of the cilium for another round of IFT.

1.1.2.2 IFT complexes

In addition to containing motor proteins, the multimeric IFT machinery also harbors two separate protein complexes: IFT subcomplex A (IFT-A) and subcomplex B (IFT-B). From a biochemical purification of the IFT machinery in *Chlamydomonas*, it was discovered that IFT-A and IFT-B contains at least 6 and 16 subunits each, respectively (Fan et al., 2010; Ishikawa et al., 2014; Piperno et al., 1998; Wang et al., 2009). These IFT subcomplexes interact with the anterograde and retrograde motor proteins. IFT-B interacts with the heterotrimeric kinesin-2 in *Chlamydomonas* lacking homodimeric kinesin-2*,* and the mouse IFT-B subunits can be pulled down with both the heterotrimeric and homodimeric kinesin-2 motors (Baker et al., 2003; Howard et al., 2013; Liang et al., 2014). Based on genetic and time-lapse video microscopy studies in *C. elegans*, it is thought that IFT-B associates with OSM-3, and that IFT-A binds to kinesin-II in *C. elegans* (**Figure 1.5**). The evidence stems from the observation that disruption of the BBS complex causes the dissociation of the IFT-A and IFT-B subcomplex subunits; IFT-A remains associated with and moves at kinesin-II speeds, whereas IFT-B remains associated with and moves at OSM-3 speeds (Hao et al., 2011a). There is evidence that the inactive dynein-2 motor docks to IFT-B during anterograde trafficking but is activated and binds to IFT-A for retrograde movement at the tip of the cilium (Chien et al., 2017).

When IFT-B is knocked down, the resultant cells possess short or no cilia, similar to cells carrying defective kinesin-II (Adhiambo et al., 2009; Brazelton et al., 2001; Follit et al., 2006; Haycraft et al., 2003; Pazour et al., 2000; Sun et al., 2004; Tsao and Gorovsky, 2008). This suggests that the role of IFT-B is likely related to anterograde trafficking, rather than retrograde movement. Supporting this notion, IFT-B is responsible for the delivery of tubulin to the cilium. Bhogaraju et al. have been shown that two components of IFT-B (IFT74 and IFT81) can bind α/β tubulins. After IFT81 siRNA knockdown, ciliogenesis is significantly decreased in human RPE-1 cells indicating the IFT-B is essential for ciliary assembly (Bhogaraju et al., 2013). In addition, the IFT-B is involved in the import as well as export of the Hh signaling components to the cilium (Keady et al., 2012; Yang et al., 2015a).

IFT-A mutants, on the other hand, enable assembly of the cilia but develop unusual bulge structures filled with IFT proteins, like *dynein-2* mutants (Blacque et al., 2006; Efimenko et al., 2006; Iomini et al., 2001; Iomini et al., 2009; Piperno et al., 1998;

Tran et al., 2008; Tsao and Gorovsky, 2008). This suggests that IFT-A plays an important role in retrograde trafficking. Furthermore, G protein-coupled receptors (GPCRs), such as somatostatin receptor type 3 (Sstr3) and melanin-concentrating hormone receptor 1 (Mchr1), require IFT-A-dependent trafficking for their ciliary localization of in RPE-1 cells (Mukhopadhyay et al., 2010).

To summarize, both IFT complexes are involved in the trafficking of certain types of ciliary cargos and the IFT-B complex is additionally important for cilium assembly.

1.1.2.3 BBS complex

The last component group of the IFT machinery is called the BBS protein complex, or BBSome. Bardet-Biedl syndrome (BBS) is a very rare genetic disorder caused by ciliary dysfunction, with BBS patients showing symptoms such as blindness, obesity, polydactyly and renal failure (Reiter and Leroux, 2017). At least eight evolutionarily conserved BBS proteins form the BBSome complex in mammalian cells, *C. elegans*, and other organisms, and have known ciliary functions including targeting of membrane protein GPCRs and trafficking of signaling molecules (Nachury et al., 2007). In the mouse brain, deletion of BBS genes abolishes ciliary localization of Sstr3 and Mchr1, and loss of *Chlamydomonas* BBS proteins causes accumulation of signaling molecules within its motile cilium (Berbari et al., 2008; Jin et al., 2010; Lechtreck et al., 2009). As mentioned above, the BBSome also helps to maintain the structural/functional integrity of the IFT machinery, maintaining the IFT-A and IFT-B subcomplexes together during anterograde transport.

1.1.3 Ciliopathies

Cilia with functional or structural anomalies can cause ciliopathies. Although some ciliopathies are organ-specific, most manifest multi-systemic symptoms that include retinal dystrophy, renal disease, brain malformations, polydactyly, and obesity (Reiter and Leroux, 2017). This is due in part because cilia support the functions of nearly all cell types (Jensen and Leroux, 2017). Furthermore, cilia need to be correctly assembled to become functional. The major steps of ciliogenesis are docking of the basal body to the plasma membrane, formation of the transition zone, and extension of the axoneme by the IFT system (Reiter et al., 2012). These cilium-building pathways require a large number of cellular components, and indeed, over 400 genes are known to be associated with ciliary functions (Reiter and Leroux, 2017). Of these, nearly one half have been reported to be mutated in patient presenting with at least 35 different types of ciliopathies (Reiter and Leroux, 2017).

Cilia that have compromised functions but lack major structural defects can also result in ciliopathies. For example, loss of, or abnormal motility in normally motile cilia often leads to PCD, which is characterized by fertility and breathing problems amongst other clinical ailments (Reiter and Leroux, 2017). Sensory ciliopathies including retina degeneration and anosmia result from functional defects in the primary cilia found in sensory organs (Nikopoulos et al., 2016; Omori et al., 2010). Sensory cilia detect environmental cues such as light and odor molecules and initiate signal transduction, whereas other primary cilia mediate intracellular signaling pathways, such as the Hh transduction pathway, essential for physiology and development (Mukhopadhyay and Rohatgi, 2014). When hedgehog signaling molecules bind to PTCH1 receptors on the cilia, Hh signal transduction is triggered. As a result, Hh signaling components are relocated to, or out of, the cilia and GLI proteins are converted to activators which induce target gene transcription. Disrupting these intracellular signaling pathways results in ciliopathies exhibiting developmental abnormalities, such as short-rib polydactyly (Paige Taylor et al., 2016). The IFT machinery, which plays a role in ciliogenesis by delivering tubulin, also dynamically transports signaling molecules in and out of cilia; for example, IFT-A, IFT-B, and BBS proteins are involved in the trafficking of certain GPCRs and Hh signaling proteins. As such, mutations in many different IFT proteins are implicated in skeletal ciliopathies such as JATD, MSS, and Sensenbrenner syndrome (Perrault et al., 2012; Reiter and Leroux, 2017; Waters and Beales, 2011).

1.1.4 Studying cilia in *C. elegans*

C. elegans, which lacks motile cilia, represents an excellent multicellular model organism to study the biogenesis and fundamental functions of non-motile sensory cilia, and it has helped uncover the components and molecular etiologies associated with ciliopathies, such as BBS, MKS, and PKD (Ansley et al., 2003; Bae et al., 2006; Barr and Sternberg, 1999; Blacque et al., 2005; Blacque et al., 2004; Efimenko et al., 2005; Jauregui and Barr, 2005). A hermaphrodite worm contains 60 ciliated sensory neurons (~20% of its total neurons), while a male worm has additional 52 ciliated neurons (Inglis et al., 2007). All of the sensory cilia are present at the distal ends of dendrites, which extend from the cell bodies. Cilia are largely (but not exclusively) responsible for the ability of *C. elegans* to sense its environment and modulate behavior. Cilium-dependent sensory processes include chemosensation, olfaction, mechanosensation and thermosensation (Inglis et al., 2007).

To perform these functions, many cilia are exposed to the external environment through channels created by socket cells, in the head and tail of the animal (Inglis et al., 2007). The amphid (head) channel contains single rod-like cilia (ASE, ASG, ASH, ASI, ASJ, and ASK) and double-rod cilia (ADF and ADL) whose length is between 7 to 8 μm (Doroquez et al., 2014). The phasmid (tail) cilia (PHA and PHB) are single rod-like cilia, slightly shorter than amphid channel cilia (Hall and Russell, 1991). Other amphid cilia (AWA, AWB, AWC, and AFD) are embedded in sheath cells rather than exposed to the environment (Inglis et al., 2007). Unlike other chemosensory cilia mentioned above, AFD cilia are responsible for thermosensation (Inglis et al., 2007). Still other amphid cilia (CEP and OLQ) are required for mechanosensation and terminate in the cuticle near *C. elegans*' lips (Inglis et al., 2007). Given their functions, it is not surprising that defects in the sensory cilia affect worm's behaviors, such as the ability to move towards attractants or away from repellants, and navigate temperature and oxygen gradients to find their optimal growth conditions (Inglis et al., 2007). Cilia also control the entry of the organism into a stress-resistant alternate life stage (dauer larva), and influence body size, indicating that the cilia in *C. elegans* are involved in developmental processes (Fujiwara et al., 2002; Inglis et al., 2007).

A key advantage of studying cilia in *C. elegans* is that the organelles are not essential for life. In contrast, mouse cilia mutants that affect the function of ciliogenesis

(*e.g.*, IFT) show embryonic lethality (Chih et al., 2011; Dowdle et al., 2011; Garcia-Gonzalo et al., 2011; Sang et al., 2011; Weatherbee et al., 2009). Mutations in the *C. elegans* orthologs of human ciliary genes can, on the other hand, be readily studied in the context of individual cells and the entire animal (Jensen et al., 2015; Li et al., 2016; Williams et al., 2011). A large number of *C. elegans* ciliary mutants have been characterized and are readily available, and precise gene editing using the CRISPR/CAS9 system is straightforward (Dickinson et al., 2015; Thompson et al., 2013). Furthermore, behavioral assays (for example, chemotaxis and osmotic avoidance) are well established in *C. elegans*, and investigating how ciliary dysfunction changes neuronal functions and consequently affects the worm's behaviors is possible. Lastly, using *C. elegans* as a disease model system allows us to study pathomechanisms for ciliopathies at the cellular and molecular levels.

1.2 Ciliary length regulation

Cells have different lengths of cilia in different tissues, and each cell type maintains an appropriate cilium length for optimal function (Keeling et al., 2016). Impairment of this length regulation, therefore, leads to interruption of ciliary functions such as cell locomotion and cell signaling, and has the potential to cause ciliopathies (Nguyen et al., 2005; Paige Taylor et al., 2016). Links between the regulation of ciliary length and various ciliopathies are known: for example, long cilia are implicated in MKS, tuberous sclerosis and juvenile cystic kidney disease (DiBella et al., 2009; Husson et al., 2016; Sohara et al., 2008; Tammachote et al., 2009), while short cilia are associated with primordial dwarfism and PKD (Huang and Lipschutz, 2014; Shaheen et al., 2012).

To explain cilium length control, Marshall and Rosenbaum proposed a balance-point model using findings largely obtained using *Chlamydomonas* as a model system. In brief, this generally-accepted cilium length control model suggests a fine balance between assembly and disassembly of microtubules at the ciliary tip (the plus ends of microtubules) (**Figure 1.6**) (Marshall and Rosenbaum, 2001). While cilium assembly rates decrease as the axoneme grows, disassembly is length-independent and has a constant rate. If the assembly rate is higher than the disassembly rate, ciliary axonemes grow. Conversely, if the disassembly rate exceeds the assembly rate, cilia shorten. An equilibrium between assembly and disassembly therefore sets a defined, stable cilium length. Hence, partial reduction of IFT, which is required for ciliary assembly, decreases the assembly rate and as a result, leads to short cilia in *Chlamydomonas*. On the other hand, a long flagellar mutant has a decreased disassembly rate compared to wild-type animals (Marshall and Rosenbaum, 2001).

The assembly of the ciliary axoneme is IFT-dependent. IFT loads ciliary cargos, including microtubule building blocks (tubulins) and other structural components of the axoneme at the ciliary base, and delivers them to the assembly site (Broekhuis et al., 2013; Kubo et al., 2016). Wren et. al. showed that ciliary cargo loading on IFT is length-dependent. In *Chlamydomonas*, the amount of an axonemal protein of the nexin-dynein regulatory complex, DRC-4, transported into the cilium by IFT, decreases as the cilium grows (Wren et al., 2013). Therefore, alterations of not only ciliary cargo delivery mediated by IFT, but also the cargo loading on IFT affect the assembly rate and influences cilium length.

In contrast, the disassembly of microtubules is IFT-independent and relies on the activity of two kinesin families (kinesin-8 and kinesin-13), called depolymerizing kinesins which remove tubulin from microtubules. For example, the mammalian kinesin-8 family (KIF19A) and the kinesin-13 family (KIF2A and KIF24) localize to cilia and regulate ciliary disassembly (Kim et al., 2015; Miyamoto et al., 2015; Niwa et al., 2012).

In addition to IFT and depolymerizing kinesins, posttranslational modifications of tubulins present in the ciliary axoneme (*e.g.*, polyglutamylation, acetylation, detyrosination) can influence the structure and/or stability of the microtubules and represent a factor in cilium length regulation (Avasthi and Marshall, 2012; Wloga and Gaertig, 2010). For example, tubulin acetylation stabilizes microtubules, and a tubulin deacetylase is involved in cilium disassembly (Pugacheva et al., 2007). A doublecortin (DC) domain protein, which binds tubulins and enhances polymerization, is also implicated in ciliary length control. Overexpression of DC domain proteins, including DCDC2 and RP1, results in cilia lengthening in mammalian hippocampal neurons and photoreceptors, respectively (Massinen et al., 2011; Omori et al., 2010).

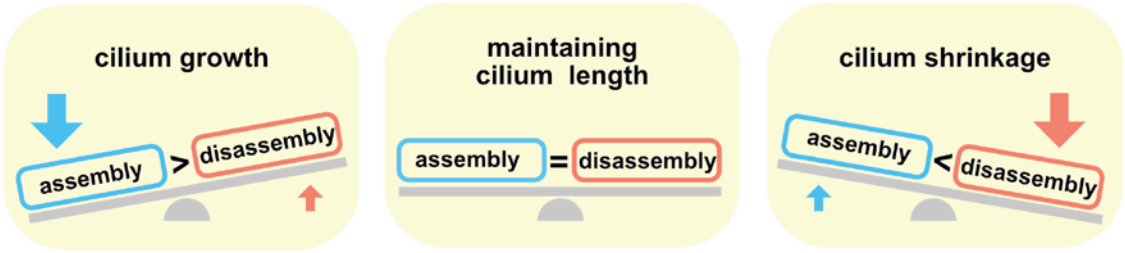

Figure 1.6 Model for cilium length regulation. A cilium disassembles with a constant rate and this process is length-independent. However, the cilium assembly rate is length-dependent and decreases as cilium length increases. In a growing cilium, the assembly rate is higher than that of disassembly (left). When cilium assembly and disassembly are balanced, a cilium maintains a specific length (center). On the other hand, when a cilium exceeds its desired length, disassembly predominates over assembly, resulting in shrinkage of cilium (right).

1.2.1 Protein kinases implicated in cilium length regulation

Protein kinases are involved in virtually all cellular processes, including cell signaling and the cell cycle. Of particular importance to this thesis work, there is increasing evidence that protein kinases are implicated in the ciliary formation and length regulation. When looked at in the context of the entire human kinase complement ('kinome'), kinases with roles in cilium length control mainly belong to three kinase groups/families: the CMGC group, which includes CDKs, mitogen-activated protein kinases (MAPK), glycogen synthase kinases (GSK), and CDC-like kinases (CLK); the never-in-mitosis-A (NIMA)-Related Kinase family, which consists of several NEK proteins; and finally, the Aurora kinase family (Berman et al., 2003; Broekhuis et al., 2014; Burghoorn et al., 2007; Hu et al., 2015a; Husson et al., 2016; Omori et al., 2010; Phirke et al., 2011; Shalom et al., 2008; Sohara et al., 2008; Tam et al., 2013; Tam et al., 2007; Wilson and Lefebvre, 2004; Yang et al., 2013) (**Figure 1.7**). Most of these kinases functionally associate with cellular factors important for the assembly and/or disassembly of the cilium, such as IFT, depolymerizing kinesins, and tubulin deacetylases.

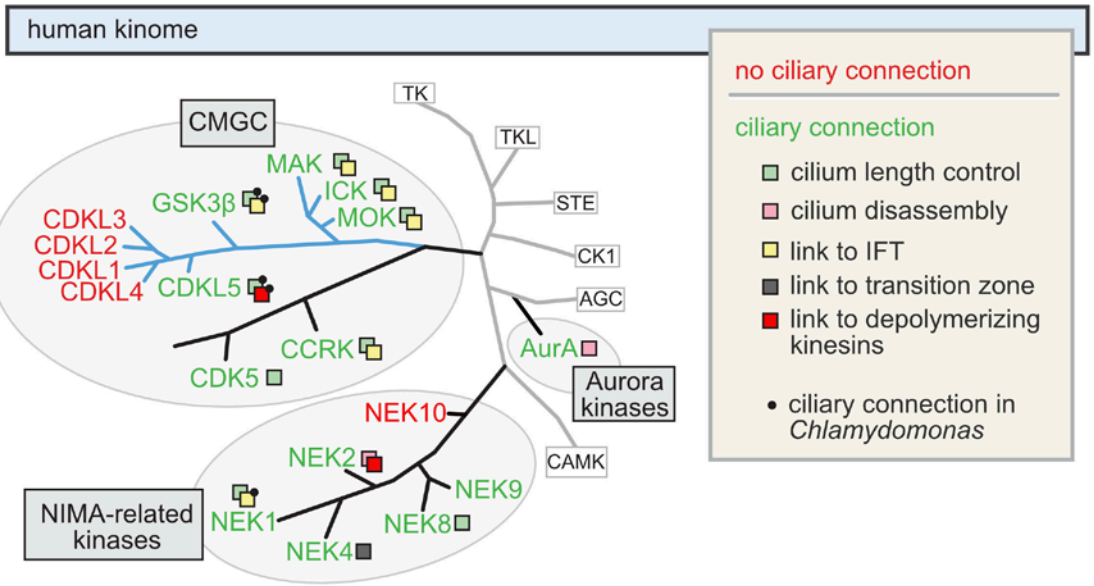

Figure 1.7 Phylogenetic distribution of CMGC group kinases, NIMA-Related Kinases (NEKs) or Aurora-A kinases with known ciliary functions. Protein kinases involved in cilium length control and disassembly, association with intraflagellar transport (IFT), depolymerizing kinesins, and TZ localization are shown in green. A branch of the CMGC group (blue) includes several kinases (mammalian MAK, ICK, and MOK; Chlamydomonas GSK3β and CDKL5) that regulate cilium length, by either influencing either IFT or depolymerizing kinesins. Human CDKL1, CDKL2, CDKL3, and CDKL4 (shown in red) have no previously known links to cilia.

1.2.1.1 CMGC kinases

The CMGC group includes several kinases involved in cilium length control that are found in one specific branch, namely the *ros-cross* hybridizing kinase (RCK) family kinases, glycogen synthase kinase 3 beta (GSK3β) and cyclin-dependent kinase-like (CDKL). One additional branch sports two other kinases, the cell cycle related kinase (CCRK) and cyclin-dependent kinase 5 (CDK5) (**Figure 1.7**).

1.2.1.1.1 CCRK and CDK5

CCRK negatively regulates ciliary length in mammals, C*hlamydomonas* and *C. elegans* (Snouffer et al., 2017; Yang et al., 2013). CCRK knockdown results in ciliary length elongation and its overexpression leads to a decrease in ciliary length in mouse fibroblast cells. When CCRK is depleted, intestinal cell kinase (ICK), a known CCRK substrate and ciliary length regulator, accumulates at the tip of the cilium. As CCRK does not appear to specifically localize to cilia, it may indirectly regulate the length of the cilium via ICK. This latter kinase is discussed in more detail below.

Similarly, the *Chlamydomonas* ortholog of CCRK, LF2 (long flagella 2), is not cilium-localized protein. Rather, it combines with LF1 and LF3 to form the so-called length regulatory complex (LRC) in cytoplasm. The *lf2-3* mutant, containing mutations which affect the activity of the protein, has abnormally long flagella in comparison to wild-type (Asleson and Lefebvre, 1998; Tam et al., 2007). In contrast, the *C. elegans* ortholog, DYF-18, is transported to the ciliary distal segment by the IFT machinery, as a cargo. In the absence of DYF-18, some IFT proteins abnormally localize in the elongated cilia and unlike in wild-type cilia, the heterotrimeric kinesin-2 motor enters to the distal segment, suggesting DYF-18 modulates ciliary length by controlling IFT motor activity (Phirke et al., 2011; Yi et al., 2018).

Depletion of CDK5 results in reduction of ciliary length in RPE-1 cells (Maskey et al., 2015). In addition, either inhibition with pan CDK inhibitor treatment or knockdown using siRNA of CDK5 in *juvenile cystic kidneys* (*jck*) mice, which have significantly long cilia on kidney epithelial cells, leads to shorter cilia. In *jck* mice, CDK5 controls ciliary length via its substrate CRMP2, apparently by affecting microtubules dynamics, rather than by regulating IFT (Husson et al., 2016).

1.2.1.1.2 RCK kinase family

RCK kinases have three members, namely male germ cell associated kinase (MAK), MOK (MAPK/MAK/MRK Overlapping Kinase), and MAK-like intestinal cell kinase (ICK) (Broekhuis et al., 2014; Chaya et al., 2014; Yi et al., 2018). Each has been shown to localize to cilia and play a crucial role in governing ciliary length, mainly by regulating the IFT machinery.

LmxMPK9 and DYF-5*, L. mexicana* and *C. elegans* orthologs of mammalian MAK, negatively regulate the length of cilia (Bengs et al., 2005). Overexpression of either *LmxMPK9* or *dyf-5* results in very short or no cilia, whereas *null* mutants have significantly long cilia. *C. elegans* DYF-5 is directly associated with the correct function of IFT proteins, which is important for ciliary assembly and maintenance. In *dyf-5* mutant cilia, IFT proteins atypically accumulate and IFT frequencies (numbers of moving IFT particles over time) are also reduced (Burghoorn et al., 2007; Yi et al., 2018). Notably, DYF-5 influences two anterograde IFT motors. In the *dyf-5* mutant, the kinesin-2 motor—normally found from ciliary base to the end of the middle segment—ectopically enters the distal segments, and OSM-3 exhibits a reduced velocity.

Mammalian MAK similarly plays a role in cilium length regulation. Mouse embryonic fibroblast (NIH 3T3) cells overexpressing *Mak* have short cilia. On the other hand, *Mak-knockout* mouse photoreceptor cilia are elongated, and their outer segment contains abnormally-accumulated IFT components, including a subunit of the anterograde kinesin-2 motor protein, KIF3A (Omori et al., 2010). MAK also modulates ciliary length by directly phosphorylating a DC domain-containing protein, RP1, which is a positive ciliary length regulator. RP1 stabilizes and enhances the polymerization of microtubules, and thus its overexpression results in the assembly of longer cilia. However, co-expression with *Mak* reduces the length of cilia (Omori et al., 2010). These observations suggest that mammalian MAK acts as a negative regulator of ciliary length by controlling the functions of IFT as well as DC domain proteins.

MOK also negatively controls the length of cilia in IMCD3 cells. Although it travels with IFT, it does not appear to influence the ciliary localization or speed of IFT particles (Broekhuis et al., 2014). One possibility is that MOK modulates other properties of IFT. Indeed, green algal cells assemble aberrantly long cilia upon disruption of LF4, the *Chlamydomonas* ortholog of mammalian MOK. In comparison to wild-type, *lf4* mutant

exhibits elevated injection rates of IFT particles into cilia, which results in an increased rate of ciliary assembly (Berman et al., 2003; Hilton et al., 2013; Ludington et al., 2013).

ICK has been shown to regulate cilium length, by modulating IFT, and in a manner that is cell type-specific. Depletion of ICK leads to excessively long cilia in mouse renal epithelial (IMCD3) and mouse fibroblast NIH 3T3 cells indicating that it is a negative regulator of ciliary length (Broekhuis et al., 2014; Moon et al., 2014). In IMCD3 cells, ICK is transported by IFT and influences the speed of the IFT machinery (Broekhuis et al., 2014). Depletion of ICK makes anterograde IFT move faster, and its overexpression results in a decrease in retrograde IFT velocity. In contrast, in mouse embryonic fibroblast (MEF) cells, loss of ICK results in short cilia, and its overexpression leads to cilia elongation (Chaya et al., 2014). IFT components abnormally accumulate in *Ick* null as well as ICK-overexpressed MEFs. ICK regulates an IFT motor protein, a subunit of kinesin-2 (KIF3A), by phosphorylation (Chaya et al., 2014).

1.2.1.1.3 GSK3β

GSK3β has functions in microtubule dynamics, polymerization, and stabilization by phosphorylating microtubule binding proteins (MBPs), such as Collapsin Response Mediator Protein 2 (CRMP-2), Adenomatous Polyposis Coli (APC), Microtubule-Associated Protein 1B (MAP1B) (Zhou and Snider, 2005). There is also evidence that GSK3β is involved in ciliary length regulation, perhaps because cilia are microtubule-base organelles. Expressing kinase-dead GSK3β induces long cilia in zebrafish (Yuan et al., 2012). Moreover, GSK3 from *Chlamydomonas* is a cilium-localized protein that regulates ciliary length (Wilson and Lefebvre, 2004). When the kinase activity of GSK3β is inhibited by lithium treatment, cilia elongate, and the amount of the anterograde IFT motor protein increases. While the *Chlamydomonas* studies suggest that GSK3β likely regulates IFT functions to regulate ciliary length, we cannot exclude a possibility that GSK3β also regulates other microtubule-associated proteins to achieve this role.

1.2.1.1.4 CDKL kinase family

The unicellular Choanoflagellate, the closest ancestor of multicellular animals (metazoans), expresses two genes of the CDKL family, which has five members in mammals (King et al., 2008). One is closely related to mammalian *CDKL1-4* and the other is orthologous to *CDKL5*. CDKL1-4 are similar each other but distantly related to CDKL5 (**Figures 1.7** and **2.1A**). Among CDKL family members, CDKL5 has been implicated in ciliary length control in *Chlamydomonas*. Long Flagella 5 (LF5) and FLagellar Shortening 1 (FLS1), *Chlamydomonas* orthologs of CDKL5, localize to the base of the cilia. While LF5 negatively regulates ciliary length, FLS1 functions in cilium shortening during ciliary resorption by regulating the phosphorylation of a microtubule depolymerizing kinesin (CrKinesin13) and a *Chlamydomonas* Aurora/Ipl1p-Like protein Kinase (CALK) which is implicated ciliary disassembly (Hu et al., 2015a; Tam et al., 2013).

Other CDKL members (CDKL1-4) are more poorly studied, but are suggested to have roles in cell proliferation, development, learning, and cancer progression (Bonifaci et al., 2010; Dubos et al., 2008; Gomi et al., 2010; Jaluria et al., 2007; Li et al., 2014; Lin et al., 2015b; Song et al., 2015; Sun et al., 2012; Tang et al., 2012). Although disruption of zebrafish *cdkl1* leads to dysregulated sonic hedgehog signaling and several developmental defects which are reminiscent of cilia function anomalies (Hsu et al., 2011), there is no clear experimental evidence that it has ciliary function(s). *Drosophila* and *C. elegans* lack a CDKL5 ortholog but encode a single protein related to CDKL1-4. This suggests that the CDKL1-4-related protein may be necessary and sufficient to fulfill the core functions of CDKL family in these invertebrates, and that other CDKL family members may have shared but specialized cellular or tissue-specific functions in vertebrates/mammals. Based on the above, we hypothesized that similar to CDKL5, CDKL 1-4 family members also potentially paly roles in cilia, and more specifically, in cilium length regulation. This possibility is discussed in more detail in section **2**.

1.2.1.2 NIMA-related kinases

1.2.1.2.1 *Tetrahymena* NIMA-related kinase (Nrk) family

Tetrahymena Nrk1p, Nrk2p, Nrk17p, and Nrk30p localize to cilia, and when overproduced, cells shorten their cilia; this indicates that the four Nrks negatively regulates ciliary length (Wloga et al., 2006). Consistent with this, cells overexpressing of a kinase-inactive Nrk2p have elongated cilia. Overproduction of Nrk2p, Nrkp30p, and Nrk17p results in rapid cilia shortening, but these kinases utilize different mechanisms. IFT is upregulated in shortening cilia mediated by Nrk2p, which promotes rapid removal of depolymerized microtubules. On the other hand, resorption is not associated with upregulation of IFT in cells overexpressing Nrk30p. Resorbing cilia caused by excessive Nrk30p have bulges and are filled with scattered materials, indicating removals of ciliary membrane and the breakdown products are not synchronized with the depolymerization of axonemal microtubules. Differing from Nrk2p and Nrk30p, Nrk17p appears more specific for the removal of the central pair microtubules at the proximal end, and it later prompts depolymerization of the rest of axonemal microtubules.

1.2.1.2.2 *Chlamydomonas* NIMA-related kinases

Chlamydomonas encodes 12 NIMA-related kinases, including four, Cnk2p, Cnk4p, Cnk11p and Fa2p, which are implicated in ciliary functions such as assembly, disassembly and length regulation (Parker et al., 2007). Cnk2p is an axonemal protein and its level affects the length of cilia by altering the disassembly rate. Excessive Cnk2p results in short cilia because of a high disassembly rate. Conversely, *cnk2* mutant cells show a slow disassembly rate and have long cilia (Bradley and Quarmby, 2005; Hilton et al., 2013). Another ciliary protein, Cnk4p, also influences ciliary length. Interestingly, *cnk4* null mutant cells show a long flagellar (*lf*) phenotype with bulge structures containing IFT proteins. The *cnk4* mutant cilia contains an excess of IFT proteins, which may result in ciliary elongation. In the absence of Cnk4p, IFT velocity is unchanged, but IFT frequency is reduced, indicating that CNK4 may control the IFT entry into the ciliary compartment (Meng and Pan, 2016). Cnk11p regulates the tubulin turnover at the ciliary tip, and its disruption partially rescues the short ciliary phenotype in mutants with structural defects (Lin et al., 2015a). Lastly, Fa2p, related to *Chlamydomonas* Cnk4p and *Tetrahymena* Nrk17p, not only regulates axonemal microtubule severing at the

proximal end of cilia during deflagellation, but also possibly ciliary regeneration (Mahjoub et al., 2002; Mahjoub et al., 2004; Wloga et al., 2006). Fa2p requires its kinase activity for the microtubule severing.

1.2.1.2.3 Mammalian NIMA-related kinases

Mutations in mammalian *Nek1* are associated with ciliopathies, such as short-rib polydactyly syndrome and polycystic kidney disease. NEK1 localizes to the basal body and has ciliary functions, such as ciliogenesis and cilium length regulation. Both mouse and human fibroblast cells lacking functional NEK1 display reduced ciliation. In addition to the ciliogenesis defects, human patient cells have abnormally short cilia, whereas long and branched cilia are observed in the *Nek1* mutant mouse fibroblasts, indicating that NEK1 is involved in the ciliary length regulation. The different cilium length phenotypes potentially result from different mutations in NEK1 (Shalom et al., 2008; Thiel et al., 2011; Wang et al., 2014).

Similar to NEK1, NEK8 mutations are associated with polycystic kidney disease in zebrafish, mice and humans (Smith et al., 2006; Sohara et al., 2008; Zalli et al., 2012). Nek8 localizes to the proximal region of primary cilia from mouse kidney tissues, and regulates cilium length. *jck* (juvenile cystic kidneys) mice has a NEK8 missense mutation which results in not only increased expression, but also mislocalization of NEK8 (Mahjoub et al., 2005). *Nek8* mutant mice exhibit abnormally long renal primary cilia.

NEK2 is implicated in cilium disassembly (Kim et al., 2015; Spalluto et al., 2012). Depletion of *Nek2* by RNAi results delayed cilium disassembly, whereas overexpression of *Nek2A* reduces ciliation and the length of cilia in RPE-1 cells. NEK2 activates a depolymerizing kinesin, KIF24, by direct phosphorylation to regulate cilium disassembly from the basal body. NEK2-KIF24-mediated cilium disassembly is distinct from the Aurora A-HDAC6 pathway which is discussed in more detail below (section **1.2.1.3**).

NEK4 mostly localizes at the basal body and the ciliary rootlet in various ciliated rat tissues, and is also present at the connecting cilium (transition zone) in rat retina (Coene et al., 2011). NEK4 knockdown reduces cilium assembly in RPE-1 cells.

Lastly, *NEK9* mutations in humans result in skeletal dysplasias, and patient fibroblasts lacking full-length NEK9 show reduction in cilia number as well as length, indicating that NEK9 plays roles in regulating cilium assembly and length (Casey et al., 2016).

1.2.1.3 Aurora kinases

Aurora kinases are implicated in cilium disassembly. In *Chlamydomonas*, aurora protein kinase (CALK) is essential for ciliary degeneration, and thus depletion of CALK inhibits ciliary resorption (Pan et al., 2004). The status of phosphorylation at the T193 residue of the activation loop and the C-terminus of CALK are altered during ciliary assembly and disassembly. When cilia regenerate after detachment, the level of CALK phosphorylated on T193 (T193 CALK) gradually increases concomitant with cilium length increases. However, the C-terminus is dephosphorylated after cilia reach half-length. When cilia shortening is initiated, the amount of T193 CALK greatly increases, and the CALK C-terminus become phosphorylated (Cao et al., 2013; Pan and Snell, 2005). Interestingly, FLS1, a *Chlamydomonas* ortholog of mammalian CDKL5, regulates CALK phosphorylation and enrichment of the T193 form upon initiation of disassembly (Hu et al., 2015a). The level of T193 CALK continuously reduces, but C-terminally phosphorylated CALK remains unchanged until completion of ciliary resorption. The regulation of the amount of T193 CALK is perturbed in the long flagellar mutant, *lf4,* during ciliary assembly and disassembly.

In human RPE-1 cells, Aurora A (AurA) localizes to the basal body and plays a role in cilium disassembly (Pugacheva et al., 2007). AurA activates the microtubule deacetylase HDAC6 by phosphorylation, and the activated HDAC6 induces destabilization of the ciliary axoneme, which promotes cilium resorption. When either AurA or HDAC6 is depleted by RNAi, cilium disassembly is greatly reduced.

1.2.2 Depolymerizing kinesins

Among 14 kinesin families, kinesin-8, kinesin-13, and kinesin-14A have microtubule-depolymerizing activities and consequently, regulate microtubule dynamics (Walczak et al., 2013). In particularly, kinesin-8 and kinesin-13 are implicated in ciliary assembly, disassembly, and length regulation in various organisms (Kim et al., 2015; Kobayashi et al., 2011; Miyamoto et al., 2015; Niwa et al., 2012).

1.2.2.1 Kinesin-8 family

Kinesin-8 family members use their ATP-driven motor to walk toward and depolymerize microtubules at the plus end of microtubules. For example, *S. cerevisiae* kinesin-8, Kip3p, regulates microtubule length by removing tubulins from the microtubules (Gupta et al., 2006; Varga et al., 2006). Mammalian kinesin-8 family have four members (KIF18A, KIF18B, KIF19A, and KIF19B), and one of which, KIF19A, has been implicated in cilium length regulation (Miki et al., 2005; Niwa et al., 2012). KIF19A localizes at and depolymerizes the distal end (microtubule plus end) of the axoneme of mouse motile cilia. KIF19A is a negative regulator of cilium length. KIF19A knockout female mice have elongated motile cilia in oviducts which fail to create a proper fluid flow, and as a result are infertile.

1.2.2.2 Kinesin-13 family

Unlike the kinesin-8 family, kinesin-13 family proteins diffuse toward the both the plus and minus ends of microtubule and remove tubulin subunits from microtubules (Desai et al., 1998; Hu et al., 2015b; Walczak et al., 2013). They play roles in cilium length regulation by controlling ciliary assembly and disassembly in different organisms. For example, in *Leishmania* and *Tetrahymena*, kinesin-13 proteins depolymerize the distal end of the axoneme, and thus their overexpression results in short cilia (Blaineau et al., 2007; Vasudevan et al., 2015). Moreover, when the GiKinesin-13 variant, carrying a mutation which disrupts its microtubule depolymerizing activity, is overexpressed, cilia elongate in *Giardia* (Dawson et al., 2007). *Chlamydomonas* kinesin-13 (CrKinesin-13) is associated with both ciliary assembly and disassembly (Piao et al., 2009; Wang et al.,

2013). CrKinesin-13 localizes to the basal body of cilia in steady-state cells. However, it is transported to the ciliary axoneme in an IFT-dependent manner and disassembles microtubules during ciliary resorption. When cilia regenerate after amputation, CrKinesin-13 is deactivated by phosphorylation and targets to the cytoplasmic microtubules. After its activity is restored, potentially by dephosphorylation, CrKinesin-13 depolymerizes the cytoplasmic microtubules to provide tubulin precursors for ciliary regeneration. Indeed, in CrKinesin-13-depleted cells, cilia are short, and their assembly rate is reduced. Similarly, loss of *Tetrahymena* kinesin-13 causes reduction of both the cilium length and assembly rate, but the kinesin-13 is not involved in production of tubulins required for cilium assembly. Rather, the kinesin-13 may also have a nonconventional function (*e.g.*, promoting cilium assembly) in *Tetrahymena* (Vasudevan et al., 2015).

In humans, there are four kinesin-13 family members, namely KIF2A, KIF2B, KIF2C and KIF24. Two of these, KIF24 and KIF2A, are implicated in cilium assembly and disassembly. During cilium resorption, KIF24 prevents cilium formation at the basal body via its microtubule depolymerizing activity, which is stimulated by NEK2-mediated phosphorylation (Kim et al., 2015; Kobayashi et al., 2011). KIF24 also controls cilium formation through recruitment of its interaction partner, CP110, to the mother centriole (basal body). CP110 is important for ciliogenesis; its overexpression suppresses cilium formation in quiescent cells, whereas its depletion result in formation of aberrant cilia in cells that are unable to form cilia (Kobayashi et al., 2011). In the absence of KIF24, CP110 is no longer present at the mother centriole, and this induces inappropriate ciliogenesis in cycling cells. Similar to KIF24, KIF2A localizes to the base of cilia. However, it plays a role in cilium disassembly, not in ciliogenesis, through its depolymerizing activity. This activity is enhanced by Polo-like kinase 1 (PLK1)-mediated phosphorylation (Miyamoto et al., 2015).

1.3 Functions of cilia in *C. elegans* sensory reception and development

Primary cilia, enriched with receptors and signaling molecules, function as cellular antenna; they receive extracellular (and potentially intracellular) cues and mediate cellular signaling pathways that influence sensory functions and development. The *C. elegans* hermaphrodite has 302 neurons, of which ~ 20 % (60) are ciliated and play a role in chemosensation, mechanosensation and thermosensation. For example, *C. elegans* senses and responds to changes in osmotic strength and increased levels of carbon dioxide (CO_2) through different sensory neurons and specialized cilia. Furthermore, sensory cilia-mediated signaling pathway also influences a major alternate developmental switch—namely formation of stress-resistant dauer larva—and also regulates the body size of worms.

1.3.1 Osmotic avoidance

Worms are repelled by high concentrations of sugar, which have a high osmotic strength (Culotti and Russell, 1978). However, mutations in cilium-associated genes, such as *osm-3* and *osm-6*, show abnormal osmotic avoidance behavior. Both OSM-3 and OSM-6 are IFT proteins, and cilia are severely shortened in *osm-3* and *osm-6* mutants (Perkins et al., 1986). This suggests that cilia are required for the detection of the high osmotic strength. In particular, the ciliated ASH neuron is important for the high osmolarity perception and avoidance behavior (Srinivasan et al., 2008).

1.3.2 Carbon dioxide (CO_2) avoidance

C. elegans displays an acute avoidance response to high concentrations of CO_2, which can cause anesthesia or death due to hypoxia (Hallem and Sternberg, 2008). This avoidance behavior is a chemosensory response which depends on several ciliated amphid neurons, including BAG, AFD, and ASE; together, they are involved in CO_2 detection and activation of a neural circuit which mediates the rapid avoidance response (Bretscher et al., 2011; Hallem et al., 2011; Hallem and Sternberg, 2008). BAG neurons

in particular play a major role in acute CO_2 avoidance via cilium-mediated cGMP signaling; this pathway involves the receptor-type guanylate cyclase (GCY-9) and the cGMP-gated channel (TAX-2/TAX-4) (Hallem and Sternberg, 2008; Martinez-Velazquez and Ringstad, 2018). *tax-2* and *tax-4* are also expressed in other amphid neurons and their proteins localize to the cilia. Furthermore, the receptor guanylyl cyclase *daf-11*, which is expressed in some of the amphid ciliated neurons but not in BAG neurons, is required for the CO_2 avoidance response. Therefore, DAF-11, TAX-2, and TAX-4 may work together in other amphid neurons to mediate acute CO_2 avoidance.

1.3.3 Body size regulation

In *C. elegans*, several signaling pathways are involved in the regulation of body size. The TGF-β DBL-1 pathway, which is activated by the ligand DBL-1, is a key regulator of body size (Brenner, 1974; Savage-Dunn, 2005). When DBL-1 binds to SMA-6/DAF-4 receptors, DAF-4 activates SMA-6 by phosphorylation. Thereafter, receptor-regulated signal transducers (R-Smads) are phosphorylated by the activated SMA-6, and form a heterotrimer complex with common mediator Smad (co-Smad) in the cytoplasm. This complex translocates to the nucleus to regulate gene transcription. *dbl-1* is expressed in neurons and is a dose-dependent regulator for body-size. While *dbl-1* overexpression causes a long-body phenotype, loss-of-function mutations in *dbl-1* leads to a marked reduction in length and volume. The size of L1 larvae of *dbl-1* mutants are similar to that of wild-type, but then postembryonic growth is reduced. In *dbl-1* mutant adults, cell size is reduced, but not the number of cells.

In addition to acting in chemosensory pathways (*e.g.*, CO_2 sensing, as discussed above), the cGMP signaling pathway also participates in body size control. The cGMP-dependent protein kinase *egl-4*, which is expressed in neurons—including some of ciliated sensory neurons—acts downstream of ciliated-mediated signaling and upstream of the TGF-β DBL-1 pathway (Fujiwara et al., 2002). Loss-of-function mutations in *egl-4* results in a long body size, and supresses the small body size phenotype of *che-2* mutant, which is unable to receive and process sensory input due to defects in cilia (CHE-2 is an IFT-B component). Furthermore, the *dbl-1* mutant, which displays small body size, fully suppresses the *egl-4* body size phenotype. GCY-12, a receptor-type

guanylyl cyclase (generates cGMP), and PDE-2, a cyclic nucleotide phosphodiesterase (breaks down cGMP), work together to regulate cGMP levels, and thus modulate function of the cGMP-binding EGL-4 in body size regulation (Fujiwara et al., 2015). In addition, mutations in other ciliary gene (*che-3*, *osm-6*, *tax-2* and *tax-4*), which are important for cilium formation and function, are implicated in body size regulation. *che-3* and *osm-6* mutants have defective cilia, which potentially lead to defects in signaling pathway(s) including cGMP signaling. TAX-2 and TAX-4, the cGMP-gated channel subunits, localize to cilia and are essential for cGMP signaling pathway-dependent neuronal activation.

In parallel with TGF-β DBL-1 signaling pathway, insulin signaling, TOR kinase, Hippo-Warts pathway, MAPK signaling and signal from the gonad also have an influence on worm body size, but play relatively minor roles (Cai et al., 2009; Clark et al., 2018; Jones et al., 2009; McCulloch and Gems, 2003; Watanabe et al., 2007). Disruption of an insulin receptor DAF-2 results in large body size, whereas mutations in *sma-5* (*C. elegans* ortholog of a *MAP* kinase), *wts-1*(Hippo-Warts pathway component *warts*), and *lpo-6* (TORC2-specific component *Rictor*) lead to a small body size. They all show synergetic effects with mutants of dbl-1 pathway components. Moreover, removal of the gonad from *dbl-1* mutant animals causes an increase in body size, suggesting that signal(s) from this reproductive tissue is involved in regulating body size and is DBL-1-independent.

1.4 Research aims

Loss of LF5, a *Chlamydomonas* homolog of human CDKL5, results in cilium elongation and its related protein, FLS1, is implicated in cilium disassembly (Hu et al., 2015a; Tam et al., 2013). CDKL family consists of five members (CDKL1-5) in humans and phylogenetically most closely related to other protein kinases linked to cilium length regulation, in a distinct branch of the CMGC group of kinases. In this kinase branch, ICK and MAK affect the functions of the IFT machinery in mammals and *C. elegans*, and *Chlamydomonas* CDKL5 regulates the phosphorylation of a depolymerizing kinesin to perform their ciliary functions (Chaya et al., 2014; Hu et al., 2015a; Omori et al., 2010). However, whether CDKL1/CDKL2/CDKL3/CDKL4 are also have ciliary functions remains uncertain, although zebrafish *zcdkl1* knockdown experiments suggest ciliary defect-like phenotypes, such as brain malformation and reduced sonic hedgehog signal ((Hsu et al., 2011); cilia were not examined, however).

Based on the limited evidence, we initially hypothesized that the CDKL protein family as a whole may carry out ciliary functions, and perhaps more specifically, play roles in cilium length control. As *C. elegans* has a single CDKL family protein (CDKL-1), which is closely related to CDKL human CDKL1-4, and more distantly related to CDKL5, we set out to study *C. elegans* CDKL-1 to explore whether it performs an evolutionarily conserved function in cilia and potentially, cilium length regulation. After obtaining evidence that CDKL-1 does indeed modulate cilium length in *C. elegans*, we further hypothesized that this kinase may perform this activity by regulating the functions of the IFT system and/or depolymerizing kinesins. Furthermore, we sought to understand how CDKL-1 cooperates with other protein kinases to perform its functions, and the impact of disrupting CDKL-1 on the nematode's sensory and developmental systems.

2 CDKL-1, localized to the transition zone, regulates ciliary length

This chapter is a modified version of two papers published in *PLOS Biology* (Li et al., 2016) and *Cell Reports* (Canning et al., 2018). The authors and their affiliation are listed below:

PLOS Biology

Chunmei Li[1], Victor L. Jensen[1,§], Kwangjin Park[1,§], Julie Kennedy[2], Francesc R. Garcia-Gonzalo[3,¤a], Marta Romani[4], Roberta De Mori[4], Ange-Line Bruel[5], Dominique Gaillard[6], Bérénice Doray[7], Estelle Lopez[5], Jean-Baptiste Rivière[5,8], Laurence Faivre[5,9], Christel Thauvin-Robinet[5,9], Jeremy F. Reiter[3], Oliver E. Blacque[2], Enza Maria Valente[4,10], Michel R. Leroux[1*]

[1]Department of Molecular Biology and Biochemistry and Centre for Cell Biology, Development and Disease, Simon Fraser University, Burnaby, British Columbia, Canada

[2]School of Biomolecular & BiomedicalScience, University College Dublin, Belfield, Dublin 4, Ireland

[3]Department of Biochemistry and Biophysics, Cardiovascular Research Institute, University of California, San Francisco, San Francisco, California, United States of America

[4]Neurogenetics Unit, Mendel Laboratory, IRCCS Casa Sollievo dellaSofferenza, San Giovanni Rotondo, Italy

[5]EA4271 GAD Génétique des Anomalies du Développement, FHU-TRANSLAD, Université Fédérale Bourgogne Franche-Comté, Dijon, France

[6]Service de Génétique clinique, CHU Reims, Reims, France

[7]Service de Génétique clinique, CHRU Strasbourg, Strasbourg, France

[8]Laboratoire de Génétique moléculaire, Plateau Technique de Biologie, CHU Dijon, Dijon, France

[9]Centre de Génétique, FHU-TRANSLAD, Hôpital d'Enfants, CHU Dijon, Dijon, France

[10]Department of Medicine and Surgery, University of Salerno, Salerno, Italy

[¤a]Current address: Departamento de Bioquímica, Facultad de Medicina, and Instituto de Investigaciones Biomédicas "Alberto Sols" UAM-CSIC, Universidad Autónoma de Madrid, Madrid, Spain

[§]These authors equally contributed

*corresponding author

As a co-second author of the manuscript, I designed and performed experiments, analyzed data, and contributed to writing the accepted manuscript. Chunmei Li designed and performed most experiments, interpreted data, and created figures of the manuscript. Dr. Victor L. Jensen also performed experiments and data analysis, made figures and contributed to the writing of the manuscript. Julie Kennedy performed the transmission electron microscopy analysis in the manuscript. Dr. Christel Thauvin-Robinet conceived and designed the experiments. Dr. Francesc R. Garcia-Gonzalo conceived, designed, and performed the experiments of the manuscript. Dr. Marta Romani, Dr. Roberta De Mori, Dr. Ange-Line Bruel, Dr. Dominique Gaillard, Dr. Bérénice Doray, Dr. Estelle Lopez, Dr. Jean-Baptiste Rivière, and Dr. Laurence Faivre performed the experiments of the manuscript. Drs. Jeremy F. Reiter, Oliver E. Blacque, Enza Maria and Valente contributed to the conception, interpretation, and writing of the manuscript. Dr. Michel Leroux supervised the research and wrote the manuscript.

Cell Reports

Peter Canning[1,6,§], Kwangjin Park[2,§], João Gonçalves[3,4], Chunmei Li[2], Conor J. Howard[5], Timothy D. Sharpe[1,7], Liam J. Holt[5,8], Laurence Pelletier[3,4], Alex N. Bullock[1,*], and Michel R. Leroux[2,*]

[1]Structural Genomics Consortium, University of Oxford, Old Road Campus, Roosevelt Drive, Oxford OX3 7DQ, UK

[2]Department of Molecular Biology and Biochemistry, and Centre for Cell Biology, Development, and Disease, Simon Fraser University,8888 University Drive, Burnaby, BC V5A 1S6, Canada

[3]Lunenfeld-Tanenbaum Research Institute, Mount Sinai Hospital, 600 University Avenue, Toronto, ON M5G 1X5, Canada

[4]Department of Molecular Genetics, University of Toronto, Toronto, ON M5S 1A8, Canada

[5]Department of Molecular & Cell Biology, University of California, Berkeley, Berkeley, CA 94720, USA

[6]Present address: LifeArc, SBC Open Innovation Campus, Stevenage SG1 2FX, UK

[7]Present address: Biophysics Facility, Biozentrum, University of Basel, 4056 Basel, Switzerland

[8]Present address: Institute for Systems Genetics, New York University, New York, NY 10016, USA

[§]co-first author

*co-corresponding author

I'm the co-first author of this manuscript. I designed the research, performed the experiments and data analysis in *C. elegans*, generated figures, and wrote the manuscript. Chunmei Li made **Figures 2.1C** and **2.2B-C**. Dr. Peter Canning designed the research, solved crystal structures of CDKL proteins with Dr. Timothy D. Sharpe, prepared figures and wrote the manuscript. Under the supervision of Dr. Liam J. Holt, Conor J. Howard performed *in vitro* kinase assay shown in **Figure 2.4D,** and both wrote the manuscript. Dr. João Gonçalves, who is under the supervision of Dr. Laurence Pelletier, collected and interpreted data shown in **Figures 2.5A and B,** and wrote the manuscript. Dr. Alex N. Bullock and Dr. Michel Leroux supervised the project and wrote the manuscript.

2.1 Introduction

Several members from a specific branch of CMGC kinases (**Figure 1.7**) regulate cilium length, namely ICK, MAK, MOK, GSK3β, and CDK-Like 5 (CDKL5). Human CDKL5 belongs to a family of CDKL kinases encompassing CDKL1, CDKL2, CDKL3, and CDKL4. However, aside from CDKL5, little is known about CDKL protein function, and no CDKL family member has been structurally characterized. CDKL proteins share a high degree of sequence similarity with CDKs and contain the MAPK TXY phosphorylation motif needed for activity (Yee et al., 2003). They also have putative cyclin-binding domains, but there is no evidence of interaction with cyclins. Here we present the crystal structures of CDKL proteins, including that of the Rett syndrome- and epileptic encephalopathy-associated CDKL5, and reveal an unusual αJ helix important for CDKL2 and CDKL3 function. Furthermore, we study the sole *C. elegans* CDKL protein (CDKL-1) which is closely related to human CDKL1-4 to provide insights into the function of the CDKL family. We show that CDKL-1 localizes to the ciliary TZ, but does not regulate the ciliary 'gate' or diffusion barrier function that most known TZ proteins are involved in. Instead, CDKL-1 regulates cilium length, in a kinase activity- and αJ helix C-terminal region-dependent manner. We present evidence that human CDKL5 is a ciliary protein with a potential role in ciliogenesis, and *C. elegans* CDKL-1 variants modeling CDKL5 human patient mutations exhibit cilium length defects, with or without loss of TZ localization. Our study reveals that CDKL proteins may share a common function in cilium length control, and show that CDKL5-associated Rett syndrome may stem, at least in part, from ciliary dysfunction.

2.2 Methods

2.2.1 Transcriptional and translational constructs

1.8 kb promoter of *cdkl-1A* amplified from the genomic DNA was fused to GFP to create the transcriptional construct. For the various *cdkl-1A* (Y42A5A.4A) translational fusions, all introns and exons of *cdkl-1A* with its 5' UTR were fused to GFP or tdTomato with the *unc-54* 3' UTR or *cdkl-1* 3' UTR without any fluorescent protein tags. The mutations found in CDKL5 human patients (G20R, P180L, and L220P) or kinase-dead (CDKL5 K42R) mutation were introduced into the *cdkl-1* gene by replacing the corresponding residues, and they were fused to tdTomato to assess localization.

Plasmids encoding tdTomato-tagged or untagged CDKL-1A variants harboring CDKL5 mutations, and those encoding CDKL-1A(ΔαJ) (residues 1–286) with/without mNeonGreen, were prepared with the CloneJET PCR Cloning kit.

2.2.2 *C. elegans* mutant and transgenic strains

mks-5 (*tm3100*), *cep-290* (*gk415029*), *nphp-1* (*ok500*), *nphp-4* (*tm925*), *tmem-231* (*tm5963*) and *cdkl-1*(*tm4182*) mutant strains were obtained from the *C. elegans* Gene Knockout Consortium or National BioResource Project. *cdkl-1* kinase-dead (*nx131*, p. K33R) and *cdkl-1* null (*nx132*, c. 85-89 deletion) mutants were generated with the CRISPR/CAS9 system (Friedland et al., 2013; Kim et al., 2014). The *cdkl-1* CRISPR guide RNA sequence (5'-AGGGATACTGGACAAATTG-3') was predicted by the CRISPR Design Tool (http://crispr.mit.edu/) and was substituted for *unc-119* sequence in pU6::*unc-119* small-guide RNA (sgRNA) vector (Addgene #46169) by site-directed mutagenesis using overlap extension PCR (Zoller, 1991). The *nx131* allele was made by CRISPR-mediated homologous recombination. 2Kb homologous donor DNA template of *cdkl-1A* harboring two mutations, V30V (silent mutation in PAM site) and K33R (kinase-dead), was amplified by stitch-PCR (Reikofski and Tao, 1992) and cloned into a pJET1.2 vector. 50ng/µl each of *cdkl-1* sgRNA vector, Cas9 plasmid (Addgene #46168), and pRF4::*rol-6* (*su1006*) with or without the *cdkl-1* donor plasmid were mixed and injected into 20 young adult worms. F1 heterozygous (roller) and F2 homozygous (non-roller) worms of either the *nx131* or the *nx132* mutant were identified by tetra-primer ARMS-PCR (Ye et al., 2001) and confirmed by DNA sequencing.

Transgenic animals carrying separate extrachromosomal DNA arrays with different mutant backgrounds were created by worm microinjection and classical genetic methods. The extrachromosomal array [*Psrh220::ift-20::gfp*; *cc::gfp*] was integrated into the chromosome with 1.5 krads of X-ray irradiation for 135 seconds at 145kilovolts/5milliamps (TORREX150D X-Ray Inspection System) for ADL ciliary length measurement and analysis (McKay et al., 2003). The X-ray integrated strains were outcrossed with wild-type six times to remove X-ray-induced mutations. All strains were grown and maintained at 20°C. All nematode strains used in this chapter are described in **Appendix A.**

2.2.3 ADL ciliary length measurement and statistical analysis

After mounting on a 5% agar pad, worms were immobilized with 1 µl of 10mM levamisole and 0.1 micron polystyrene microspheres mixture for microscopy. Microscopy images were obtained using either epifluorescence or spinning disc confocal microscope (WaveFX spinning disc confocal system, Quorum Technologies) and were analysed with Volocity 6.3 software (PerkinElmer). ADL cilia lengths (from the TZ to the tip) of L4 larvae were measured and plotted using Dot and Boxplots in R software. The distribution of each dataset was determined by the Shapiro-Wilk test. The statistical significance (*p*-value) was calculated by using the Dunn's Kruskal-Wallis Multiple Comparisons test with the Holm-Sidak adjustment.

2.2.4 Phylogenetic analysis

The phylogram showing human and *C. elegans* CDKL protein evolutionary relationships was generated using PHYML (bootstrap 1,000) at http://www.atgc-montpellier.fr/phyml and www.phylogeny.fr (Altschul et al., 1997; Chevenet et al., 2006; Dereeper et al., 2010; Dereeper et al., 2008; Edgar, 2004; Guindon et al., 2010). Branch support values (%) are displayed. Protein sequences: *Hs* CDKL1 (Uniprot Q00532), *Hs* CDKL2 (Q92772), *Hs* CDKL3 (Q8IVW4), *Hs* CDKL4 (Q5MAI5), *Hs* CDKL5 (O76039) and *Ce* CDKL-1 (Q9U2H1)

2.2.5 Cloning of human CDKL kinase domains

Bacmids were prepared in *E. coli* strain DH10Bac and used to generate baculoviruses in Sf9 insect cells. For activity assays, wild-type sequences (residues corresponding to CDKL1, 1-357; CDKL1(ΔαJ), 1 -287; CDKL2, 1-312; CDKL2(ΔαJ), 1-287; CDKL3, 1-313; CDKL3(ΔαJ), 1-286; CDKL5, 1-831; CDKL5(ΔαJ), 1-299) were cloned into a 2 µm P_{GAL1}-kinase-TAP plasmid (pRSAB1234 backbone, originally a gift from Erin O'Shea) for expression in *S. cerevisiae*. Purification and structure determination of CDKL kinase domains, and *in vitro* kinase assays were conducted as described (Canning et al., 2018).

2.2.6 Dye-filling assay

C. elegans L4 larvae were exposed to the lipophilic dye, DiI (Invitrogen; 1:1,000-fold dilution of 1 mM stock in M9 buffer), to assay for uptake of dye through intact, environmentally exposed ciliary structures (Williams et al., 2011). Stained worms were imaged with fluorescence microscopy, and intensities were analyzed with ImageJ.

2.2.7 Human CDKL5 constructs

A Gateway entry clone with the coding sequence of human CDKL5(NM_003159.2) was obtained from the LTRI plasmid repository, and it was used to clone CDKL5 fused to GFP in the pcDNA5-FRT/TO-GFP vector. The GFP-CDKL5 fusion was subsequently subcloned into the lentiviral vector pHR-SIN-SFFV to generate the pHR-SIN-SFFV-GFP-CDKL5 plasmid. More details of generation of the hTERT RPE-1 GFP-CDKL5 stable cell line and mammalian RNAi analysis in (Canning et al., 2018).

2.3 Results

2.3.1 CDKL-1 assembly at the TZ requires central proteins, MKS-5 and CEP-290

To investigate the collective function of CDKL proteins, we chose to study the sole member encoded by *C. elegans*, CDKL-1. This kinase is most closely related to mammalian CDKL1/CDKL2/CDKL3/CDKL4 and more distantly related to CDKL5 (**Figure 2.1A**). Among three isoforms (A-C) of *C. elegans cdkl-1*, we investigated the isoform A, as it is specifically expressed in ciliated sensory neurons (**Figure 2.1B**), likely due to the presence of an X-box motif found in the promoters of most ciliary genes (Blacque et al., 2005). We found that the CDKL-1A protein localized to ciliary TZs in head (amphid) and tail (phasmid) neurons (**Figure 2.1C**).

In *C. elegans*, most known TZ proteins, except for MKS-5, fit genetically within the MKS or NPHP module. MKS-5 is the core TZ assembly factor, which shows interaction with both modules. Moreover, CEP-290 is the central organizing protein for the MKS module and is dependent on MKS-5 for TZ localization (Li et al., 2016). We

further investigated if *cdkl-1* is associated with either MKS or NPHP module using genetic interaction and dye-filling studies. CDKL-1A still localized to TZ when core MKS (MKS-2) or NPHP (NPHP-4) module proteins were removed (**Figure 2.1D**). While synthetic dye-filling defect between MKS and NPHP module mutants was observed due to severe disruption of ciliary structures (Li et al., 2016; Williams et al., 2011), combining the *cdkl-1* mutant with either the *mks-2* mutant or the *nphp-1* mutant does not cause a synthetic dye-filling defect (**Figure 2.1E**). Hence, CDKL-1 cannot be assigned to either the MKS or NPHP module. However, CDKL-1 not only requires MKS-5 for its TZ localization but also depends on CEP-290, suggesting CDKL-1 is CEP-290-associated protein (**Figures 2.1D and E**).

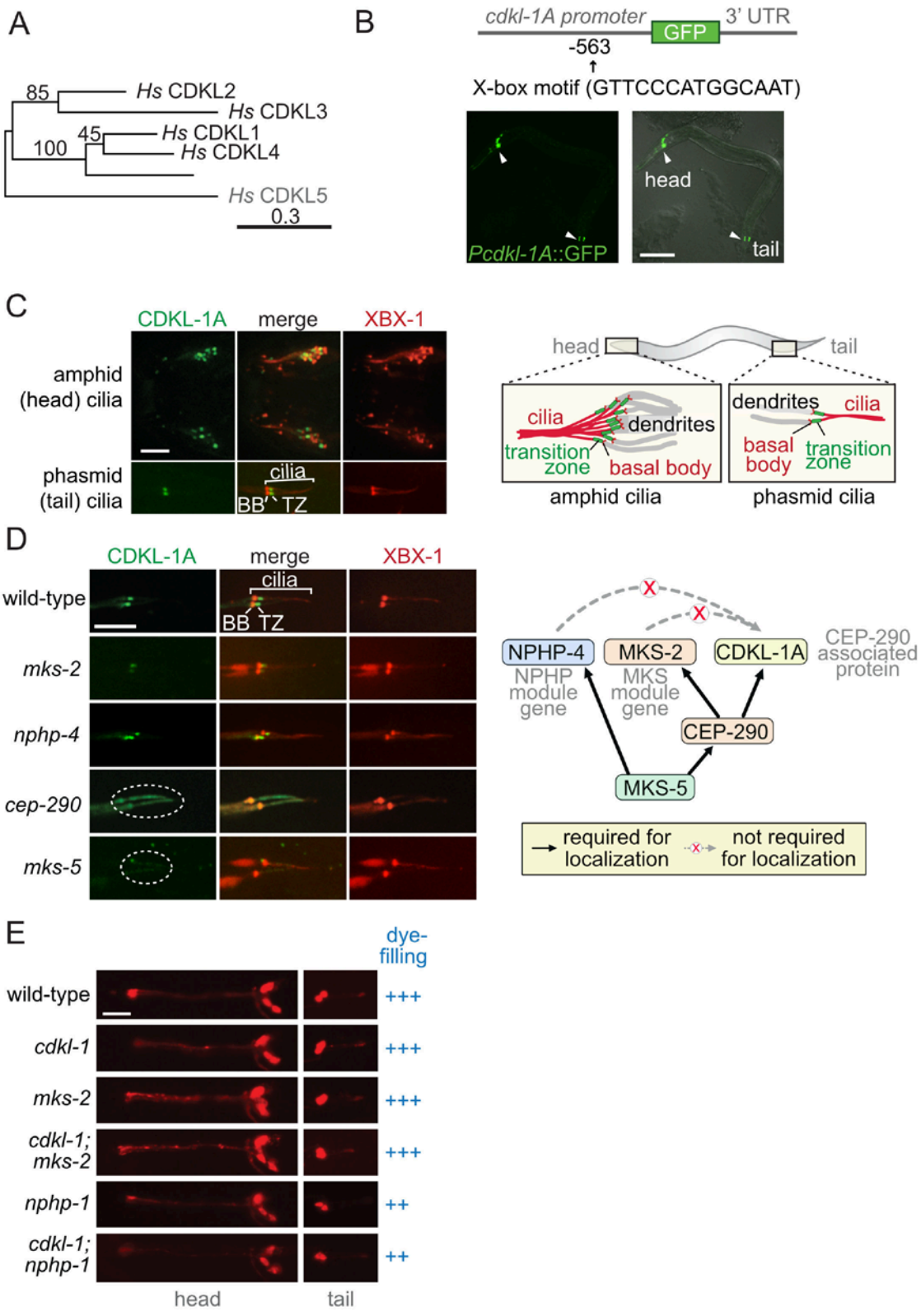
A
85
Hs CDKL2
Hs CDKL3
45
Hs CDKL1
100
Hs CDKL4
Hs CDKL5
0.3
B
cdkl-1A promoter
GFP
3' UTR
-563
X-box motif (GTTCCCATGGCAAT)
Pcdkl-1A::GFP
head
tail
C
CDKL-1A
merge
XBX-1
amphid (head) cilia
phasmid (tail) cilia
cilia
BB
TZ
head
tail
cilia
dendrites
transition zone
basal body
dendrites
cilia
basal body
transition zone
amphid cilia
phasmid cilia
D
CDKL-1A
merge
XBX-1
wild-type
mks-2
nphp-4
cep-290
mks-5
cilia
BB
TZ
X
X
NPHP-4
NPHP module gene
MKS-2
MKS module gene
CDKL-1A
CEP-290 associated protein
CEP-290
MKS-5
required for localization
not required for localization
E
dye-filling
wild-type
cdkl-1
mks-2
cdkl-1; mks-2
nphp-1
cdkl-1; nphp-1
+++
+++
+++
+++
++
++
head
tail

Figure 2.1 CDKL-1A requires MKS-5 and CEP-290 for their transition zone localization and is functionally independent of the MKS or NPHP module.

(A) Phylogenetic relationship between *H. Sapiens* (*Hs*) and *C. elegans* (*Ce*) CDKL proteins. **(B)** The *C. elegans cdkl-1A* promoter-GFP transcriptional fusion shown in the schematic (and containing a ciliogenic X-box regulatory motif) is specifically expressed in head and tail ciliated sensory neurons (arrow head), as shown in the fluorescent and DIC overlay images. Scale bar, 100 µm. **(C)** GFP-tagged CDKL-1A specifically localizes at the transition zone (TZ) in head and tail cilia; the tdTomato-XBX-1 IFT protein serves to mark the basal body (BB) and axonemes in head (amphid) and tail (phasmid) sensory neuron cilia (see schematic). Scale bar, 4 µm. **(D)** GFP-tagged CDKL-1A (green) requires MKS-5 (dotted ellipse) but not other "core" MKS (MKS-2) or NPHP (NPHP-4) module proteins for its TZ localization. Scale bar, 4 µm. Schematic showing interdependent organizational hierarchy of MKS-5, CEP-290, CDKL-1A, MKS and NPHP components. **(E)** Dye-filling assays of head and tail sensory neurons reveal that *cdkl-1* does not genetically interact (i.e., shows synthetic dye-filling phenotype) with either MKS (*mks-2*) or NPHP (*nphp-1*) module mutants. Scale bar, 40 µm.

2.3.2 CDKL-1 is dispensable for cilium gate function

The TZ functions as a membrane diffusion barrier, or ciliary gate, that maintains the protein composition of the organelle (Reiter et al., 2012). Since CDKL-1 localizes to the TZ, we therefore wondered if it plays a role in ciliary gating. To test this, we probed if two proteins normally found at the periciliary membrane, namely TRAM-1a and RPI-2, could inappropriately enter the ciliary compartment in strains lacking CDKL-1. The *cdkl-1* (*tm4182*) mutant contains a large out-of-frame deletion (850 bp) of exons 3-7 and is likely null, and another null (*nx132*) mutant generated using CRISPR-cas9 has a 5-bp deletion in the first coding exon, causing an early stop (**Figure 2.2A**).

TRAM-1a and RPI-2 entered cilia in most TZ mutants tested (Huang et al., 2011; Jensen et al., 2015; Williams et al., 2011). In contrast, they remained at the periciliary membrane in the *cdkl-1* mutants, as in the wild-type control (**Figures 2.2B** and **C**). We also queried for the leakage of ARL-13 from its normal localization (ciliary middle segment) to the periciliary membrane, as seen in various TZ mutants (Cevik et al., 2013; Li et al., 2016). ARL-13 ciliary localization was unchanged in the *cdkl-1* mutants, similar to wild-type (**Figure 2.2D**). Altogether, TRAM-1a, RPI-2, and ARL-13 localization remained unperturbed in this *cdkl-1* mutant (**Figures 2.2B-D**), providing further evidence that CDKL-1 performs a non-canonical function unrelated to ciliary gating at the TZ.

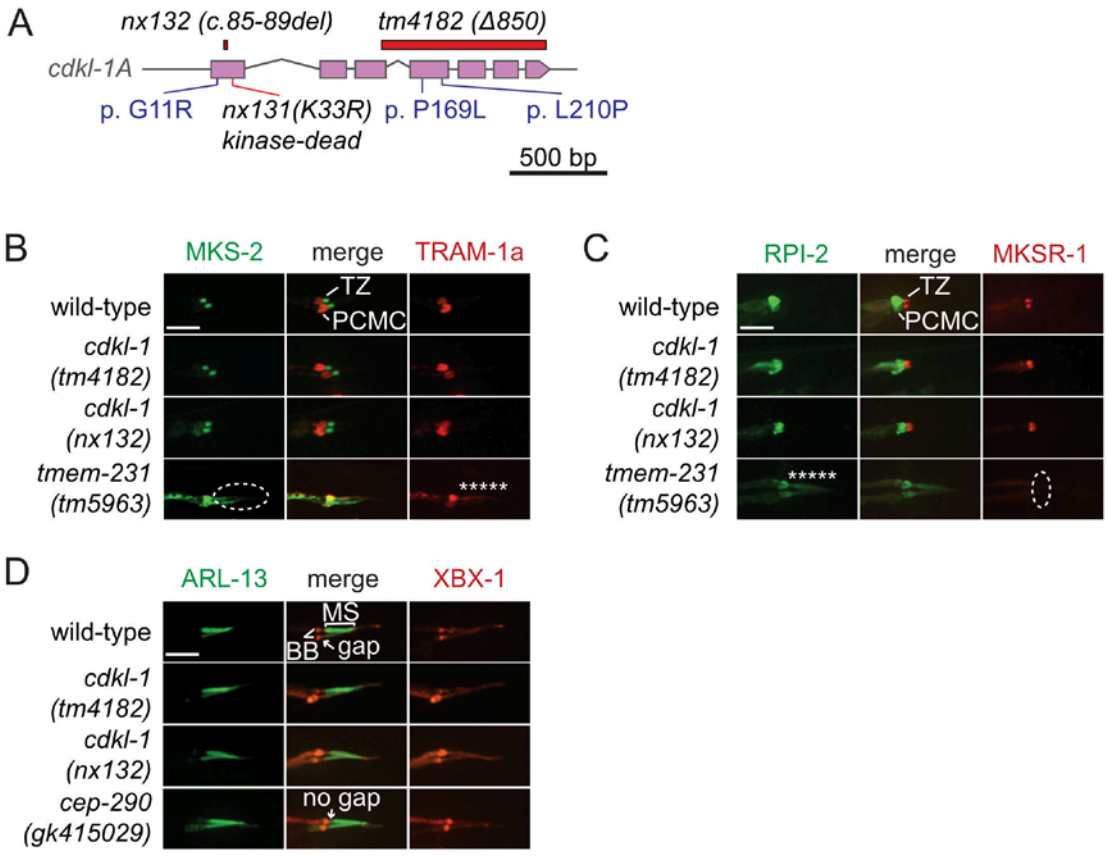

Figure 2.2 *C. elegans* CDKL-1 appears dispensable for cilium gate function. (A) Gene structure of *cdkl-1A*, highlighting the deletion or missense mutants analyzed. **(B-D)** Disruption of CDKL-1 does not visibly influence cilium gate function. The plasma membrane proteins TRAM-1a **(B)** and RPI-2 **(C)** concentrate just outside of cilia at the periciliary membrane compartment (PCMC) in wild-type animals and *cdkl-1* mutants, indicating the presence of a normal diffusion barrier; these proteins leak into cilia in transition zone (TZ) mutant (*tmem-231*) (asterisk) where TZ function is known to be compromised. In the *tmem-231* mutant, the TZ protein co-markers, MKS-2 and MKSR-1, mislocalize (dotted ellipse). ARL-13 **(D)** localizes correctly in the middle segment (MS) in wild-type and *cdkl-1* mutants, indicating an intact ciliary gate. However, ARL-13 leaks out of cilium in the TZ mutant known to affect gate function, *cep-290*(*gk415029*). XBX-1 marks the basal body (BB) and axoneme. PCMC, periciliary membrane compartment. Scale bar, 4 μm.

2.3.3 CDKL-1 modulates cilium length

Given that MAK, ICK, MOK, GSK3β, and CDKL5 regulate cilium length (**Figure 1.7**), we hypothesized that *C. elegans* CDKL-1 plays a similar role. To test this, we expressed GFP-tagged IFT-20 in the bi-ciliated ADL neuron to measure cilium length

accurately (Mohan et al., 2013). IFT-20::GFP, which marks the basal body and entire axonemal region, was introduced into wild-type and *cdkl-1* mutant (*tm4182* and *nx132*) animals (**Figure 2.3A**). Whereas the median length of wild-type ADL cilia was 8.0 µm, *cdkl-1* mutant cilia were 9.6 µm, or ~20% longer (**Figure 2.3B**). As *C. elegans* only encodes one CDKL protein, related to CDKL1–4, our results provide the first evidence for a CDKL1–4-related protein in cilium length regulation. Moreover, it suggests that both CDKL5 and CDKL1–4 proteins may share functions in cilium length regulation.

Since longer cilia may be curved and not guided into amphid channels formed by sheath and socket cells, as for example seen in the *dyf-5* ciliary mutant (Burghoorn et al., 2007), we tested for this using a socket cell marker (Hunt-Newbury et al., 2007). We confirmed that the long ADL cilia correctly penetrated amphid channels (**Figure 2.3C**). Next, we sought to rescue the cilium length defect of *cdkl-1* mutants by expressing wild-type *cdkl-1A*, but we found that this shortens ciliary length by ~11%, to 7.1 µm (**Figure 2.3B**). Similarly, overexpressing *cdkl-1A* in a wild-type background reduced ciliary length. Therefore, loss of or increased levels of CDKL-1 activity led to longer or shorter cilia, suggesting that the correct level of CDKL-1 is needed to maintain correct cilium length.

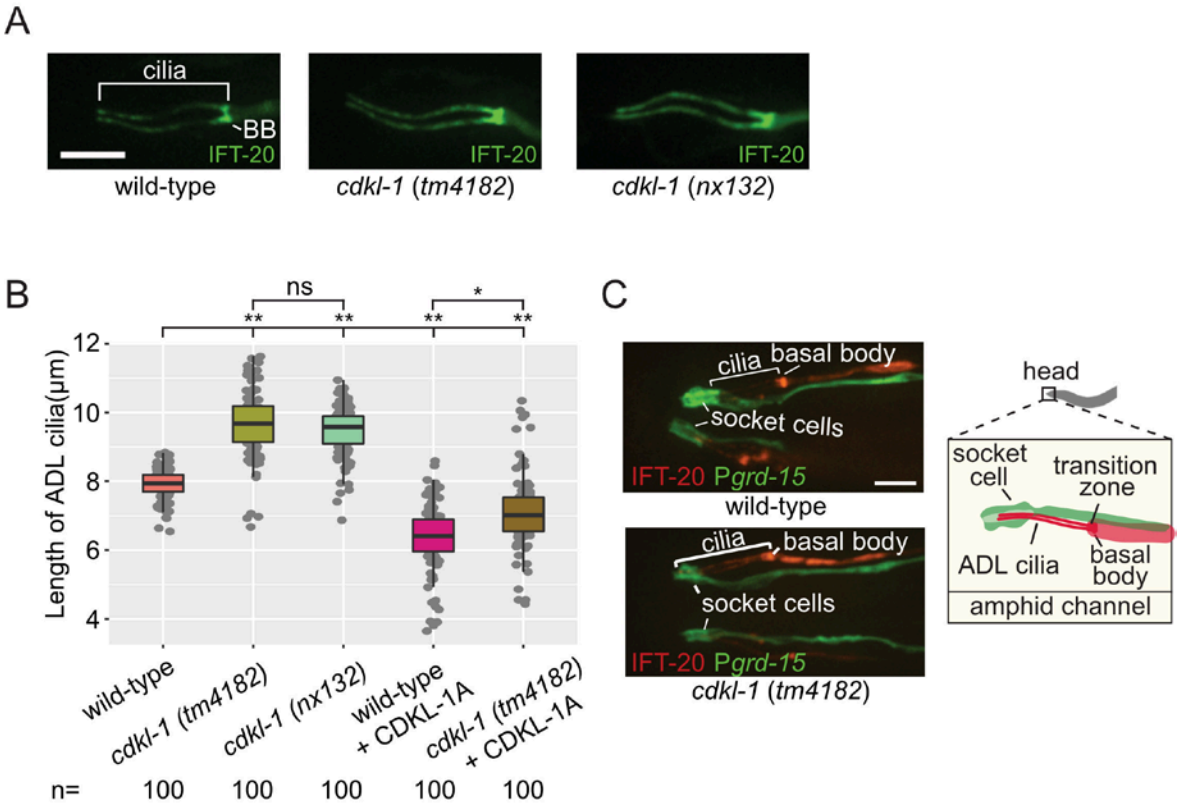

Figure 2.3 CDKL-1 regulates cilium length. (A) Representative images of the GFP-tagged IFT-20 marker expressed specifically in ADL neurons (L4 larvae), used to measure the length of cilia in wild-type and *cdkl-1* mutants (*tm4182* and *nx132*). ADL doublet cilia are longer in mutants than wild-type. BB, basal body. Scale bar, 4 μm. **(B)** ADL cilia lengths (L4 larvae) of wild-type and *cdkl-1* mutants with/without expression of wild-type CDKL-1A construct. Each dot represents one cilium. Kruskal-Wallis test (Dunn Kruskal-Wallis multiple comparison [Holm-Sidak method]) was used for significance. *$p < 0.01$ and **$p < 0.001$; ns, not significant. **(C)** The cilia of ADL in L3 larvae of wild-type and *cdkl-1* (*tm4182*) mutant are correctly guided into amphid channels (Inglis et al., 2007). The schematic depicts how ADL cilia (red) penetrate an amphid channel formed by the sheath and socket (green) cells. The fluorescence images from wild-type or *cdkl-1* mutant animals show a cilium marker (tdTomato-tagged IFT-20 expressed in the neuron using the *srh-220* promoter) and socket cell marker (GFP expressed using the *grd-15* promoter). Scale bar, 4 μm.

2.3.4 Kinase activity and C-terminal αJ helix region of CDKL-1 is required for cilium length control

We examined if CDKL-1 kinase activity is required for cilium length control. Using CRISPR-Cas9, we generated a *cdkl-1* kinase-dead mutant (*nx131*) by converting a conserved lysine (K) in the ATP-binding site to arginine (R) (**Figure 2.2A**). Similar to the

cdkl-1 (*tm4182*) null mutant, the kinase-dead mutant exhibited cilia ~20% longer than wild-type (**Figure 2.4A**). In addition, the CDKL-1A(K33R) protein no longer concentrated at the TZ; it became dispersed in the dendrite and ciliary axoneme (**Figure 2.4B**). Thus, CDKL-1 kinase activity is critical for regulating cilium length and proper TZ localization of the protein.

Our collaborators (Canning and his colleagues) solved the crystal structures of the CDKL kinase domains (CDKL1, CDKL2, CDKL3 and CDKL5) at resolutions from 1.5 to 2.4 Å. The prototypical structure, exemplified by CDKL2, conformed to the classic bilobal kinase architecture, but is distinct from both the CDK and MAPK families (**Figure 2.4C**) (Canning et al., 2018). Interestingly, the packing and orientation of the αJ helix was distinct from the C-terminal extensions of other kinases, such as PAK1, CDK2, BUB1, and NEK1 (Canning et al., 2018). CDKL2 and CDKL3 showed an unusual amphipathic helix, αJ, while the constructs for CDKL1 and CDKL5 were truncated and lacked this region (Canning et al., 2018). To determine the functional relevance of the αJ, wild-type proteins were expressed in and purified from yeast, and subjected to *in vitro* kinase assays (**Figure 2.4D**). Proline-directed activity was observed against an Ime2 peptide substrate (RPRSPGARR), consistent with other CMGC kinases. Turnover was low (<10 phosphorylations/min) for all CDKLs, perhaps reflecting a requirement for activating partners. Notably, deleting the αJ region reduced the activities of CDKL2 and CDKL3, whereas CDKL1 and CDKL5 were largely unchanged. These results are consistent with the observed structures, and they further show the importance of the unprecedented αJ helix for CDKL2 and CDKL3 function.

We further probed for a potential role of the αJ helix in *C. elegans* CDKL-1 function. An mNeonGreen-tagged CDKL-1A(ΔαJ) protein variant was expressed, and it was found to localize correctly to the TZ, suggesting that this region does not overtly affect protein stability (**Figure 2.4E**). However, unlike wild-type CDKL-1A, the CDKL-1A(ΔαJ) protein only partially rescued the cilium length defect in a *cdkl-1* mutant, suggesting that the αJ helix region is important for cilium length control (**Figure 2.4F**).

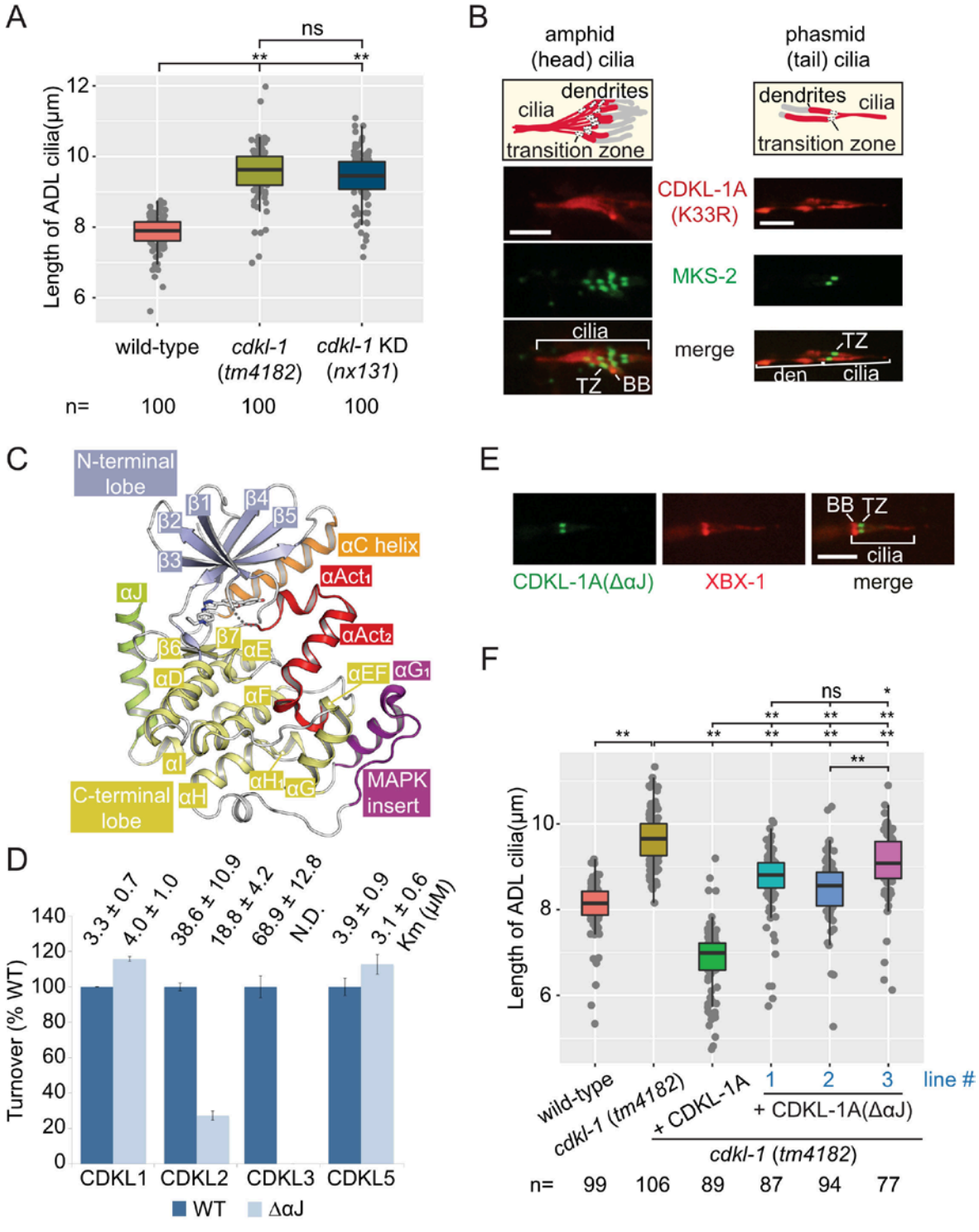
A
ns
**
**
Length of ADL cilia(μm)
12
10
8
6
wild-type
cdkl-1 (tm4182)
cdkl-1 KD (nx131)
n= 100 100 100
B
amphid (head) cilia
phasmid (tail) cilia
dendrites
cilia
transition zone
CDKL-1A (K33R)
MKS-2
merge
TZ
BB
den
C
N-terminal lobe
β1
β2
β3
β4
β5
αC helix
αAct1
αAct2
αJ
β6
β7
αE
αD
αF
αEF
αG1
αI
αH1
αG
αH
C-terminal lobe
MAPK insert
D
3.3 ± 0.7
4.0 ± 1.0
38.6 ± 10.9
18.8 ± 4.2
68.9 ± 12.8
N.D.
3.9 ± 0.9
3.1 ± 0.6
Km (μM)
Turnover (% WT)
140
120
100
80
60
40
20
0
CDKL1
CDKL2
CDKL3
CDKL5
WT
ΔαJ
E
BB TZ
cilia
CDKL-1A(ΔαJ)
XBX-1
merge
F
ns
*
**
Length of ADL cilia(μm)
10
8
6
wild-type
cdkl-1 (tm4182)
+ CDKL-1A
1
2
3
line #
+ CDKL-1A(ΔαJ)
cdkl-1 (tm4182)
n= 99 106 89 87 94 77

Figure 2.4 *C. elegans* CDKL-1 requires its kinase activity and C-terminal region (including αJ helix) to regulate cilium length. (A) ADL cilia length in wild-type, *cdkl-1* null (*tm4182*), and *cdkl-1 kinase-dead* (*KD*) (*nx131*) mutant L4 larvae. Dot, one cilium. The *p*-values of the dataset in **(A)** and **(F)** were calculated using Kruskal-Wallis test; Dunn Kruskal-Wallis multiple comparison [Holm-Sidak method]. ***p* < 0.001; ns, not significant. **(B)** The kinase-dead variant CDKL-1A(K33R)::tdTomato no longer concentrates at the TZ (marked by MKS-2::GFP); it mislocalizes to dendrites (den) and cilia in amphid and phasmid neurons. BB, basal body. Scale bar, 4μm. **(C)** Structural features of the CDKL2-TCS2312 complex, the most complete/ordered CDKL structure. **(D)** A radiometric *in vitro* kinase assay reveals that the αJ region is critical for CDKL2 and CDKL3 activities but dispensable for CDKL1 and CDKL5. K_m values are shown for the Ime2 peptide substrate. N.D. denotes not determined for CDKL3(ΔαJ) due to diminished catalytic activity. **(E)** CDKL-1A(ΔαJ)::mNeonGreen protein predominantly accumulates at the TZ in cilia. The BB and ciliary axoneme are marked by XBX-1::tdTomato. Scale bar, 4 μm. **(F)** ADL cilia lengths (L4 larvae) measured in wild-type, *cdkl-1* null (*tm4182*), and *cdkl-1* null (*tm4182*) expressing CDKL-1A or CDKL-1A(ΔαJ). Dot, one cilium. **p* < 0.05 and ***p* < 0.001; ns, not significant.

2.3.5 CDKL-1 variants carrying human CDKL5 pathogenic mutations disrupt ciliary length regulation

CDKL5 mutations, most occurring in the kinase domain, are linked to neurological disorders, including epilepsy, atypical Rett syndrome, and autism (Castren et al., 2011; Kilstrup-Nielsen et al., 2012; Tao et al., 2004; Weaving et al., 2004). We sought to model such CDKL5 mutations using *C. elegans* CDKL-1, but first we wanted to reveal a functional connection between human CDKL5 and cilia to ensure the relevance of our studies. As a ciliary role for mammalian CDKL5 has not been reported, our collaborators (Gonçalves and his colleagues) determined the subcellular localization of GFP-tagged human CDKL5. It localized at the basal body, as well as ciliary tip in ciliated RPE-1 cells (**Figure 2.5A**). Compared to serum-starved wild-type RPE-1 cells, cells expressing GFP-CDKL5 exhibited compromised ciliogenesis (**Figure 2.5B**). This negative effect of GFP-CDKL5 overexpression was rescued by RNAi-mediated depletion of CDKL5 (**Figure 2.5B**). These findings provide evidence for an association between vertebrate/mammalian CDKL5 and cilia.

We chose to model three pathogenic CDKL5 missense mutations (G20R, P180L, and L220P) present in patients with epileptic encephalopathy, severe mental retardation, and developmental delay (Archer et al., 2006; Rosas-Vargas et al., 2008; White et al., 2010). These residues are conserved in all human CDKL proteins and *C. elegans* CDKL-1 (**Figure 2.5C**). The corresponding mutations (G11R, P169L, and L210P) were introduced in *C. elegans* CDKL-1 to explore their influence on TZ localization (**Figures**

2.5C-E). Strikingly, CDKL-1A proteins harboring the G11R or L210P mutations no longer concentrated at the TZ (**Figure 2.5E**). CDKL-1A(G11R) were primarily dispersed in the ciliary axoneme, whereas CDKL-1A(L210P) showed weak localization to cilia and periciliary membrane. In contrast, CDKL-1A(P169L) localized to the TZ, similar to wild-type.

Next, we assessed the functionality of each CDKL-1 variant by testing their effect on ADL cilium length when expressed in a *cdkl-1* mutant. Relative to wild-type CDKL-1A, expression of each variant gave statistically longer cilia in almost all lines, with the phenotypic severity ranked as L210P > G11R > P169L (**Figure 2.5F**). Substituting proline in the L210P variant likely disrupts the α helix structure, potentially causing protein misfolding and, thus, dysfunction due to mislocalization and/or loss of kinase activity. The G11R missense mutation was predicted to preclude ATP binding (**Figure 2.5D**). This may have reduced CDKL-1 catalytic activity and, similar to the kinase-dead mutant (**Figure 2.4B**), induced mislocalization. The weaker P169L phenotype may have reflected a partial loss of function (2 of 3 independent lines showed different ciliary lengths), with the protein remaining localized to the TZ (**Figure 2.5E**). Together, our modeling of CDKL5 patient mutations using *C. elegans* CDKL-1 suggests that cilium length may, at least in part, cause the observed neurological phenotypes present in patients with CDKL5 mutations.

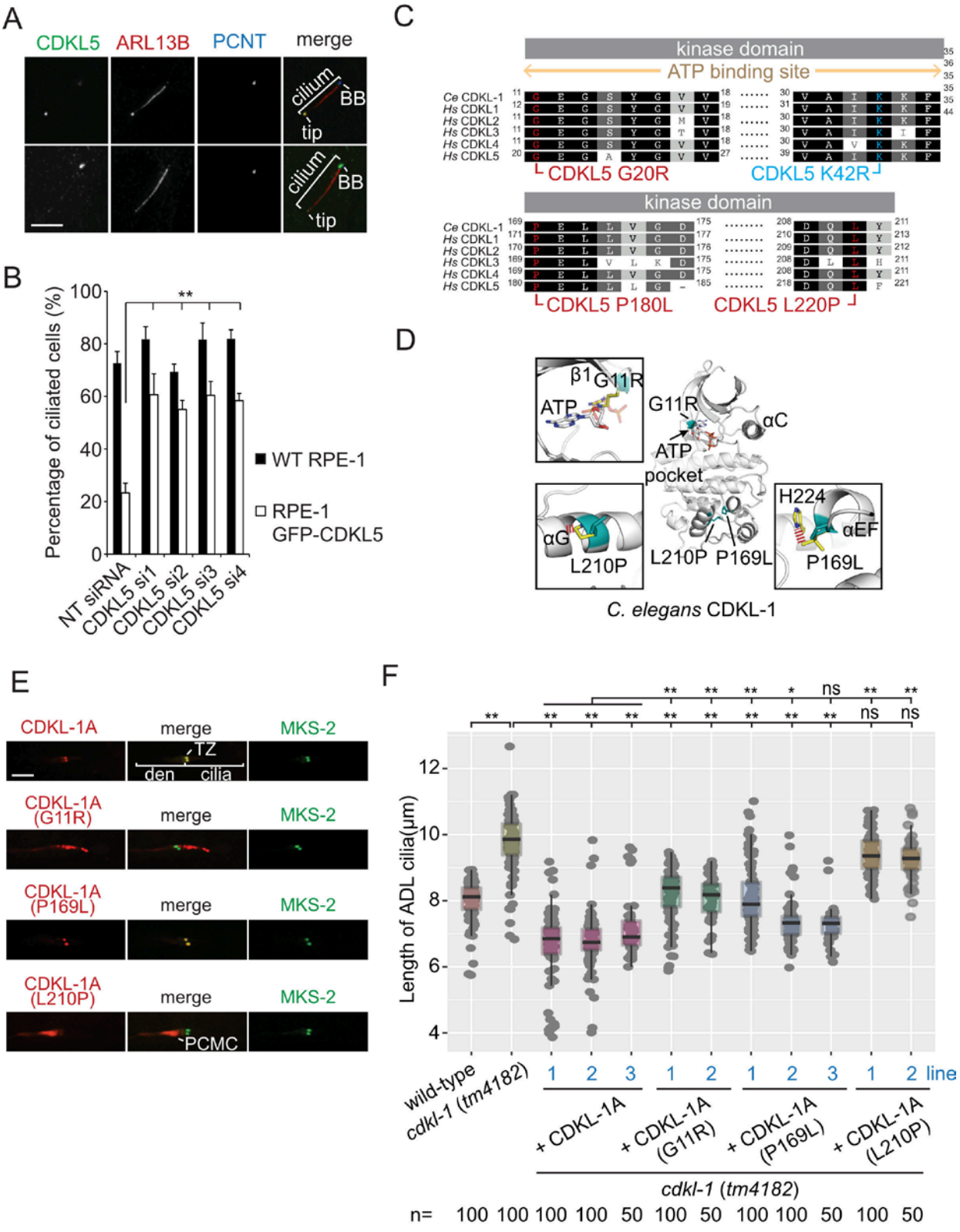
A
CDKL5
ARL13B
PCNT
merge
cilium
BB
tip
B
Percentage of ciliated cells (%)
WT RPE-1
RPE-1 GFP-CDKL5
NT siRNA
CDKL5 si1
CDKL5 si2
CDKL5 si3
CDKL5 si4
C
kinase domain
ATP binding site
CDKL5 G20R
CDKL5 K42R
CDKL5 P180L
CDKL5 L220P
D
G11R
ATP
αC
ATP pocket
αG
L210P
P169L
H224
αEF
C. elegans CDKL-1
E
CDKL-1A
merge
MKS-2
TZ
den
cilia
CDKL-1A (G11R)
CDKL-1A (P169L)
CDKL-1A (L210P)
PCMC
F
Length of ADL cilia(μm)
wild-type
cdkl-1 (tm4182)
+ CDKL-1A
+ CDKL-1A (G11R)
+ CDKL-1A (P169L)
+ CDKL-1A (L210P)
line
cdkl-1 (tm4182)
n=

Figure 2.5 Human CDKL5 localizes to cilium and affects ciliogenesis when overexpressed in RPE-1 cells, and mutations modeled in *C. elegans* CDKL-1A disrupt localization and/or cilium length regulation. (A) Immunofluorescence analysis of serum-starved hTERT RPE-1 cells expressing GFP-CDKL5 stained with antibodies against GFP, ARL13B (cilium marker), and PCNT (centrosome marker). The top and bottom panels are representative images showing different levels of GFP-CDKL5 localization to the BB and cilium tip. Scale bar, 5 µm. **(B)** Bar graph shows mean percentage of ciliated cells (n > 300 cells per sample, 3 independent experiments) in the serum-starved populations (72 hr) of hTERT RPE-1 and hTERT RPE-1GFP-CDKL5 cells transfected with the indicated siRNAs. Error bars indicate SD. $^{**}p < 0.01$ (Student's two-tailed t test). **(C)** Conserved CDKL5 missense mutations associated with neurological disorders (red) and catalytic lysine residue (blue) highlighted in a partial sequence alignment of human (*Hs*) and *C. elegans* (*Ce*) CDKL kinase domains. **(D)** Locations of missense mutation residues (cyan) in a homology model of the *C. elegans* CDKL-1 structure (gray) prepared using SWISS-MODEL (Biasini et al., 2014). Inset boxes show wild-type (cyan) and mutant side chains (yellow) modelled using the DUET server (Pires et al., 2014). Steric clashes are indicated by red bars. **(E)** Wild-type CDKL-1A and the P169L variants localize to the TZ, whereas the G11R mutant localizes along the length of cilia, and the L210P mutant accumulates in dendrites (den) and is weakly present at the periciliary membrane compartment (PCMC). MKS-2 is a TZ marker. Scale bar, 4 µm. **(F)** ADL cilia lengths (L4 larvae) of wild-type and strains expressing CDKL-1A variants. Expressing wild-type CDKL-1A leads to short cilia. Similar levels of length reduction are not seen upon expression of the G11R and L210P variants, or lines 1 and 2 of the P169L variant (line 3 is not significant), suggesting functional defects with these variants. Dot is one cilium. Significance (*p* value) was calculated by Dunn Kruskal-Wallis multiple com-parison (Holm-Sidak adjustment). $^{*}p < 0.01$ and $^{**}p < 0.001$; ns, not significant.

2.4 Discussion

Phylogenetic distribution of CDKL protein family members

The phylogenetic distribution of CDKL proteins suggests that the ciliated last eukaryotic common ancestor had two family members. Most extant ciliated protists and metazoans generally encode one CDKL5-related member, and one or more protein(s) most closely related to CDKL1-4. The closest unicellular ancestor of metazoans (multicellular animals), the Choanoflagellate, has two such members. Vertebrates/mammals possess a CDKL5 orthologue as well as CDKL1, CDKL2, CDKL3 and CDKL4 proteins. Interestingly, both *C. elegans* and *Drosophila* lack a CDKL5 orthologue but retain one CDKL1-4-related protein. Hence, in these invertebrates, the single CDKL1-4 family member may be sufficient to fulfill the core function(s) of CDKL proteins, whereas in vertebrates/mammals, the different members likely have shared but specialised cellular functions.

Modelling of CDKL5 human patient mutations

Using *C. elegans* CDKL-1 to model three patient mutations found in CDKL5 (G20R, P180L, and L220P) revealed two potential pathogenic mechanisms that are not mutually exclusive. The first is disruption of function, as all three variants exhibit cilium length defects (longer cilia) compared to a wild-type control when expressed in the worm. Similar cilium length phenotypes are observed in the *cdkl-1* null and kinase-dead mutants. The second mechanism is protein mislocalization, where *C. elegans* CDKL-1A(G11R) and CDKL-1A(L210P), as well as the kinase-dead variant, no longer concentrate at the TZ. One variant, however, remains at the TZ: CDKL-1A(P169L). Notably, as seen in our CDKL1/2/3/5 crystal structures, all three mutations cluster in the kinase domain (**Figures 2.5C and D**). Dissecting the relationship between kinase activity, TZ localisation, and mechanism of ciliary length regulation will necessitate further studies.

Model for CDKL protein regulation of cilium length

One specific branch of the kinome (**Figure 1.7**) is enriched with proteins having ciliary functions (Avasthi and Marshall, 2012). ICK, MOK, and MAK localize to cilia and negatively regulate their length (Broekhuis et al., 2014; Chaya et al., 2014; Omori et al., 2010). Notably, IFT components accumulate inside cilia when ICK or MAK are lost. Moreover, ICK phosphorylates a subunit of kinesin-2 and affects IFT speeds, consistent with the link between cilium length control and IFT. *Chlamydomonas* orthologs of CDKL5 and GSK3β (LF5/FLS1 and GSK3) also localize to, and control the length of, cilia (Hu et al., 2015a; Tam et al., 2013; Wilson and Lefebvre, 2004). *Chlamydomonas* CDKL5 (LF5) localizes at the ciliary base and its disruption lengthens cilia (Tam et al., 2013), similar to loss of *C. elegans* CDKL-1. Interestingly, *Chlamydomonas* CDKL5 moves to the ciliary tips in long-flagella (*lf*) mutants, suggesting a link to length control. Specifically, *Chlamydomonas* CDKL5 is influenced by LF3, whose loss-of-function causes IFT protein accumulation at ciliary tips (Tam et al., 2003). This is of interest, since human CDKL5 localizes at the base, and also tip, of cilia (**Figure 2.5A**). Hence, CDKL5 (and perhaps other CDKL proteins) may influence IFT from the base, or tip, of cilia to regulate cilium length. Consistent with such a role, overexpressing CDKL5 impairs cilium formation in

RPE-1 cells. Interestingly, *C. elegans* CDKL-1A localizes to the TZ, whereas human CDKL5 and another CDKL5-related *Chlamydomonas* protein (FLS1) are at the basal body (Hu et al.,2015) (**Figure 2.6**). Hence, CDKL proteins exist in three regions at the ciliary base—basal body, TZ, and immediately distal to the TZ (**Figure 2.6**). At any of these locations, CDKL proteins may be well positioned to interact with the IFT machinery. Such a transient interaction with IFT proteins has been described for the TZ protein B9D1 (Zhao and Malicki, 2011). Another possibility, not mutually exclusive, is that CDKL5 and perhaps other CDKL proteins act via depolymerizing kinesin(s). This is reported for *Chlamydomonas* FLS1, which regulates phosphorylation of a kinesin-13 member in flagella (Hu et al., 2015a). In mammals, two cilium base-localized kinesin-13 proteins, KIF2A and KIF24, regulate cilium disassembly/length control (Kim et al., 2015; Kobayashi et al., 2011; Miyamoto et al., 2015) (**Figure 2.6**). CDKL proteins may also influence another depolymerizing kinesin, KIF19A, found at the ciliary tip (Niwa et al., 2012). In summary, CDKL proteins may control cilium structure and length through the IFT machinery and/or depolymerizing kinesins, at the ciliary base and/or tip (**Figure 2.6**). Understanding their ciliary roles may be relevant to human neurological disorders, including epilepsy.

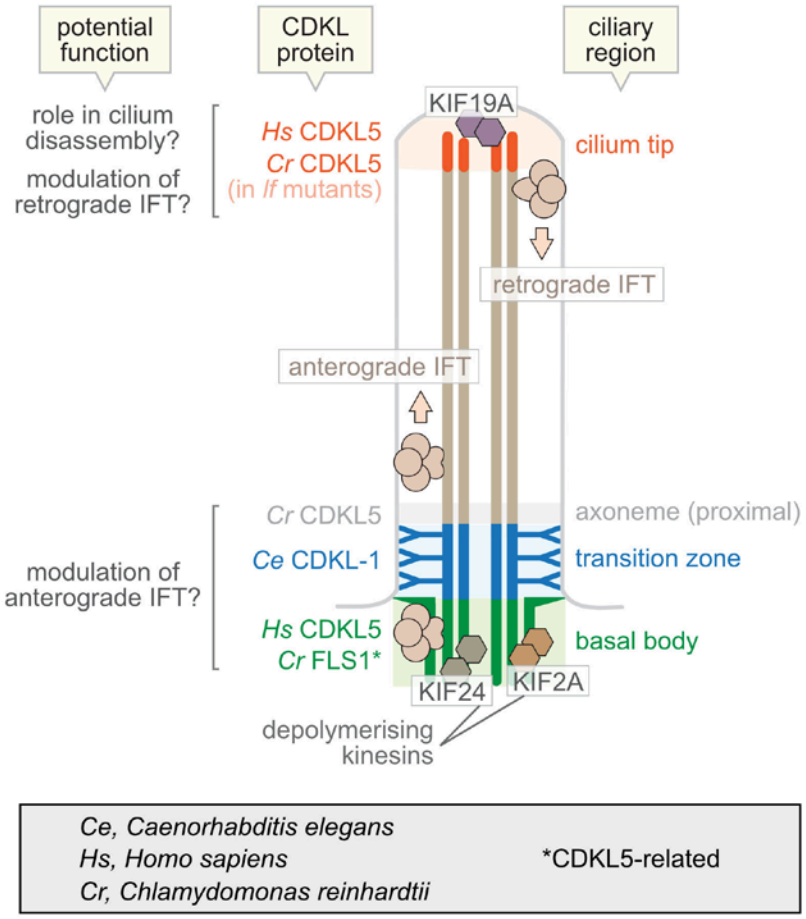

Figure 2.6 Model for CDKL protein ciliary localization and potential roles in cilium length regulation. CDKL proteins localize to the base and/or tip of cilia, and they likely influence IFT (anterograde/retrograde) machinery and/or depolymerizing kinesins to regulate cilium growth and disassembly, respectively, and thus control cilium length.

3 CDKL-1 controls intraflagellar transport to maintain cilium length, and influences sensory perception and body size in *C. elegans*

This chapter is a modified version of a manuscript prepared for publication. The authors and their affiliation are listed below:

Kwangjin Park[1], Chunmei Li[1], João Gonçalves[2,3,¤a], Nils Lambacher[1], Tiffany Timbers[1,¤b], Christine Kondratev[1], Laurence Pelletier[2,3], Michel R Leroux[1*]

[1]Department of Molecular Biology and Biochemistry, and Centre for Cell Biology, Development, and Disease, Simon Fraser University,8888 University Drive, Burnaby, BC V5A 1S6, Canada

[2]Lunenfeld-Tanenbaum Research Institute, Mount Sinai Hospital, 600 University Avenue, Toronto, ON M5G 1X5, Canada

[3]Department of Molecular Genetics, University of Toronto, Toronto, ON M5S 1A8, Canada

[¤a]Current address: Deep Genomics, MaRS Centre, 661 University Ave, Suite 480, Toronto, ON M5G 1M1, Canada

[¤b]Current address: Department of Statistics, University of British Columbia, 2329 West Mall, Vancouver, BC V6T 1Z4, Canada

*Corresponding author

As the first author of this manuscript, I conceived and designed the research, performed most experiments, analyzed data, interpreted results, generated figures and wrote the manuscript under the supervision of Dr. Michel Leroux. Chunmei Li created nematode transcriptional/translational fusion constructs and strains, performed imaging in **Figures 3.5E, 3.6A-B, 3.7A, and 3.8A-C** and contributed valuable discussions. Dr. João Gonçalves, who is under the supervision of Dr. Laurence Pelletier, collected data in human cells shown in **Figure 3.2E**. Dr. Nils Lambacher performed the fluorescence

recovery after photobleaching (FRAP) assay in **Figure 3.2A-B**. Dr. Tiffany Timbers set up multi-worm tracker (MWT) machine, analyzed CO_2 avoidance results and generated **Figure 3.10B**. Christine Kondratev helped make and maintain *C. elegans* strains, and contributed to establishing the behavioral and biochemical assays. Dr. Michel Leroux contributed to the conception, interpretation, and writing of the manuscript.

3.1 Introduction

We previously discovered that the sole *C. elegans* CDKL protein (CDKL-1), which is most closely related to mammalian CDKL1-4 and more distantly related to CDKL5, controls cilium length in a kinase activity-dependent manner at the transition zone (Canning et al., 2018). However, our findings still did not clarify the process by which CDKL family proteins function as negative regulators of cilium length.

The length of cilia is determined by a fine balance between ciliary assembly and disassembly (**Figure 1.6**). Cilia grow when the balance is shifted towards assembly, and when ciliary assembly is slower than disassembly, cilia shorten. When cilium assembly and disassembly occur at an equal rate, the cilium maintains its normal length. The IFT machinery plays a significant role in the assembly and maintenance of cilia, as it delivers microtubule building blocks (tubulin subunits) to the ciliary tip (assembly site) (Marshall and Rosenbaum, 2001). There is also clear evidence for a link between IFT and ciliary length control. For example, the amount of the anterograde IFT motor proteins increases in elongated flagella in *Chlamydomonas*, and *C. elegans* ciliary axonemes become shorter when IFT function is abrogated in *che-10* mutants (Mohan et al., 2013; Wilson and Lefebvre, 2004). Cilium disassembly is thought to be IFT-independent (Engel et al., 2012) but relies on the activity of two kinesin families (Kinesin-8 and Kinesin-13), called depolymerizing kinesins, which induce tubulin depolymerization. Kinesins-8 family walks toward and removes tubulins at the plus end of the microtubules. For example, the mammalian kinesin-8 family (KIF19A) localizes at and depolymerizes the distal end of the ciliary axoneme (the plus end of microtubules in cilium). In contrast, kinesin-13 family, instead of walking along the microtubules, diffuses toward both the plus and minus ends and show microtubule depolymerizing activity at either location. Among

mammalian kinesin-13 family members, KIF2A and KIF24 participate in the process of cilium disassembly through their depolymerizing activities at the ciliary base.

Proteins kinases, also implicated in cilium length control, are known to influence the functions of either IFT or depolymerizing kinesins. For instance, mammalian ICK directly phosphorylates an IFT kinesin-II subunit, KIF3A, and affects IFT speed (Broekhuis et al., 2014; Chaya et al., 2014). Loss-of-function of ICK increases anterograde IFT speed, whereas retrograde velocities are decreased when overexpressed. In cultured cells, down-regulation of *ick* results in cilium elongation (Moon et al., 2014). *Chlamydomonas* CDK-like kinase (FLS1) regulates the phosphorylation of CrKinesin-13, a depolymerizing kinesin involved in flagellar resorption (Hu et al., 2015a). In addition, NEK2 regulates microtubule depolymerizing activity of KIF24 by phosphorylation (Kim et al., 2015).

Based on the above-mentioned roles of kinases in regulating both IFT and depolymerizing kinesins, we therefore hypothesized that CDKL family members might modulate the length of cilia possibly by regulating one or both processes. In this study, we reveal that the *C. elegans* CDKL-1 protein is partially mobile and travels along the ciliary axoneme as an IFT cargo. CDKL-1 mainly regulates the length of the middle segment by acting on the IFT machinery, rather than depolymerizing kinesins. Furthermore, we performed genetic interaction studies with either protein kinase mutants implicated in cilium length control (*dyf-5*, *dyf-18*, *nekl-1*, and *nekl-4*) or depolymerizing kinesin mutants (*klp-13* and *klp-7*). The studies suggest that CDKL-1 utilizes a unique pathway to regulate the cilium length. Dysregulation of cilium length in *cdkl-1* mutants affects not only sensory functions but also body development possibly owing to defects in cilia-mediated signaling pathways, such as cGMP signaling pathways. Notably, we find that the *C. elegans* kinesin-13 family member KLP-7 positively regulates cilium length at the transition zone. Mutations in KIF2A, a human kinesin-13 family member, is associated with microcephaly, a potential ciliopathy-linked phenotype (Poirier et al., 2013). Introducing the corresponding pathogenic mutations of KIF2A (S317N and H321D) into *C. elegans* KLP-7 cause its mislocalization, and cilium length defects. These data suggest that the abnormal brain development shown in KIF2A patients possibly results from ciliary dysfunctions arose from cilium length defects.

3.2 Methods

3.2.1 *C. elegans* transgenic constructs

To examine the subcellular localization of different CDKL-1 isoforms, the *bbs-8* promoter (370 bp) was stitched to either the cDNA of the *cdkl-1B* (Y42A5A.4B) or *cdkl-1C* (Y42A5A.4C) isoforms, and each stitched gene was fused to GFP with the *unc-54* 3' UTR. *klp-7A* constructs were prepared for protein localization and rescue experiments. The *bbs-8* promoter (370 bp) was fused to all exons and introns of *klp-7A* and GFP carrying the *unc-54* 3' UTR. The KIF2A missense mutations found in patients (S317N and H321D) were introduced into the *klp-7A* gene by substituting the corresponding residues (S414N and H418D) (Q5 site-directed mutagenesis kit, New England BioLabs). *klp-7A* including exons, introns and 3' UTR were amplified from genomic DNA and fused to the *bbs-8* promoter for rescue experiments. cDNA of klp-13C is stitched to the *bbs-8* promoter (941bp) and then GFP with the *unc-54* 3' UTR is C-terminally fused to the stitched product. For the NIMA-related kinase genes, GFP with 1.8kb *nekl-1* 5' UTR were N-terminally fused to cDNA and 3' UTR of *nekl-1*. 5' UTR (2 kb) containing X-box motif, all exons and introns of *nekl-4* were amplified from genomic DNA and were fused to GFP with the *unc-54* 3' UTR.

3.2.2 *C. elegans* strains

The *nekl-1(gk516661)* and *nekl-4(tm4910)* mutant strains were obtained from Dr. Blacque, and *klp-7(tm2143)* was obtained from Dr. Srayko. Dr. Peterman kindly provided strains generated using Mos1-mediated single-copy insertion (EJP13[KAP-1::EGFP], EJP16[OSM-3::mCherry], EJP76[OSM-6::EGFP], EJP81[CHE-11::mCherry], and EJP206[XBX-1::EGFP]). *klp-7* variants (*syb603* and *syb613 alleles*) carrying the corresponding mutations (S414N and H418D) found in KIF2A human patients were made using CRISPR/CAS9-meditated homologous recombination (Suny Biotech; http://www.sunybiotech.com). The *cdkl-1* mutant alleles (*nx163*, *nx164* and *nx166*) were generated by CRISPR-mediated homologous recombination. *dpy-10* sgRNA sequence (5'-gctaccataggcaccacgag-3') was inserted after 3xFlag tags sequence in pDD282 (addgene # 66823) using Gibson assembly (a donor vector for generating *nx163* allele).

50 ng/µl each of *cdkl-1* sgRNA vector, Cas9 plasmid (Addgene #46168), and the donor plasmid (modified pDD282 carrying *dpy-10* sgRNA) were mixed and injected into 20 wild-type young adult worms. F1 heterozygous (roller) and F2 homozygous (roller) worms that survived hygromycin treatment (final concentration of ~250 µg/ml) were picked. *nx163* allele were identified by PCR screening. The *nx164* allele was generated by removing the selectable marker in *cdkl-1*(*nx163*) mutant using heat shock. *cdkl-1(nx164*) mutant was confirmed by DNA sequencing. To create the *nx166* allele, a donor vector was prepared. The 5' UTR (700 bp), exons, and introns of *cdkl-1A* were fused to mNeonGreen with 700bp 3' UTR of *cdkl-1A*. The stitched gene was cloned into the pJET1.2 vector. The *dpy-10* sgRNA vector was prepared as described in (Canning et al., 2018). 50 ng/µl each of *dpy-10* sgRNA vector, Cas9 plasmid, the donor plasmid carrying *cdkl-1A::mNeonGreen*, *and* the plasmid encoding neomycin-resistance gene were mixed and injected into 20 *cdkl-1*(*nx164*) mutant worms. The surviving F1 heterozygous (dumpy) treated with neomycin (G418; final concentration of ~1.25 mg/ml) were transferred to new plates without neomycin. F2 homozygous (dumpy) worms containing the *cdkl-1*(*nx166)* allele were identified by PCR and confirmed by DNA sequencing. To remove the dumpy phenotype, the *cdkl-1*(*nx166)* mutant was outcrossed once. All strains used in this chapter are described in **Appendix B**

3.2.3 CO_2 avoidance analysis

Wild-type and *cdkl-1*(*tm4182*) animals were synchronized and grown at 20°C for 4 days. After 100 seconds of putting individual plate on a Multi-Worm Tracker (MWT), worms were exposed to 4% CO_2 and their reversal responses were recorded. Data were visualized using R software (pheatmap and gplots packages).

3.2.4 Osmotic avoidance assay

Five worms each for wild-type, *osm-3*, *cdkl-1* null (*tm4182* and *nx132*) and *cdkl-1* kinase-dead (*nx131*) strains were placed inside of an 8M glycerol ring (110mm

diameter). The percentage of worms which remained inside the osmotic barrier for 10 minutes were counted. Four independent experiments were performed.

3.2.5 Imaging, intraflagellar transport (IFT) analysis, and fluorescence recovery after photobleaching (FRAP) assay

Microscopy images and time-lapse imaging of cilia were obtained using either WaveFX spinning disc confocal microscope (Quorum Technologies) or LSM880 laser scanning microscope with Airyscan (Zeiss). They were analysed with either Volocity 6.3 software (PerkinElmer) or ZEN 2.3 software. IFT speed and flux in wild-type and *cdkl-1* mutant animals were calculated from particle track data on kymographs created using the ImageJ plug-in multi-kymograph (https://imagej.net/Multi_Kymograph). For the FRAP assay, either the transition zone or the middle segment was photobleached after 5 frames (pre-photobleach) using the 488nm laser, and then images were recorded at varying time points including 0 second time point post-photobleach.

3.2.6 Body size and length measurements

L4 stage worm of wild-type, *cdkl-1* null (*tm4182*), *dbl-1* null (*nk3*), *cdkl-1;dbl-1*(*nk3*), *dbl-1* over-expression (+), and *cdkl-1;dbl-1*(+) animals were picked and grown at 20°C for 48 hours. Worms were imaged using Axioscope, and body size (length of the perimeter of the worm body) and length (length of the midline of worm body) were measured using ImageJ software. *p*-values were calculated based on Tukey's honestly significant difference (HSD).

3.3 Results

3.3.1 *C. elegans* CDKL-1 is mobile and an IFT cargo protein

CDKL family proteins localize to various regions, or subcompartments, of cilia. Human CDKL5 is observed at the basal body and ciliary tip (Canning et al., 2018). In *Chlamydomonas,* CDKL5 (LF5) is present just distal to the transition zone (TZ), whereas the LF5-related protein FLS1 is present at the ciliary base (Hu et al., 2015a; Tam et al., 2013). Interestingly, LF5 shifts to ciliary tips in various long-flagella (*lf*) mutants. *C. elegans* CDKL-1, the only CDKL family protein, encodes three isoforms. We previously reported that the shortest isoform A (CDKL-1A) localizes at the TZ (**Figures 3.1A and C**) (Canning et al., 2018). This subciliary localization was confirmed by genetically removing the TZ in the *mks-5* and *cep-290* mutants: in these mutants, CDKL-1A no longer localizes specifically at the base of the axoneme where the TZ would normally be, and instead becomes dispersed along the dendrite and axoneme (Li et al., 2016). To define the subcellular localization of other *cdkl-1* isoforms, we generated a *cdkl-1*-mNeonGreen knock-in strain using the CRISPR/CAS9 tool, which results in all of the endogenous *cdkl-1* (A, B and C) isoforms being C-terminally tagged with the mNeonGreen reporter. We found CDKL-1A/B/C proteins localize to not only the TZ, but also to the middle and the distal segments, suggesting the CDKL-1B/C isoforms localize to other ciliary subcompartments (**Figure 3.1B**). By expressing individual *cdkl-1B::gfp* and *cdkl-1C::gfp* fusion constructs, we confirmed that the B and C isoforms do not specifically accumulate at the TZ, but instead, are weakly present inside of the cilium (**Figure 3.1C**). Both isoforms are also found within the dendrite, but it possibly results from their overexpression since mNeonGreen-tagged CDKL proteins expressed from their endogenous loci do not predominantly localize to the dendrite (**Figures 3.1B** and **C**).

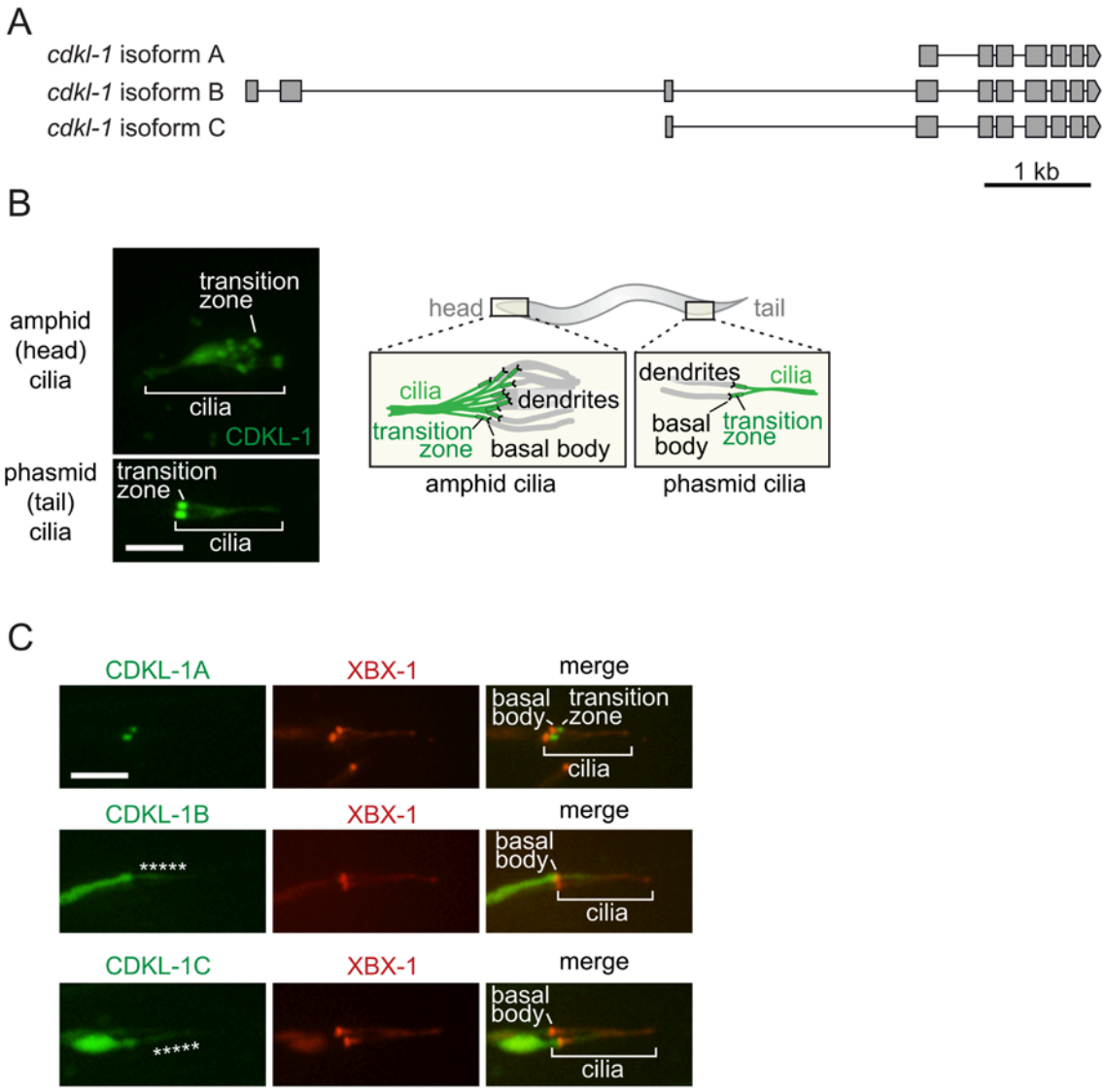

Figure 3.1 CDKL-1 protein isoforms localize to ciliary subcompartments except for the basal body. (A) Gene structures of different *cdkl-1* isoforms (A, B, and C). Exons and introns are depicted as gray boxes and solid black lines, respectively. **(B)** All three isoforms of CDKL-1 (A/B/C) tagged endogenously with mNeonGreen collectively localize to the transition zone and ciliary axoneme in amphid (head) and phasmid (tail) sensory neuron cilia (see schematic). Scale bar, 4 µm. **(C)** The overexpressed CDKL-1A isoform specifically localizes to the transition zone, whereas overexpressed CDKL-1B and CDKL-1C are found along the ciliary axoneme (asterisks) as well as within the dendrite. XBX-1 protein marks the basal body and ciliary axonemes. Scale bar, 4 µm.

The above findings suggest that the localization of CDKL-1 may not be static and restricted to the TZ. This is contrary to previous work showing by fluorescence recovery after photobleaching (FRAP) assays that TZ proteins (MKS-6, MKS-2, and TMEM-107) are largely immobile at the TZ (Lambacher et al., 2016). We therefore performed FRAP assays with different *cdkl-1* reporter strains. We found that the TZ-localized CDKL-1 proteins are not static at the TZ. When the TZ was photobleached, the strains expressing *cdkl-1A::gfp* showed a recovery within 30 seconds (**Figure 3.2A**). However, the signal in the bleached TZ area was not recovered for 15 minutes in strains carrying either CEP-290::GFP or TMEM-138::GFP, indicating that CDKL-1A proteins are less tightly anchored to the TZ than other known TZ proteins. We also examined the mobility of CDKL-1 proteins that localized within the ciliary axoneme. When the middle segments were photobleached, green fluorescence signals rapidly filled up the bleached regions, suggesting that the CDKL-1 proteins freely diffuse and/or are transported by IFT (**Figure 3.2B**). Indeed, although the data is preliminary (a small number of worms have been analyzed), we found that mNeonGreen-tagged CDKL-1 travels bidirectionally in the distal segment, with an anterograde speed of ~1.2μm/s (**Figure 3.2C**). However, the tracks of CDKL-1::mNeonGreen in the kymograph are fainter and thinner than the tracks of IFT-20::GFP, which is a core component of IFT machinery (likely present on every IFT 'train').

Together, these data suggest that CDKL-1 protein may be transported along the ciliary axoneme as an IFT cargo, rather than is a subunit of the IFT machinery. To confirm this possibility, we expressed *cdkl-1::mNeonGreen* in the temperature sensitive *che-3* (*ts-che-3*) mutant previously identified in our lab (Jensen et al., 2018). The mutation, in the IFT-dynein motor, causes a progressive disruption of retrograde IFT, and accumulation of ciliary proteins at a bulbous tip. L2-staged worms expressing *cdkl-1::mNeonGreen* (isoforms A/B/C) in the *ts-che-3 mutant* background were incubated at the non-permissive temperature (25ºC) for 48hours to disrupt retrograde IFT. Compared to the same strain maintained at the permissive temperature (15ºC), CDKL-1 proteins showed some abnormal accumulations inside of the cilia at the non-permissive temperature (**Figure 3.2D**).

Next, we questioned whether the interaction/relation between the CDKL family and IFT may be conserved in another organism. Previously, we showed that the GFP-tagged human CDKL5 proteins localize to the ciliary base and tip in RPE-1 cells

(Canning et al., 2018). Using time-laps microscopy, we discovered that CDKL5 also travels from the base to the tip in both anterograde and retrograde directions, as shown by kymograph analysis (**Figure 3.2E**). Together, these data suggest an evolutionarily conserved interaction between the CDKL protein family and the IFT family in both *C. elegans* and humans. This interaction may extend to other organisms, as *Chlamydomonas* CDKL5 abnormally localizes to the ciliary tip in the *lf* mutants, including *lf3* and *lf4*, which are known to be IFT-associated (Tam et al., 2003; Wang et al., 2019).

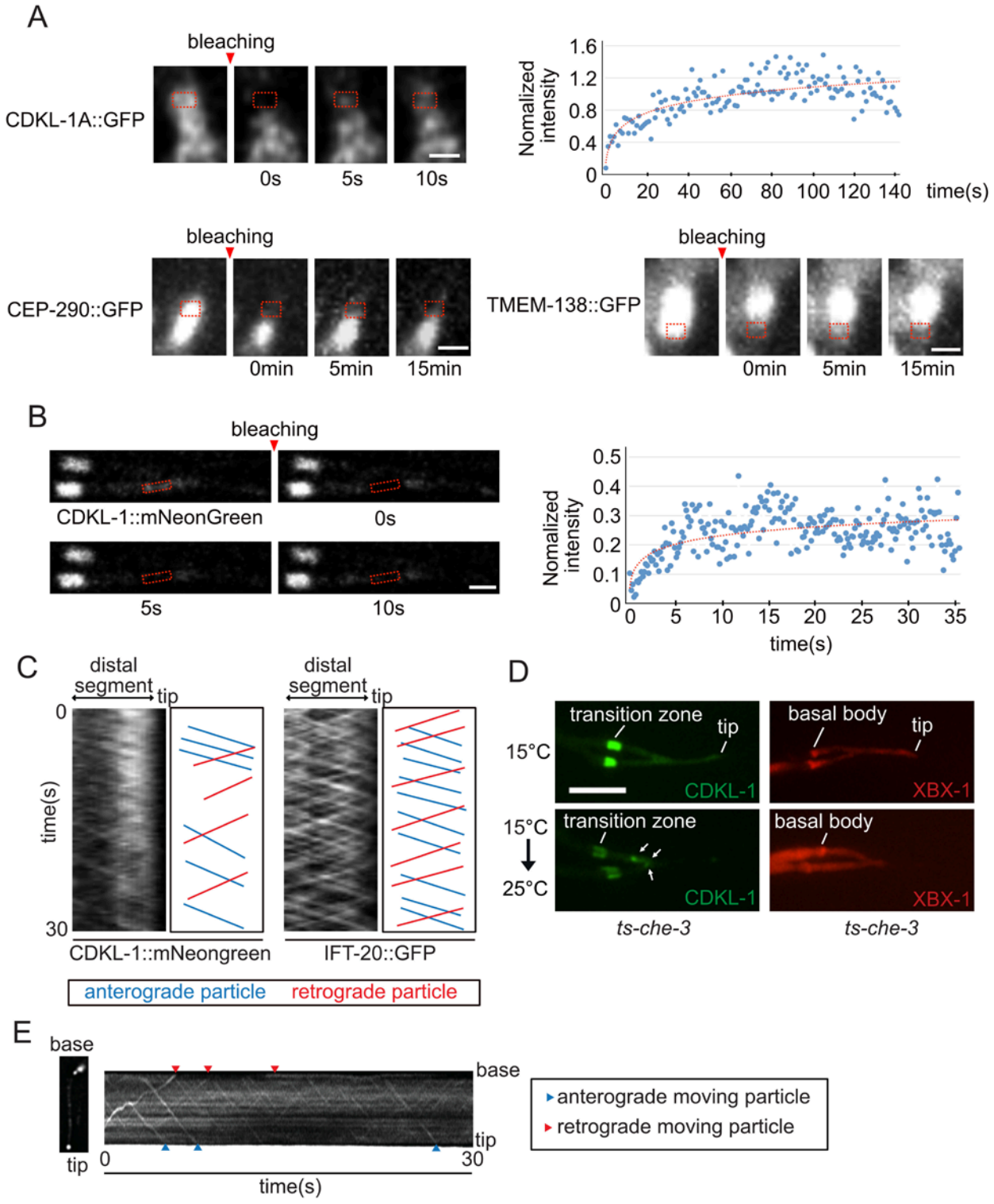
A
bleaching
CDKL-1A::GFP
0s
5s
10s
Nomalized intensity
1.6
1.2
0.8
0.4
0
0 20 40 60 80 100 120 140
time(s)
bleaching
CEP-290::GFP
0min
5min
15min
bleaching
TMEM-138::GFP
0min
5min
15min
B
bleaching
CDKL-1::mNeonGreen
0s
5s
10s
Nomalized intensity
0.5
0.4
0.3
0.2
0.1
0
0 5 10 15 20 25 30 35
time(s)
C
distal segment
tip
distal segment
tip
0
30
time(s)
CDKL-1::mNeongreen
IFT-20::GFP
anterograde particle
retrograde particle
D
15°C
transition zone
tip
CDKL-1
basal body
tip
XBX-1
15°C
25°C
transition zone
CDKL-1
basal body
XBX-1
ts-che-3
ts-che-3
E
base
tip
0
30
time(s)
base
tip
anterograde moving particle
retrograde moving particle

Figure 3.2 CDKL-1 protein is transported as a cargo by IFT. (A-B) Either the transition zone **(A)** or the middle segment **(B)** is photobleached in strains expressing indicated proteins. CDKL-1A::GFP (graph, top) and CDKL-1::mNeonGreen (graph, bottom) signals are recovered within 30 s. Pre-bleach ratios are normalized to 1. Scale bars, 0.5 μm (A) and 1 μm (B). **(C)** Distal segment kymographs of CDKL-1::mNeonGreen and IFT-20::GFP. Anterograde and retrograde IFT tracks are shown in blue and red lines, respectively. **(D)** The *ts-che-3* mutants carrying either CDKL-1::mNeonGreen or XBX-1::tdTomato are grown at the permissive (15ºC) temperature and transferred to the non-permissive (25ºC) temperature to disrupt the CHE-3 IFT retrograde motor. After incubating at the non-permissive temperature for 48 hours, XBX-1 does not move bidirectionally and CDKL-1 proteins accumulate inside of the cilia. Scale bar, 4 μm. **(E)** Serum-starved hTERT RPE-1 GFP-CDKL5 cells were imaged every 50ms for 30s. Representative kymograph showing GFP-CDKL5 particle movement along the primary cilium of a mammalian hTERT RPE-1 cell. Anterograde and retrograde moving particles are indicated by blue and red arrowheads, respectively.

To provide insights as to which IFT functional module is responsible for the ciliary localization of CDKL-1, we expressed the mNeonGreen-tagged CDKL-1 in wild-type and different IFT mutant strains. *C. elegans* IFT contains two anterograde motors: kinesin-II (the heteromeric kinesin), and OSM-3 (the homomeric kinesin-II) (**Figure 3.3**). CDKL-1 was still actively transported to the cilium, including the TZ, in kinesin-II mutant (*klp-11*); however, CDKL-1 was largely missing from the ciliary axoneme in the *osm-3* mutant (**Figure 3.3**). When the BBS protein complex, which connects the IFT-A and IFT-B complexes, is disrupted, the two anterograde motors have been shown to move separately together with the IFT-A subcomplex (kinesin-II) or the IFT-B subcomplex (OSM-3) (Pan et al., 2006). While the kinesin-II-IFT-A complex only travels between the base to the middle segments, the OSM-3-IFT-B complex moves from the base to the tip of the cilium. In the *bbs-8* mutant, the overall green fluorescence signals was slightly weaker, but the localization pattern of CDKL-1::mNeonGreen was similar to wild-type (**Figure 3.3**). This indicates that the axonemal localization of CDKL-1 largely depends on OSM-3 motor. However, CDKL-1 may be delivered to the TZ by other IFT subunits, rather than anterograde motors, or its TZ-localization is possibly IFT-independent.

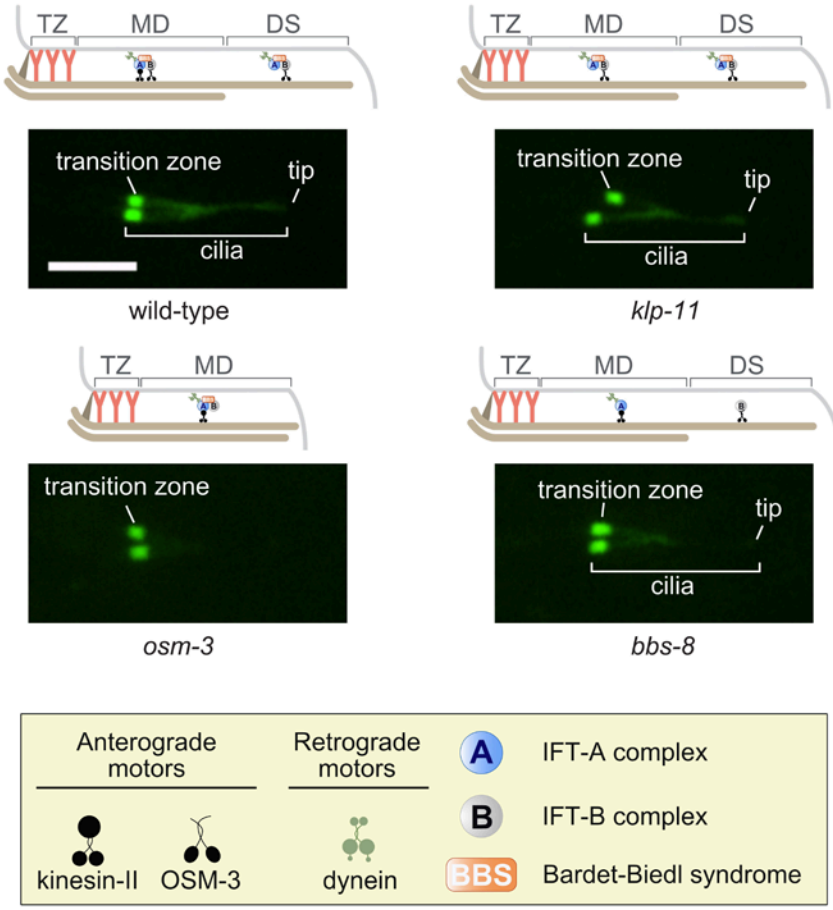

Figure 3.3 CDKL-1::mNeonGreen requires the IFT anterograde motor, OSM-3, for its axonemal localization. *cdkl-1::mNeonGreen* is expressed in wild-type, the heterotrimeric kinesin-II mutant (*klp-11*), the homomeric kinesin-II mutant (*osm-3*), and BBSome mutant (*bbs-8*). The TZ localization of CDKL-1 is not altered in all tested IFT mutants, but ciliary axonemal signals are largely absent in *osm-3* mutant animals. Scale bar, 4 μm.

3.3.2 CDKL-1 regulates the length of the middle segment by controlling IFT flux

C. elegans cdkl-1 mutant animals possess elongated cilia (Canning et al., 2018) (**Figure 3.4A**), but it is unclear which ciliary compartment gets longer. In principle, any of the ciliary compartments, including the TZ, middle segment, or distal segment, could be altered in length. To address this question, we used a strain expressing IFT-20, which marks the basal body and entire axoneme, and nephronophthisis-2 (NPHP-2), which marks the middle segment and is excluded from the TZ and distal segment (Jensen et al., 2015; Mohan et al., 2013). The markers were expressed in ADL neurons, where *cdkl-1* mutant cilia length assays have been performed. We found in the *cdkl-1* mutant, that the TZ was slightly elongated (by ~15% or 0.09 μm); most of the increased ciliary length could be accounted for by an extended middle segment (lengthened by ~39% or 1.78 μm) (**Figure 3.4A**).

This observation led us to further query the potential participation of both kinesin-II and OSM-3 anterograde IFT motors in this process, since both work cooperatively in the middle segment (OSM-3 works alone in the distal segment). In the *osm-3* mutant, which lacks the distal segment, the length of the cilium visualized with the IFT-20 marker was ~2.3μm, and the length was moderately elongated in *osm-3;cdkl-1* mutants (**Figure 3.4B**). The length of the cilium in the *kap-1* (kinesin-II) mutant, in which only the OSM-3 motor generates the anterograde movement of IFT, is similar to wild-type (**Figure 3.4C**). However, ciliary length was slightly increased in *kap-1*;*cdkl-1* double mutants, intermediate between the *kap-1* and *cdkl-1* mutants. These data support the idea that both IFT anterograde motors are required for CDKL-1-mediated cilium length regulation.

The *C. elegans* anterograde IFT train is operated by slow kinesin-II motor at the TZ. However, the IFT gradually accelerates by replacing anterograde motors from kinesin-II to OSM-3 at the handover zone which is present along the middle segment, and reaches the maximum speed at the distal segment. It has been reported that DYF-5 and DYF-18 facilitate the switching of two anterograde motors. In *C. elegans dyf-5* and *dyf-18* mutants which possess elongated cilia, kinesin-II motor abnormally enters to the distal segment (Phirke et al., 2011; Yi et al., 2018). We therefore explored whether the localization patterns of anterograde motors are altered in *cdkl-1* mutant worms. In wild-type animals, KAP-1 is mostly found at the basal body and in the proximal region of

middle segment. In contrast, KAP-1 was evenly distributed from the basal body to the distal region of the middle segment in the *cdkl-1* mutants (**Figure 3.4D**). In wild-type animals, OSM-3 is mainly localized to the distal segment (Prevo et al., 2015) (**Figure 3.4D**). However, the axonemal region predominantly occupied by OSM-3 was significantly longer in *cdkl-1* mutants, likely extending to the distal portion of the middle segment (**Figure 3.4D**). Although further additional experiments are required to investigate these phenotypes, our observations provide evidence that a property of the handover zone is modified in *cdkl-1* mutant animals.

Lastly, we examined whether CDKL-1 affects functions of the IFT machinery using GFP-tagged XBX-1, a component of the retrograde machinery. We first measured the speed of XBX-1 marker in either *xbx-1* or *xbx-1;cdkl-1* mutants. In *xbx-1* mutants, XBX-1::GFP traveled at 0.83 ±0.25 μm/s (mean ± S.D.) in the very proximal region of the middle segment (1 μm from the basal body) and at 1.19 ±0.41 μm/s in the distal segment (0.5 μm from the ciliary tip). In the absence of CDKL-1, the IFT reporter moved in those areas at the similar speed, indicating the CDKL-1 does not affect the speed of IFT machinery (**Figure 3.4E**). However, we discovered that when CDKL-1 was absent, the speed of IFT was slower in the proximal region of the middle segment (2 μm from the basal body), suggesting that the IFT machinery delays the replacement of the slow kinesin-II motor with the faster OSM-3 motor at this position. This may be explained by the handover zone being slightly shifted to the ciliary tip direction in *xbx-1;cdkl-1* mutants (**Figure 3.4D**; note how KAP-1 extends well past the base of the cilium, to the distal end of the middle segment). Additionally, we investigated the anterograde IFT flux (the numbers of IFT particles per minute) in the *xbx-1* and *xbx-1;cdkl-1* mutants, given that the IFT frequency is known to be altered in elongated cilia (Yi et al., 2018). We observed that the IFT flux was increased in *xbx-1;cdkl-1* mutants, suggesting that CDKL-1 regulates IFT entry, rather than overall IFT speed, to control the cilium length (**Figure 3.4F**).

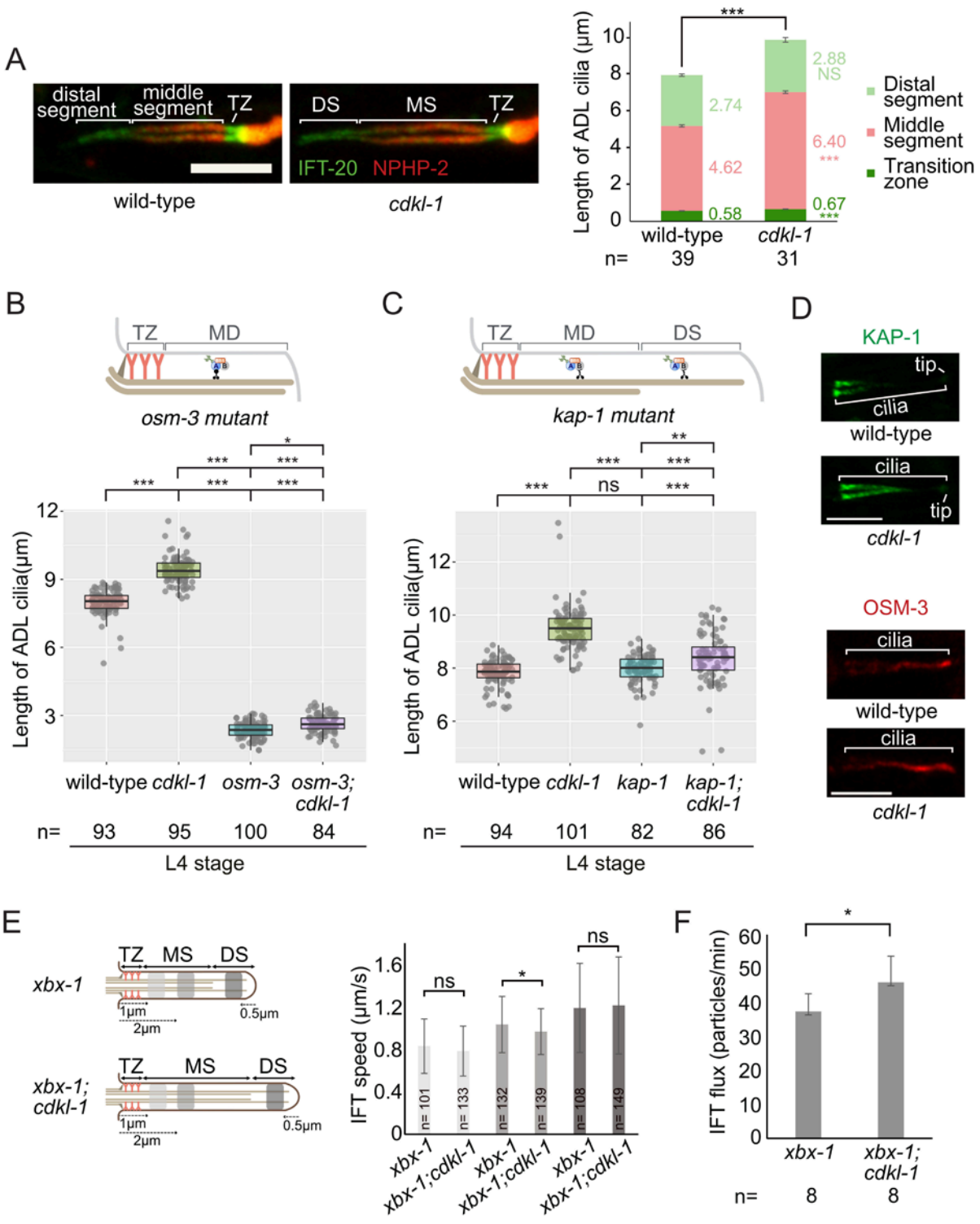
A
distal segment
middle segment
TZ
DS
MS
TZ
IFT-20
NPHP-2
wild-type
cdkl-1
Length of ADL cilia (μm)
2.74
4.62
0.58
2.88
NS
6.40
0.67
Distal segment
Middle segment
Transition zone
wild-type
cdkl-1
n=
39
31
B
TZ
MD
osm-3 mutant
Length of ADL cilia(μm)
wild-type
cdkl-1
osm-3
osm-3; cdkl-1
n=
93
95
100
84
L4 stage
C
TZ
MD
DS
kap-1 mutant
Length of ADL cilia(μm)
wild-type
cdkl-1
kap-1
kap-1; cdkl-1
n=
94
101
82
86
L4 stage
D
KAP-1
tip
cilia
wild-type
cdkl-1
OSM-3
cilia
wild-type
cdkl-1
E
xbx-1
xbx-1; cdkl-1
TZ
MS
DS
1μm
2μm
0.5μm
IFT speed (μm/s)
n= 101
n= 133
n= 132
n= 139
n= 108
n= 149
xbx-1
xbx-1;cdkl-1
F
IFT flux (particles/min)
xbx-1
xbx-1; cdkl-1
n=
8
8

Figure 3.4 *cdkl-1* mutant animals have a longer middle segment, extended kinesin-II/OSM-3 handover zone and increased IFT particle flux. (A) Length of individual subcompartments in wild-type and *cdkl-1* mutant ADL cilia (mean with standard error). NPHP-2::mCherry marks the middle segment and IFT-20::GFP represents the basal body and ciliary axoneme. The numbers of cilia analyzed are shown under the graph. DS, distal segment; MS, middle segment; TZ, transition zone. **(B-C)** Length measurement of ADL cilia in the indicated mutants. **(D)** Localization of either KAP-1::EGFP or OSM-3::mCherry in wild-type and *cdkl-1* mutant animals. Scale bar, 4 µm. **(E)** Speed of GFP-tagged XBX-1 in the middle and distal segment of either *xbx-1* or *xbx-1;cdkl-1* mutants worms. The very proximal and proximal regions of the middle segments and the distal segments (indicated by light gray, gray and dark gray in the ciliary schematics) were analyzed for IFT speeds (mean with standard deviation) and plotted in the same respective colors. The numbers of IFT tracks used for the analysis are noted in the bars. TZ, transition zone; MS, middle segment; DS, distal segment. **(F)** Eight phasmid cilia in wild-type and *cdkl-1* mutants were analyzed to obtain the flux, or numbers of IFT particles per minute (mean with standard deviation). Statistical significances were calculated using Tukey's honestly significant difference (HSD) **(A)**, Dunn's Kruskal-Wallis test [Holm-Sidak] **(B-C)**, and two-tail Student t-Test (unequal variances) **(E-F)**. *, p< 0.05; **, p< 0.005; ***, p<0.001; ns, not significant.

3.3.3 Protein kinases cooperate to fine-tune cilium length

In addition to CDKL-1, other protein kinases including DYF-5, DYF-18, NEKL-1, and NEKL-4, also negatively regulate cilium length and/or modulate the activity of IFT anterograde motors (Maurya et al., 2019; Yi et al., 2018). Therefore, we examined whether CDKL-1 functions cooperatively with these kinases, either in the same or different pathways to modulate cilium length.

First, we probed for a potential genetic interaction between CDKL-1 and DYF-5, the *C. elegans* ortholog of mammalian MAK/ICK. While IFT components improperly accumulated in the elongated cilia of *dyf-5* mutants (Burghoorn et al., 2007) (**Figure 3.5B)**, abnormal accumulation of IFT proteins was not observed in *cdkl-1* mutant animals (**Figures 2.3A, 3.4D** and **3.5A**). However, we observed that the *dyf-5;cdkl-1* double mutant has shorter cilia containing a stronger accumulation of IFT-20 proteins compared to that of the *dyf-5* single mutant (**Figure 3.5B**). We surmise that this increased accumulation of IFT particles, which prevents IFT from recycling, may be due to the increase of IFT particle entry in the *dyf-5;cdkl-1* mutants. Eventually, IFT particle entry decreases, and the imbalance of cilium assembly and disassembly causes cilium shortening. Furthermore, CDKL-1A properly localized to the TZ in *dyf-5* mutants (**Figure 3.5C**), and hence we conclude that DYF-5 and CDKL-1 regulate different aspects of IFT function that ultimately influences cilium length.

Mammalian CCRK and its orthologues in *C. elegans* and *Chlamydomonas* (DYF-18 and LF2) play roles in regulating cilium length (Maurya et al., 2019; Tam et al., 2007; Yang et al., 2013; Yi et al., 2018). Notably, LF5 (the CDKL5 orthologue in *Chlamydomonas*), enriched in the distal region of the TZ, and mislocalizes to the flagellar tip and along the axoneme in the *lf2* mutants (Tam et al., 2013). Similarly, we discovered that CDKL-1A::GFP is completely delocalized from the TZ in the *dyf-18* mutant (**Figure 3.5D**). We further investigated the localization patterns of other TZ proteins in *dyf-18* mutants, including MKS-5 and CEP-290, which are essential for the TZ localization of CDKL-1A protein itself. MKS-5 (a core TZ assembly protein), NPHP-4 (a core NPHP module protein), and CEP-290 (a core factor for MKS module proteins) all localized properly to the TZ in *dyf-18* mutant animals (**Figure 3.5E**), suggesting that loss of CDKL-1A at the TZ is not due to the absence of MKS-5 and CEP-290 proteins at the TZ. Rather, CDKL-1A likely localizes to the TZ in a DYF-18-dependent manner, implying that CDKL-1 may be a potential substrate for the DYF-18 kinase. Interestingly, DYF-18 also affects ciliary localization of DYF-5 in *C. elegans* AWA cilia (Maurya et al., 2019), indicating that DYF-18 is a functional regulator of both CDKL-1 and DYF-5 (**Figure 3.12**).

Furthermore, we measured ADL cilium length in *dyf-18* mutants and discovered that cilium length was ~9.4% increased, and the distribution of lengths was also increased, potentially owing to the considerable dysregulation of IFT in this mutant (Yi et al., 2018) (**Figure 3.5F**). Intriguingly, the cilium length was slightly elongated in *dyf-18;cdkl-1* double mutants compared to *dyf-18* single mutants (**Figure 3.5F**). This suggests that although DYF-18 is required for the TZ-localization of CDKL-1, the mislocalized CDKL-1 has not completely lost its function in *dyf-18* single mutants. Given the differences in *cdkl-1* and *dyf-18* single mutant phenotypes and the above double mutant analyses, our data suggest that CDKL-1 and DYF-18 utilize different mechanisms for cilium length control.

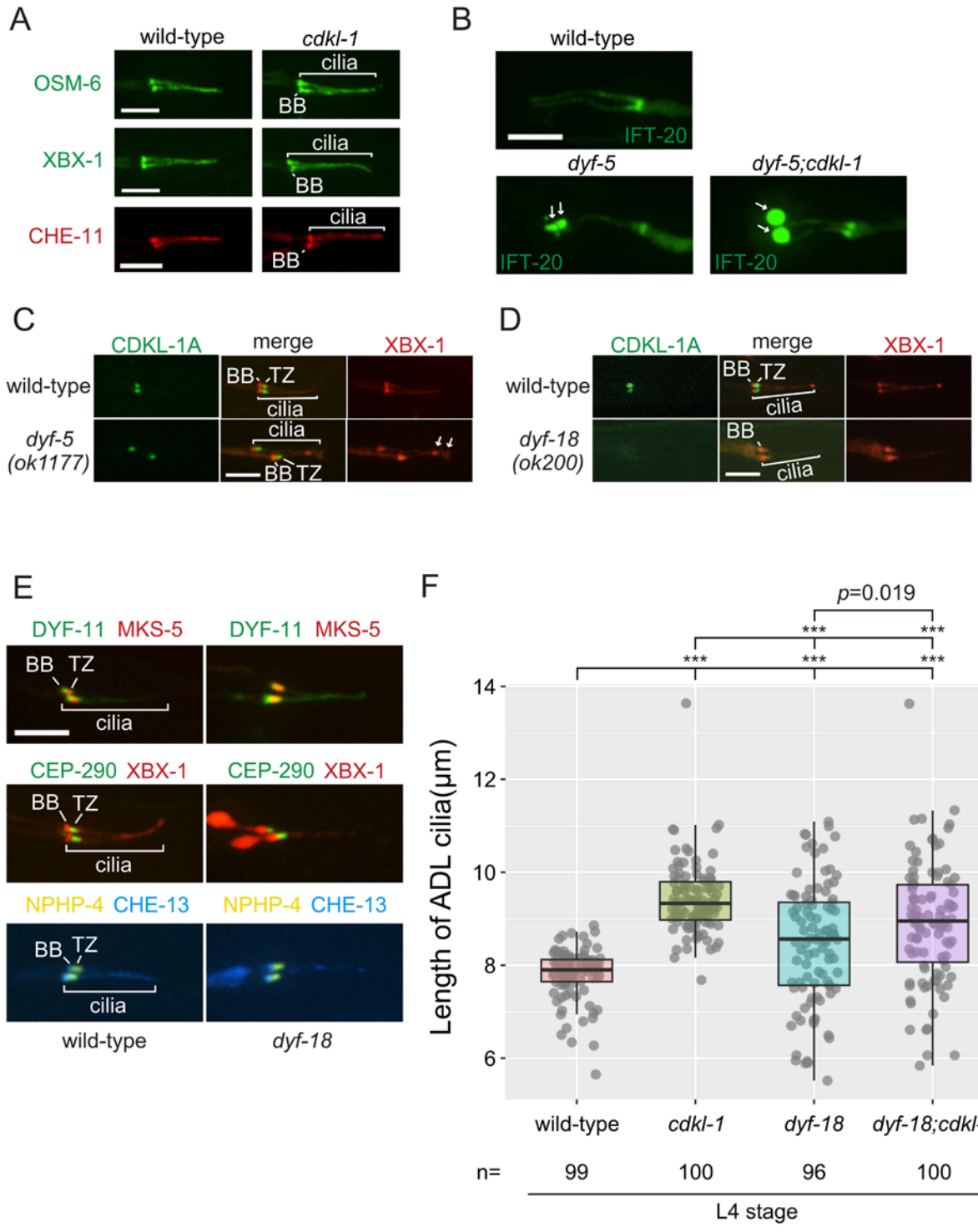
A
wild-type
cdkl-1
OSM-6
XBX-1
CHE-11
cilia
BB
B
wild-type
IFT-20
dyf-5
dyf-5;cdkl-1
C
CDKL-1A
merge
XBX-1
wild-type
dyf-5
(ok1177)
BB
TZ
cilia
D
wild-type
dyf-18
(ok200)
E
DYF-11 MKS-5
CEP-290 XBX-1
NPHP-4 CHE-13
wild-type
dyf-18
F
p=0.019
***
Length of ADL cilia(μm)
14
12
10
8
6
wild-type
cdkl-1
dyf-18
dyf-18;cdkl-1
n=
99
100
96
100
L4 stage

Figure 3.5 CDKL-1-mediated cilium length control is different from DYF-5 and DYF-18. (A) Localization patterns of indicated IFT proteins in *cdkl-1* mutant are similar to wild-type. Scale bar in **(A-E)**, 4 µm. **(B)** ADL cilia in *dyf-5;cdkl-1* mutants contain heavy accumulation (white arrows) of IFT complex B protein, IFT-20. **(C)** While XBX-1 is atypically accumulated at the tip of phasmid cilia (white arrows), CDKL-1A correctly localizes to the transition zone (TZ) in *dyf-5*(*ok1177*) mutants. BB, basal body. **(D)** CDKL-1A is largely missing from the transition zone (TZ) in *dyf-18*(*ok200*) mutants. XBX-1 is present at the basal body (BB) and extends along the ciliary axoneme. **(E)** TZ-localization of MKS-5, CEP-290, and NPHP-4 is unchanged in *dyf-18*(*ok200*) mutants. IFT proteins (DYF-11, XBX-1 and CHE-11) mark the basal body (BB) and ciliary axoneme. **(F)** ADL cilia length in wild-type and mutants (*cdkl-1*, *dyf-18* and *dyf-18;cdkl-1*). The significance was calculated using Dunn's Kruskal-Wallis test: Holm-Sidak method. One dot represents an individual cilium; ***, $p < 0.001$.

Not only CMGC group kinases, but NIMA-related kinases, including Nek8 and Nek10, are also implicated in cilium length regulation (**Figure 1.7**) (Sohara et al., 2008; Yi et al., 2018). *C. elegans* NEKL-4 is an ortholog of the mammalian Nek10. Yi and his colleagues showed that *nekl-4* mutants, carrying A486T missense mutation, moderately suppressed the short cilium length defect in the *osm-3(sa125)* kinesin mutants harboring a hinge mutation, suggesting that NEKL-4 is potentially involved in cilium length regulation (Yi et al., 2018). However, ciliary length phenotype has not been explored in a *nekl-4* loss-of-function mutant. We found that GFP-tagged NEKL-4 protein mostly accumulated at the periciliary membrane subcompartment (**Figure 3.6A**). ADL cilia of *nekl-4*(*tm4910*) mutants, harboring a deletion in the exons of the gene encoding the kinase domain, were—perhaps surprisingly—not different in length compared to wild-type (**Figures 3.6C** and **D**). Moreover, the median cilium length was similar in the *cdkl-1* mutant and *nekl-4;cdkl-1* double mutant (**Figure 3.6D**). Our data indicates that NEKL-4 is not involved in cilium length regulation. However, the A486T missense mutation possibly alters functions of NEKL-4 and affects cilium length. To test this possibility, further experiments are required.

Lastly, the kinase branch, which Nek10/NEKL-4 belongs to, also contains Nek8 and Nek9, both of which are implicated in cilium length control (**Figure 1.7**). *jck* (juvenile cystic kidneys) mice carrying Nek8 mutation have longer cilia (Sohara et al., 2008) and the fibroblasts of a Nek9 human patient with skeletal dysplasia possess short cilia (Casey et al., 2016). The worm contains one ortholog of mammalian Nek8/9, NEKL-1, which is expressed in ciliated sensory neurons (Casey et al., 2016). However, it is unclear if NEKL-1 also plays a role in cilium length modulation in *C. elegans*. We found that GFP-tagged NEKL-1 localized to dendrites and is weakly present in the ciliary

axoneme (**Figure 3.6B**). The length of ADL cilia was slightly elongated in *nekl-1* mutants (*gk516661*); notably, *nekl-1* cilium length was intermediate between the wild-type and *cdkl-1* mutant strains (**Figure 3.6C** and **D**). Remarkably, the *nekl-1;cdkl-1* double mutants had much longer cilia than the *nekl-1* or *cdkl-1* single mutants (**Figure 3.6D**). These findings suggest that CDKL-1 and NEKL-1 independently regulate ciliary length.

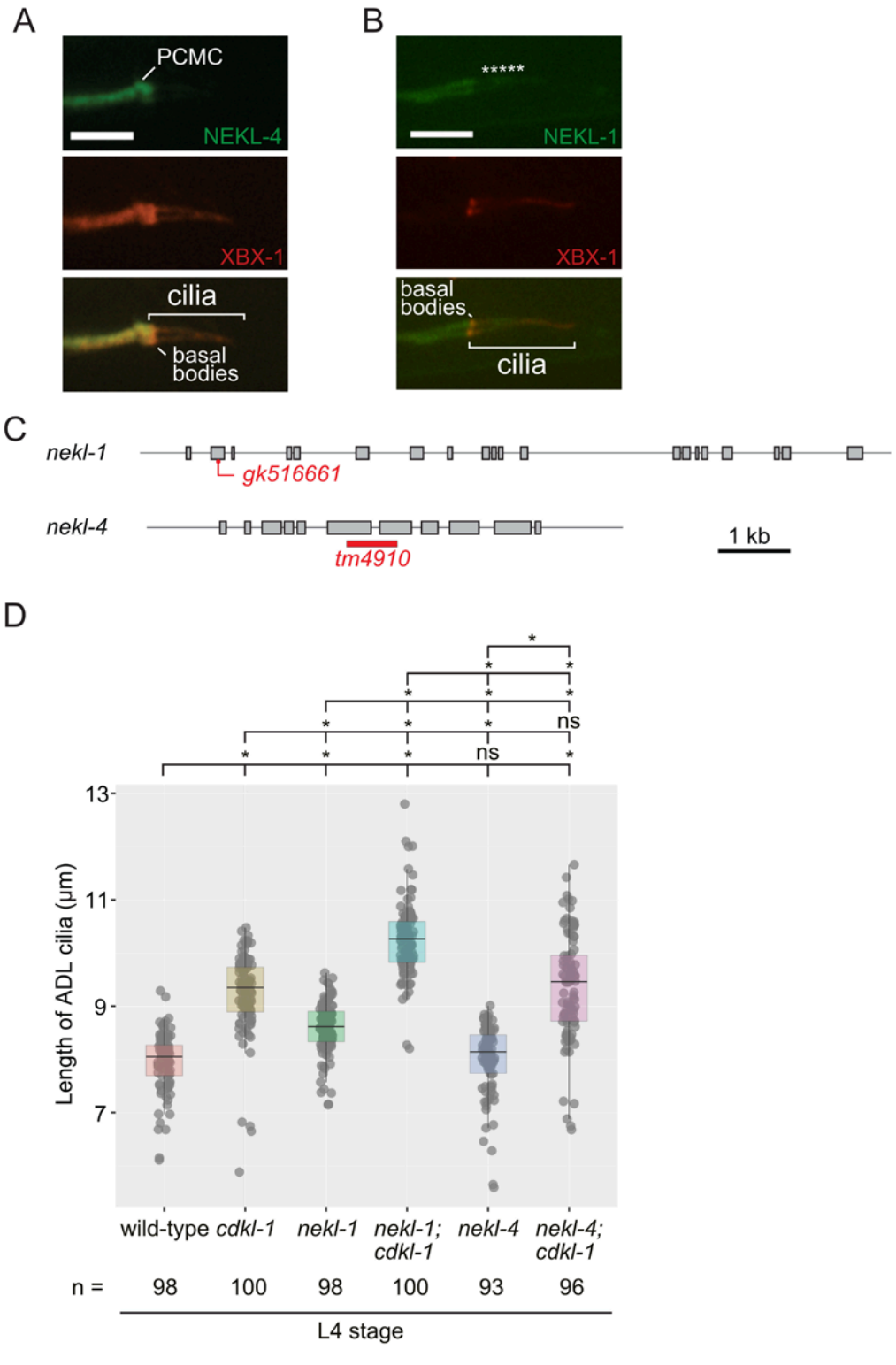
A
PCMC
NEKL-4
XBX-1
cilia
basal bodies
B
*****
NEKL-1
XBX-1
basal bodies
cilia
C
nekl-1
gk516661
nekl-4
tm4910
1 kb
D
ns
ns
Length of ADL cilia (µm)
13
11
9
7
wild-type
cdkl-1
nekl-1
nekl-1; cdkl-1
nekl-4
nekl-4; cdkl-1
n =
98
100
98
100
93
96
L4 stage

Figure 3.6 NEKL-1 negatively regulates cilium length independently from CDKL-1. (A-B) GFP-tagged NEKL-4**(A)** mostly accumulates at the periciliary membrane compartment (PCMC), whereas NEKL-1**(B)** is weakly present inside of phasmid cilia in L4-staged wild-type worms (asterisks). XBX-1 proteins mark the basal bodies and ciliary axonemes. Scale bar, 4 µm. **(C)** Gene structures of *nekl-1* and *nekl-4*, with deletion or nonsense mutants highlighted in red. **(D)** ADL cilia lengths measured in wild-type and indicated mutants. Each dot is one measured cilium. Kruskal-Wallis test (Dunn Kruskal-Wallis multiple comparison [Holm-Sidak method]) was used for significance (*p*). *, $p < 0.001$; ns, not significant.

3.3.4 KLP-13 localizes to the ciliary tip and may be involved in length modulation in non-motile cilia

CDKL-1 exerts an influence on IFT to regulate cilium length, but we cannot exclude the possibility that it also regulates the depolymerizing kinesins which induce microtubule depolymerization. Unlike other kinesin members, two depolymerizing kinesin families (the kinesin-8 and the kinesin-13) are implicated in cilium length control (Kim et al., 2015; Kobayashi et al., 2011; Miyamoto et al., 2015; Niwa et al., 2012). Mammalian Kif19A, a member of kinesin-8 family, negatively regulates motile cilium length at the ciliary tip in mice (Niwa et al., 2012). However, it is unclear whether the kinesin-8 family also regulates the length of non-motile cilia, and thus we investigated the ciliary function of KLP-13C (a *C. elegans* ortholog of KIF19A) in neuronal sensory cilia. We discovered that GFP-tagged KLP-13C was weakly present along ciliary axoneme and markedly enriched at the tip of cilia, similar to mammalian Kif19A (**Figure 3.7A**). Of two *klp-13* mutant strains (*tm3737* and *gk951285*) available, only one—*klp-13*(*tm3737*)—had mildly elongated cilia (**Figures 3.7B** and **C**).

It is possible, however, that both *klp-13* mutant strains can still produce partially functional KLP-13 proteins, and thus they do not show prominent cilium length defects. Since both CDKL-1 and KLP-13 negatively regulate the length of cilia, we further investigated if the two proteins function together in the same regulatory pathway. We therefore combined the *cdkl-1* mutant with either *klp-13* mutant, and measured ADL cilium length in both double mutant strains. Although only *klp-13*(*gk951285*);*cdkl-1* displayed a statistically significant difference, the median cilium lengths in both *klp-13;cdkl-1* strains were longer than *cdkl-1* single mutant strains (**Figure 3.7C**). We also tested whether CDKL-1 influences the localization of the depolymerizing kinesin, and found that ciliary tip enrichment of KLP-13C is not altered in the *cdkl-1* null mutant (**Figure 3.7A**). implicating that CDKL-1 and KLP-13 are distinct elements of two

separate pathways. While it may be necessary to test a clearly null *klp-13* mutant alone and in combination with the *cdkl-1* mutant, our findings suggest that CDKL-1 and KLP-13 regulate two distinct aspects of ciliary length control.

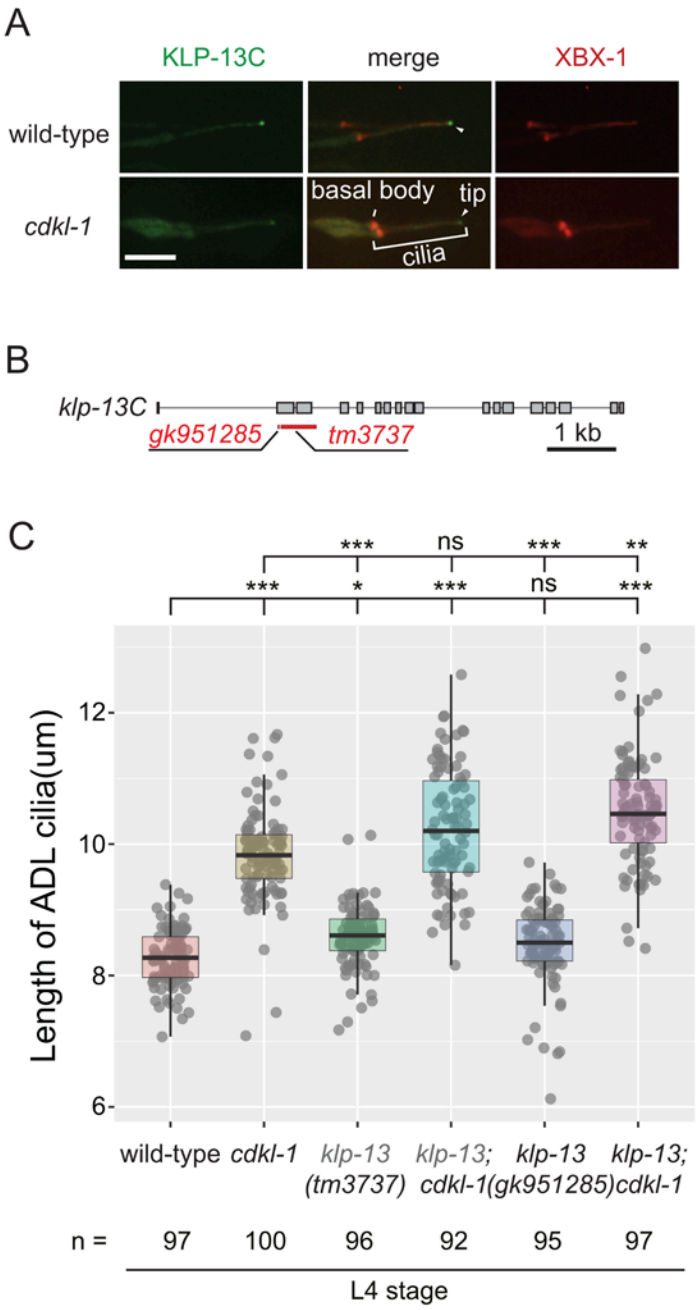

Figure 3.7 *C. elegans* KLP-13C may regulate cilium length at the ciliary tip independently from CDKL-1. (A) KLP-13C predominantly localizes to the ciliary tip in both wild-type and *cdkl-1* mutant animals. XBX-1 is used as a cilium marker. Scale bar, 4 µm. **(B)** Gene structure and potential null mutant alleles (red) of *klp-13C*. **(C)** Comparison of ADL ciliary length measurement in wild-type, *klp-13* (*tm3737* and *gk951285*) and *klp-13;cdkl-1* (*cdkl-1* with either *tm3737* or *gk951285* allele) mutants. Each dot represents one cilium. Significance (p-value) was calculated by Dunn Kruskal-Wallis multiple comparisons (Holm-Sidak adjustment). *, p <0.05; **, p <0.01; ***, p <0.001; ns, not significant.

3.3.5 KLP-7 positively controls ciliary length at the transition zone and its variants carrying KIF2A pathogenic mutations show ciliary length defects

Mammalian kinesin-13 family members (KIF2A and KIF24) have microtubule depolymerizing activity and localize at the base of primary cilia (Kobayashi et al., 2011; Miyamoto et al., 2015). KIF24 activity is regulated by a NIMA-related kinase, NEK2 (Kim et al., 2015). Moreover, the *Chlamydomonas* CDK-like (FLS1) kinase modulates the phosphorylation status of CrKinesin-13 during the shortening of distal flagella (Hu et al., 2015a). *C. elegans* has one kinesin-13 family member, KLP-7, that has been reported to localize to centrosomes and kinetochores in mitotic embryos (Han et al., 2015). However, it is unclear whether KLP-7 also localizes to the basal body ciliary apparatus and has ciliary functions.

We show that N-terminally-tagged GFP-KLP-7A predominantly accumulated at the TZ of the head and tail cilia (**Figure 3.8A**). Neither MKS nor NPHP module proteins (MKS-2 and NPHP-4, respectively) were required for the TZ localization of KLP-7A (**Figures 3.8B** and **D**). However, KLP-7A localization is partially dependent on two core TZ assembly proteins (MKS-5 and CEP-290), implying that additional proteins may be needed for the correct TZ localization of KLP-7A (**Figures 3.8B** and **D**). As CDKL-1A similarly requires MKS-5 and CEP-290 for its TZ localization, we investigated whether KLP-7A depends on CDKL-1 for its TZ localization (**Figures 3.8B** and **D**). In the absence of CDKL-1, KLP-7A still localized to the TZ (**Figure 3.8B**). Additionally, reciprocal experiment showed that the TZ localization of CDKL-1A is also independent of KLP-7 (**Figures 3.8C** and **D**). Hence, the functions of KLP-7 and CDKL-1 may be independent of each other.

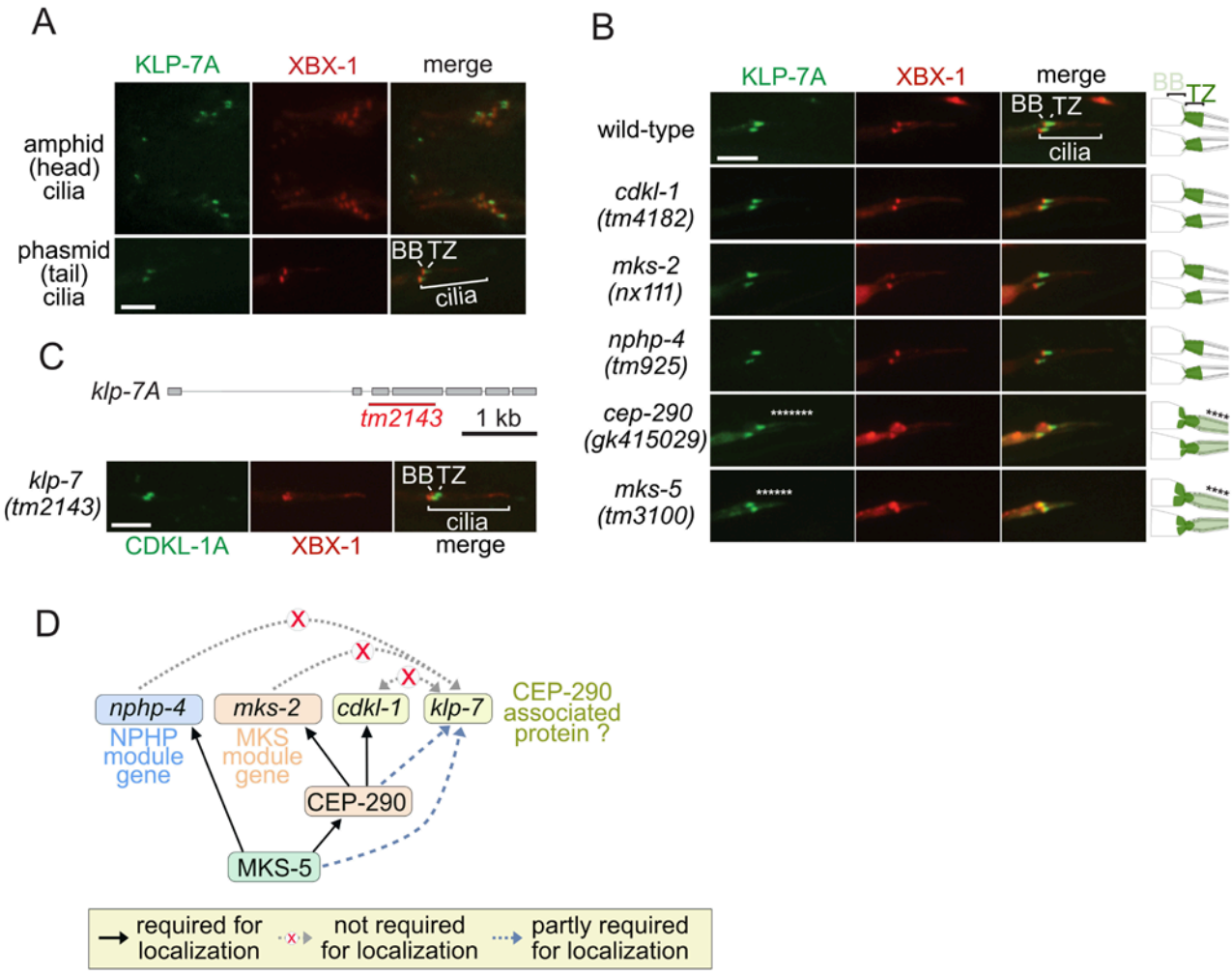

Figure 3.8 KLP-7A is a transition zone-associated protein. (A-C) GFP::KLP-7A localizes to the transition zone (TZ) in the head and tail cilia, and its TZ-localization is partially affected in *mks-5* and *cep-290* mutants (see schematic). Asterisks represent mislocalization. CDKL-1 and KLP-7 do not influence each other with respect to TZ localization. XBX-1 serves as a marker for the basal body (BB) and ciliary axoneme. Scale bar, 4µm. **(D)** Schematics showing that TZ-localization of KLP-7A is partially dependent of MKS-5 and CEP-290, but does not require the MKS, NPHP or CDKL-1 proteins.

Next, we investigated whether KLP-7 plays a role as a cilium length regulator in conjunction with CDKL-1. The *klp-7*(*tm2143*) mutant worms showed ciliary length defects (**Figure 3.9C)**. Cilia were ~25% shorter in the *klp-7* null mutant compared to wild-type and this length defect was rescued when overexpressed (**Figure 3.9D**), indicating that KLP-7 positively regulates the length of cilia. The cilium length in *klp-7;cdkl-1* double mutants was also mostly restored to the level of wild-type (**Figure 3.9C**).

Together, these data suggest that the CDKL-1 and KLP-7 proteins operate in separate pathways to exert opposite effects on cilium length regulation.

Previously, we showed that *C. elegans* CDKL-1A with corresponding CDKL5 missense mutations found in patients with epilepsy and atypical Rett syndrome caused cilium length defects, often concomitant with its mislocalization (Canning et al., 2018). Among kinesin-13 family members, two KIF2A mutations (S317N and H321D) have been reported in two unrelated patients with cortical dysplasia and microcephaly (Poirier et al., 2013). Both mutations are located near the ATP-binding pocket in the kinesin motor domain, consistent with their likely effects on motor activity. However, while KIF2A is implicated in cilium disassembly, there is no clear evidence that the brain malformations observed in the patients result from misregulation of cilium length. Since the residues are conserved in organisms from *C. elegans* to humans, we introduced the corresponding KIF2A mutations (S414N or H418D) into *C. elegans* KLP-7 to test the hypothesis that KIF2A pathogenic mutations affect the ciliary functions of KLP-7(**Figure 3.9A**). First, we determined the subcellular localization of KLP-7A variants modeling either the S414N or H418D mutation. Compared to the TZ localization of wild-type KLP-7A, both variants were delocalized to the basal body and weakly present in the TZ (**Figure 3.9B**). The KLP-7A(H418D) variants also leaked into the ciliary axoneme. Furthermore, the *klp-7(S414N)* and *klp-7(H418D)* mutant strains had short cilia to varying degrees (**Figure 3.9C**), but longer than *klp-7* null mutant animals. This suggested that the mutations do not cause a complete loss of function.

We also tested the *klp-7* patient-derived mutants in a *cdkl-1* genetic background. The cilium length was elongated in both the *klp-7(S414N);cdkl-1* and *klp-7(H418D);cdkl-1* double mutants, but shorter than the *cdkl-1* mutant (**Figure 3.9C**), confirming that both KLP-7 variants are partially functional. Together, these findings provide further evidence for CDKL-1 and a depolymerizing kinesin acting in separate pathways to regulate ciliary length, and suggests that ciliary dysfunction may lead, at least in part, to abnormal brain development in KIF2A patients—a hypothesis that will require confirmation.

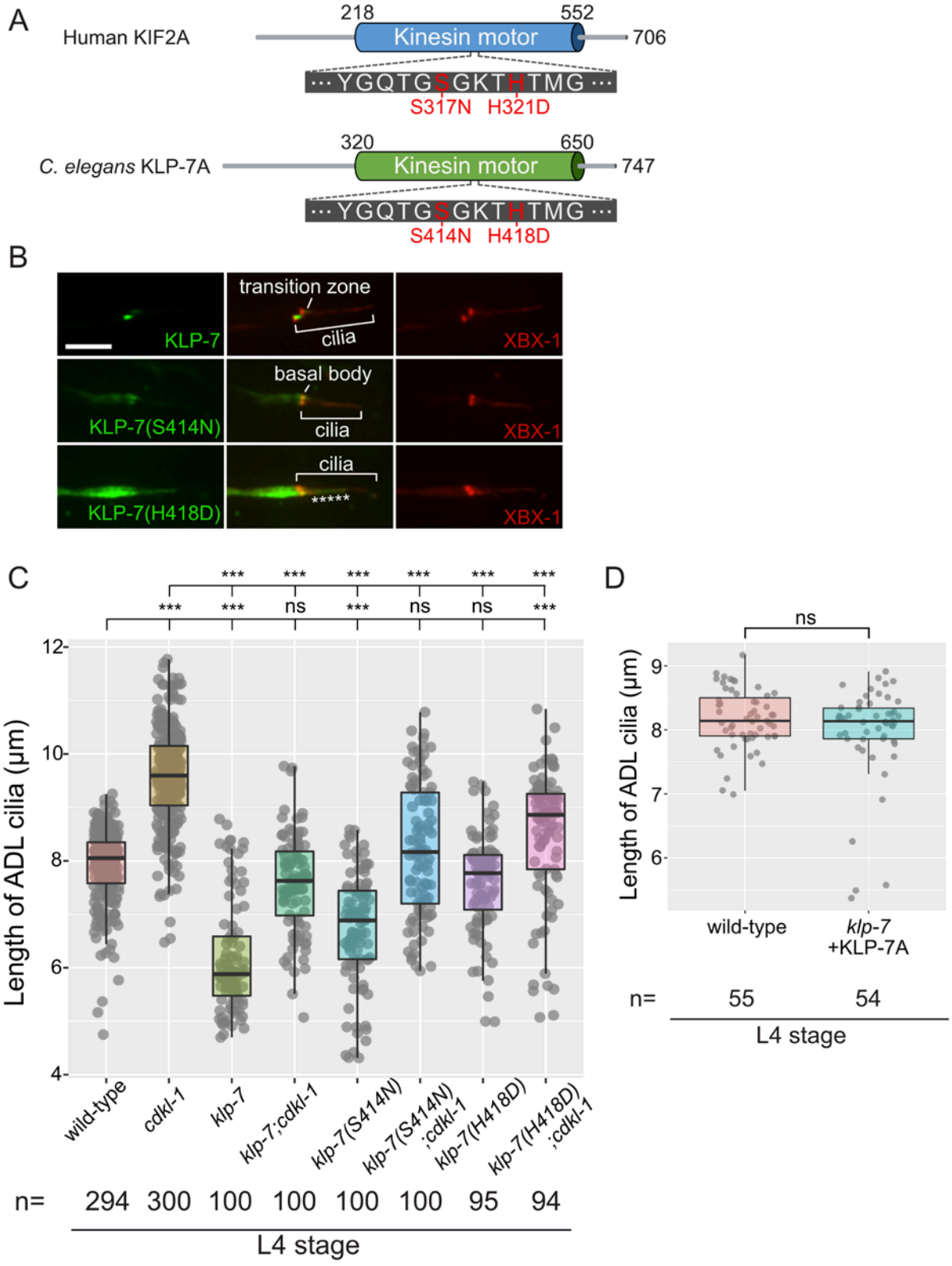
A
Human KIF2A
218
552
706
Kinesin motor
···YGQTGSGKTHTMG···
S317N
H321D
C. elegans KLP-7A
320
650
747
Kinesin motor
···YGQTGSGKTHTMG···
S414N
H418D
B
KLP-7
transition zone
cilia
XBX-1
KLP-7(S414N)
basal body
cilia
XBX-1
KLP-7(H418D)
cilia
*****
XBX-1
C
Length of ADL cilia (µm)
wild-type
cdkl-1
klp-7
klp-7;cdkl-1
klp-7(S414N)
klp-7(S414N);cdkl-1
klp-7(H418D)
klp-7(H418D);cdkl-1
n= 294 300 100 100 100 100 95 94
L4 stage
D
Length of ADL cilia (µm)
ns
wild-type
klp-7 +KLP-7A
n= 55 54
L4 stage

Figure 3.9 KLP-7 positively regulates cilium length, and pathogenic KIF2A missense mutations modeled into KLP-7 causes protein subcellular localization and ciliary length defects. (A) Two KIF2A pathogenic mutations are present in the kinesin motor domain, and their original residues are well conserved in humans and *C. elegans*. **(B)** GFP-tagged KLP-7A localizes to the transition zone, whereas KLP-7A variants harboring KIF2A patient mutations are mislocalized. XBX-1::tdTomato is used to visualize the cilia. Scale bar, 4µm. **(C-D)** Length measurements of ADL cilia in various *klp-7* and *klp-7;cdkl-1* mutants. *klp-7* mutant strains carrying corresponding KIF2A mutations were generated using the CRISPR/CAS9 tool. *klp-7* null and *klp-7* variants have shorter cilia than wild-type. However, this length phenotype is mostly rescued in double mutants. The *klp-7* mutant worms overexpressing KLP-7A has a wild-type cilium length **(D)**. Statistical significance was calculated by Dunn Kruskal-Wallis multiple comparisons with Holm-Sidak adjustment. One dot represents one cilium; ***, p <0.001; ns, not significant.

3.3.6 *cdkl-1* mutant worms show prolonged carbon dioxide avoidance behavior

Ciliary dysfunction is associated with various human sensory disorders, such as anosmia, blindness and hearing loss (Kulaga et al., 2004; Nikopoulos et al., 2016; Omori et al., 2010; Reiter and Leroux, 2017). Similarly, *C. elegans* ciliary mutants show various deficits of sensory function, such as osmosensation and gas perception, indicating defects in sensing environmental stimuli and/or signal transduction (Culotti and Russell, 1978; Hallem and Sternberg, 2008; Inglis et al., 2007). Wild-type *C. elegans* shows a cilium-associated avoidance behavior to high concentrations of sugar and carbon dioxide (CO_2) (Culotti and Russell, 1978; Hallem and Sternberg, 2008); when worms are placed inside of a high osmotic ring (8M glycerol ring) which acts as a barrier, they are not able to escape. Also, when worms are exposed to 10% CO_2, they show a rapid reversal and turns to reverse direction (avoidance response). However, some ciliary mutants, including *osm-3* which has short cilia, are defective in osmotic and CO_2 avoidance (Culotti and Russell, 1978; Hallem and Sternberg, 2008; Snow et al., 2004). *osm-3* mutant worms move freely across the barrier and exhibit reduced CO_2 avoidance compared to wild-type animals.

We therefore questioned whether *cdkl-1* mutant animals having elongated cilia have these two sensory defects. Unlike *osm-3* mutants, *cdkl-1 null* (*tm4182* and *nx132*) as well as *kinase-inactive* (*nx131*) mutant animals avoided and stayed inside of a circular 8M osmotic barrier similar to wild-type worms (**Figure 3.10A**). However, we observed that *cdkl-1* null mutant animals showed slower reversal response to CO_2 than

wild-type (**Figure 3.10B**), suggesting that dysregulation of cilium length may result in defective sensory perception, and consequently, affects the behavior of the worms. To confirm this interesting cilium-associated CO_2 phenotype, it would be useful to test other *cdkl-1* mutants and determine if their response also differs from wild-type.

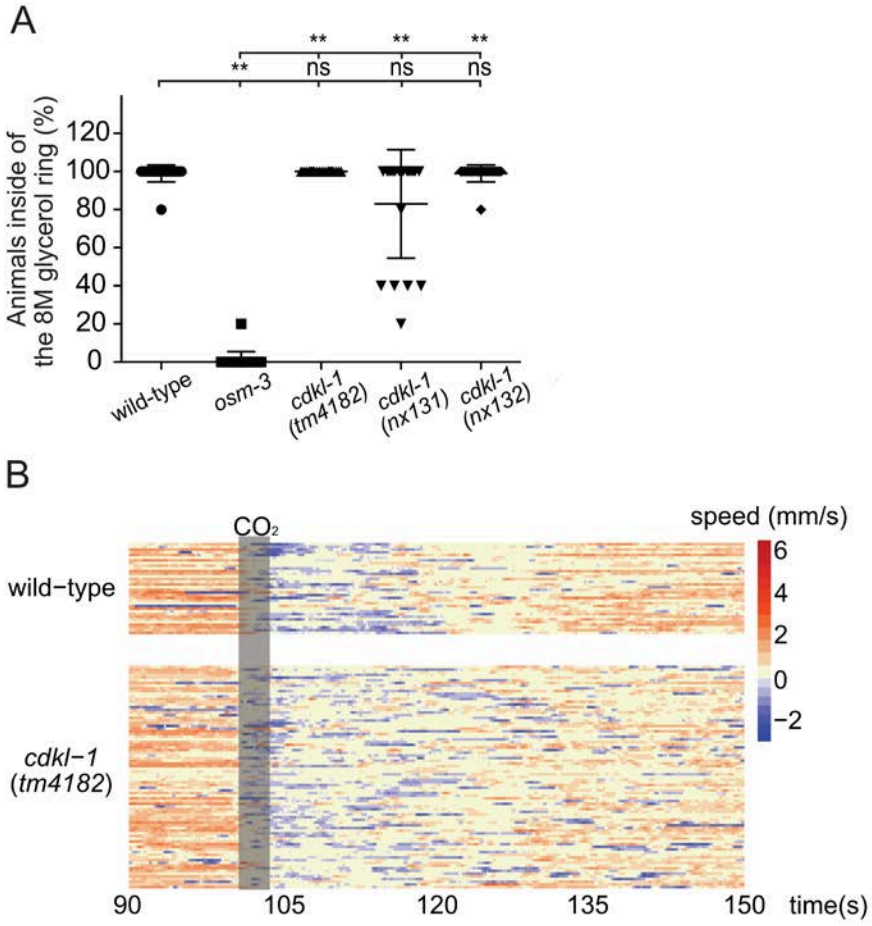

Figure 3.10 *cdkl-1* mutant worms properly avoid the high osmotic barrier, but show slow reverse movements to CO_2 exposure. (A) Osmotic avoidance behavior in wild-type, *osm-3* and *cdkl-1* mutant strains. Each dot represents 5 worms (In each strain, 100 worms are analyzed). The statistical significance was calculated by the Dunn's Kruskal-Wallis Multiple comparisons (Holm-Sidak adjustment). **, $p < 0.001$; ns, not significant. **(B)** The *cdkl-1* mutant worms show a prolonged response to CO_2 compared to wild-type. Forward movement is shown in red and reverse movement is shown in blue. Worms stop moving before changing direction and it results in zero speed.

3.3.7 *cdkl-1* loss-of-function results in a developmental (small body size) defect

Some nematode mutants with abnormal cilium length phenotypes show not only sensory, but also developmental defects (Fujiwara et al., 2002). Mutants with short cilia (*che-3, che-2*, and *osm-6*) have defective sensory functions and smaller bodies. However, it is unclear whether worms having cilium elongation also show the body size defect. To shed light into this question, we measured the overall body size and length in *cdkl-1* loss-of-function mutants. Interestingly, the *cdkl-1* mutant worms exhibit a 9% smaller body size and 8.2% smaller length than wild-type animals (**Figures 3.11A** and **B**).

We surmise that the size difference of the *cdkl-1* mutant might be due to defects in one or more cellular signaling pathways. In *C. elegans*, the transforming growth factor β (TGF-β) DBL-1 ligand pathway is known to be involved in the regulation of body size; for example, overexpressing *dbl-1* results in an increase in signaling and long body size, whereas removal of *dbl-1* causes a small body phenotype (Morita et al., 1999; Suzuki et al., 1999). We therefore investigated whether CDKL-1 regulates body size via the TGF-β DBL-1 pathway (**Figures 3.11A** and **B**). While *dbl-1*(+) animals are larger than wild-type, and *cdkl-1* mutants are smaller, *dbl-1(+);cdkl-1* double mutants exhibited an intermediate size and length. This suggests that CDKL-1 is likely to operate in a body size-regulating pathway different than TGF-β DBL-1 signaling. Consistent with this result, combining the small body size *cdkl-1* mutants with the smaller *dbl-1(nk3)* mutants resulted in even smaller-sized *dbl-1(nk3);cdkl-1* double mutants. Together, our genetic interaction experiments suggest that the developmental deficit in *cdkl-1* mutants is likely caused not by defects in the TGF-β DBL-1 signaling pathway, but rather, likely stem from alteration in other signaling pathways involved in nematode's body size regulation, including cGMP-signaling pathway.

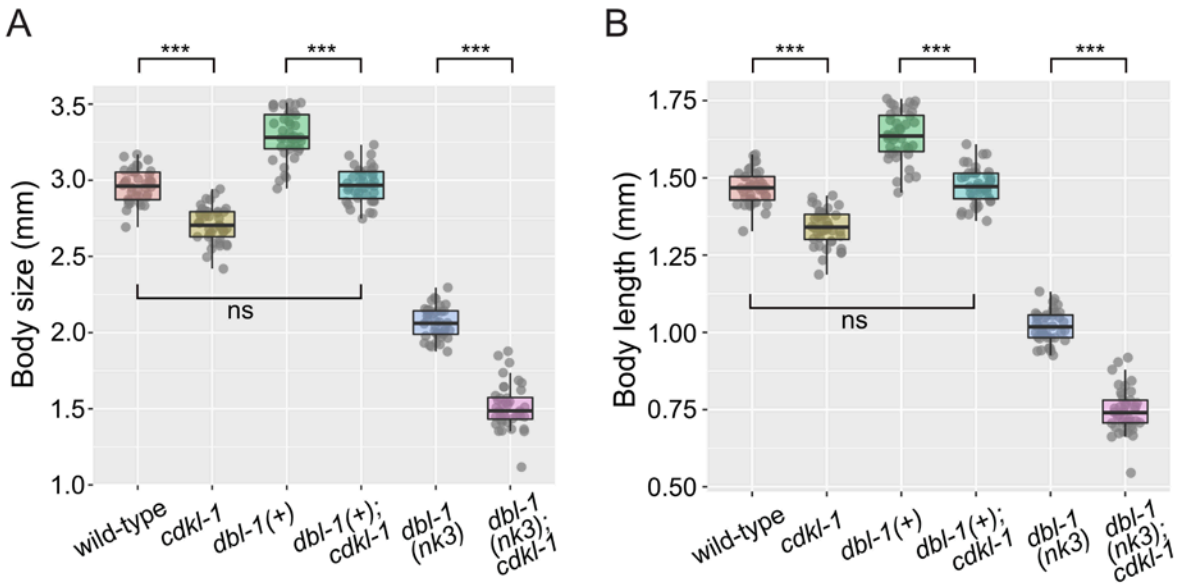

Figure 3.11 *cdkl-1* mutant animals have small bodies and it is not resulted from defects in DBL-1 TGF-β signaling pathway. (A-B) Body size (length of the perimeter of the worm body) and length (length of the midline of worm body) of *cdkl-1* mutant worms were smaller and shorter than wild-type at 48 hr after the L4 stage. Body sizes of *dlb-1(+);cdkl-1* double mutants are intermediate between *cdkl-1* and *dbl-1(+)* single mutants. *dbl-1(nk3);cdkl-1* has much smaller bodies than *dbl-1(nk3)* mutants. Tukey's honestly significant difference (HSD) was used for calculation of significance. ***, $p < 0.001$; ns, not significant.

3.4 Discussion

Model for kinase-mediated cilium length regulation in *C. elegans*

Our cellular biology and genetic interaction studies suggest that *C. elegans* sensory cilium length is regulated via several pathways and the relations among protein kinases involved in this process are complex. Although DYF-5 and CDKL-1 requires DYF-18 for their correct subcellular localization (Maurya et al., 2019) (**Figure 3.12**), these three protein kinases appear to employ distinct regulatory pathways to modulate optimal ciliary length. In both *dyf-5* and *dyf-18* mutants, IFT flux is reduced, and anterograde IFT speed in the distal segment is decreased as kinesin-II motor is not restricted to the middle segment (Yi et al., 2018). However, the major difference between the two kinases is that GFP-tagged IFT-20 accumulates at the ciliary tip in the *dyf-5* mutant, but not in *dyf-18* mutant (**Figure 3.5B**). Furthermore, the accumulation increases

and cilium length shortens in *dyf-5;cdkl-1* mutants, whereas cilia slightly elongates without abnormal protein accumulation in *dyf-18;cdkl-1* mutants, compared to *dyf-18* mutants (**Figure 3.5F**). Unlike DYF-5 and DYF-18, CDKL-1 seems to be responsible for fine-tuning of the middle segment length by regulating IFT entry, but not IFT speed (**Figure 3.12**).

C. elegans depolymerizing kinesins (KLP-13 and KLP-7) are also involved in cilium length regulation (**Figure 3.12**). However, their ciliary function as well as localization may not be regulated by CDKL-1. Instead, *C. elegans* kinesin-13 family member (KLP-7) is likely to be regulated by either Aurora kinases or NIMA-related kinases, since KLP-7 is phosphorylated by Aurora A and B *in vitro* and mammalian KIF24 activity is modulated by NEK2 (Kim et al., 2015). Interestingly, KLP-7 positively regulates cilium length, indicating that it facilitates microtubule polymerization rather than induce microtubule depolymerization in *C. elegans* sensory cilium. Such an activity by a depolymerizing kinesin is counterintuitive, but there is a precedent for this, whereby loss of *kinesin-13* in *T. thermophila* results in short cilia and decreases the cilium assembly rate (Vasudevan et al., 2015). Furthermore, our work suggests the importance of a kinesin 13 family member in human disease, as modeling patient mutations of KIF2A (human kinesin-13 family member) in KLP-7 revealed an effect on protein localization and cilium length regulation.

Lastly, we reveal *C. elegans* NIMA-related kinases (NEKL-1 and NEKL-4) are implicated in cilium length regulation through pathways that are distinct from CDKL-1 (**Figure 3.12**). These kinases may control cilium length through the IFT machinery and/or depolymerizing kinesins, and further experiments are required to address this possibility.

In brief, CMGC group kinases, NIMA-related kinases and potentially Aurora kinases function collectively to regulate cilium length by influencing the functions of IFT and/or depolymerizing kinesins in *C. elegans*. More details are discussed in **Chapter 4**.

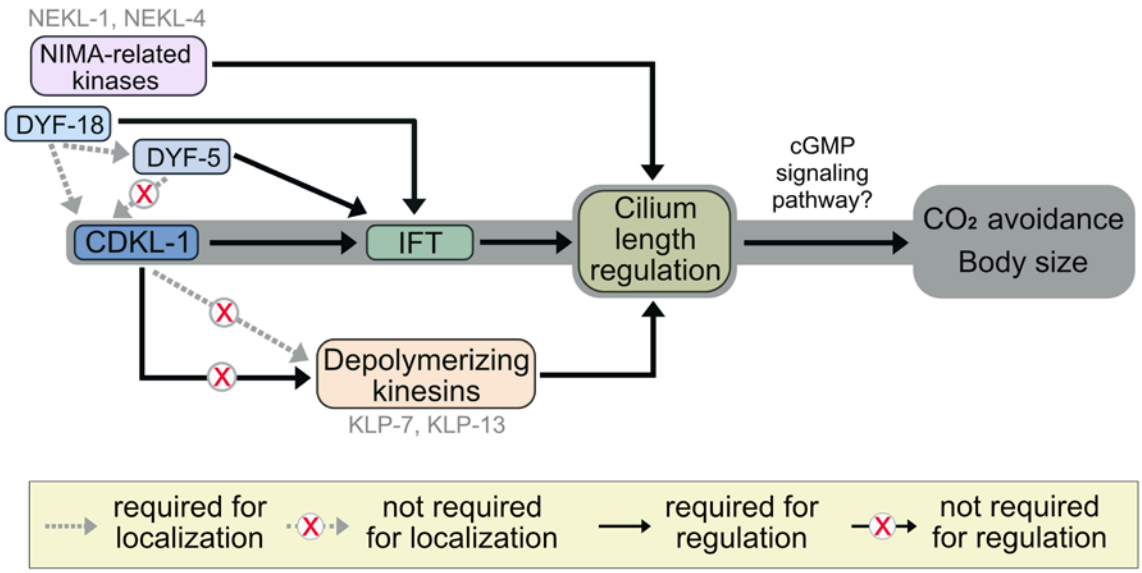

Figure 3.12 Model for kinase-mediated cilium length regulation in *C. elegans*. CDKL-1 influences the IFT machinery, but not depolymerizing kinesins to regulate cilium length. However, CDKL-1-mediated cilium length control is different from that of NIMA-related kinases, DYF-18 and DYF-5. Dysregulation of cilium length in *cdkl-1* mutants causes defects in sensory functions and worm's body development.

Possible roles of CDKL-1 in cGMP signaling pathway for CO_2 avoidance response and body size

C. elegans displays an acute avoidance response to CO_2. Ciliated neurons, including BAG, AFD, and ASE neurons (Bretscher et al., 2011; Hallem et al., 2011; Hallem and Sternberg, 2008), are important for CO_2 perception and the avoidance behavior. In particular, BAG neurons play an important role in detecting CO_2 via the receptor-type guanylate cyclase (GCY-9) and the cGMP-gated channel (TAX-2/TAX-4), both of which are localized to the BAG neuron cilia (Martinez-Velazquez and Ringstad, 2018). The cGMP-gated channel subunits (*tax-2/tax-4*) are also expressed in some of amphid channel cilia and are required for CO_2 sensing. In amphid channel cilia, TAX-2 and TAX-4 localize to the middle segment (the so-called 'inversin' compartment in vertebrate cilia) and their localization depends on NPHP-2 (Nguyen et al., 2014; Wojtyniak et al., 2013). We show *cdkl-1* mutant worms exhibit delayed avoidance

responses to CO_2 (**Figure 3.10B**). It is possible that loss of *cdkl-1* leads to perturbation of GCY-9, TAX-2, and/or TAX-4 localization in BAG and/or amphid channel cilia. One possibility is that as the middle segment is elongated in the *cdkl-1* mutant, the distribution of the cGMP-gated channel subunits is altered, and this may affect cGMP signaling, which essential for CO_2 perception and the avoidance response (**Figure 3.12**).

We also reveal that *cdkl-1* mutants have a small body, and that this phenotype does not appear to stem from defects in the DBL-1-dependent TGF-β signaling pathway, which plays an important role in body size regulation (**Figure 3.11**). As cGMP signaling, and signals from gonad and nutrients are also associated with body size regulation, CDKL-1 could modulate body size through one of these pathways. In addition to the cGMP-gated channels TAX-2/TAX-4, cGMP signaling also depends on the cGMP-dependent protein kinase (EGL-4); disrupting the activity of EGL-4 influences body size. Both *tax-2* and *tax-4* mutants have smaller bodies, whereas *egl-4* mutants have larger bodies. Although EGL-4 is responsible for small body phenotype in an IFT mutant (*che-2*), our findings suggest that CDKL-1 does not influence the activity of EGL-4 to control body size, since TGF-β DBL-1 acts downstream of EGL-4 (Fujiwara et al., 2002). Instead, CDKL-1 might modulate the cGMP-gated channel subunits (TAX-2/TAX-4), and as a result, *cdkl-1* worms have smaller bodies as well as prolonged CO_2 avoidance behavior. However, as gonadectomy and nutrient-deprivation also influence body size in *C. elegans*, we cannot exclude the possibilities that gonad and/or nutrient signals are altered in *cdkl-1* mutants.

4 Conclusions and future directions

4.1 Mechanism of CDKL-1 kinase-mediated cilium length regulation

Several different protein kinases in the CMGC group, NIMA-related kinase family, and aurora kinase family have been implicated in cilium length regulation. Most regulate the cilium length by influencing the functions of either the IFT machinery, which is essential for cilium assembly, or microtubule depolymerizing kinesin, which plays a role in cilium disassembly. Some protein kinases also control the dynamic and stability of microtubules which can induce changes to the ciliary length. The finding in 2013 that the *Chlamydomonas* ortholog of CDKL5 by the Lefebvre lab was instrumental in formulating the major hypothesis of this thesis: most if not all members of a specific branch of the CMGC kinase group are involved in cilium length control. This branch includes, in addition to CDKL5, four other cyclin-dependent kinase-like (CDKL) family members in mammals, namely CDKL1-4.

We discovered that *C. elegans* CDKL-1, whose sole CDKL protein is closely related CDKL1-4 and more distantly related CDKL5, negatively regulates the length of the ciliary axoneme middle segment. While our findings suggest that CDKL-1 influences the IFT machinery to accomplish this function, it remains unclear what the substrates of CDKL-1 are, and how the kinase specifically modulates the length of the middle segment, but not that of the distal segment.

Our findings suggest a possible mechanism. CDKL-1 may directly control the entry of IFT particles at the ciliary base (transition zone) where it localizes, rather than functions as a ‘ciliary gate’ or ‘membrane diffusion barrier’ like most other transition zone proteins. In *Chlamydomona*s, the injection rate of IFT into cilia, as well as ciliary assembly rate, increase in *lf4* (ortholog of mammalian MOK) mutants which has long cilia (Hilton et al., 2013; Ludington et al., 2013). Therefore, increasing IFT flux in *cdkl-1* mutant potentially promotes cilium assembly, since more IFT trains transport microtubule building blocks (tubulins) to the tip of the cilium. Furthermore, as the disassembly rate is raised as well in the *lf4* mutant, we speculate that the cilium disassembly rate also potentially increases in *cdkl-1* mutant. However, this elevated disassembly rate is still

lower than the assembly rate and thus the *cdkl-1* mutant worm possesses longer cilia than those of wild-type animals.

In addition to regulating the IFT flux, it is possible that CDKL-1 influences tubulin-loading on IFT particles at the transition zone. In *Chlamydomonas*, the axonemal component DRC4 is transported by IFT, and its delivery to cilia linearly decreases as ciliary length increases, suggesting that DRC4-loading on IFT trains at the flagellar base is length dependent (Wren et al., 2013). Therefore, tubulin-loading efficiency onto the IFT machinery might be elevated in the *cdkl-1* mutant, and as a result, more precursors are available at the site of cilium assembly and the cilium length increases.

Another possibility is that CDKL-1 can directly phosphorylate either or both of the IFT anterograde motors (kinesin-2 and OSM-3) to fine tune their functions. Our genetic interaction studies suggest that both anterograde motors are required for cilium elongation, and their localization patterns within cilia are altered in the *cdkl-1* mutant. In *C. elegans*, a hand-over zone, whereby IFT particles replace slowly-moving kinesin-2 motors to the faster OSM-3 motors, is present along the middle segment. Disruption of CDKL-1 causes an increase in middle segment length, which correlates with an extended hand-over zone that slows the exchange of anterograde IFT motors. CDKL-1 possibly regulates through phosphorylation how efficiently kinesin-2 can undock from the IFT train, and/or the docking of OSM-3, to generate the correct length of the middle segment.

Although CDKL-1 has observable effects on the IFT system, we cannot exclude the possibility that CDKL-1 may influence tubulin dynamics and stability, which are important for cilium assembly and disassembly, by regulating posttranslational modifications of the ciliary axoneme (*e.g.*, polyglutamylation, acetylation) and activities of microtubule associated proteins. In *C. elegans*, deletion of *dyf-5* (ortholog of mammalian MAK) or *dyf-18* (ortholog of mammalian CCRK) results in stabilization of AWA axonemal microtubules (Maurya et al., 2019). Mammalian MAK phosphorylates a tubulin-binding protein RP1, which enhances polymerization, to regulates the ciliary length. In addition, the microtubule deacetylase HDAC6 destabilizes the ciliary axoneme, and its activity is modulated by AurA.

Ultimately, understanding how CDKL-1 and other kinases regulate cilium length requires the identification of binding partners and substrates. In an effort to identify binding partners (and thus potential substrates), we are using a proximity-dependent biotin identification (BioID). This assay has been successfully used to uncover direct or indirect interacting partners, and/or adjacent proteins in various organisms, including *C. elegans* (Dang et al., 2017; Hwang and Espenshade, 2016; Mick et al., 2015; Reinke et al., 2017). An engineered pea ascorbate peroxidase (APX) harboring a single mutation (W41F) turns biotin-phenol to biotin-phenoxyl radicals in the presence of hydrogen peroxide (H_2O_2) (Martell et al., 2012; Reinke et al., 2017). These radicals have a short life span (<1ms), a small labeling radius (<20nm), and covalently react with electron-rich amino acids such as Tyrosine, Tryptophan, Histidine, and Cysteine (Rhee et al., 2013). APX-mNeonGreen knock-in strains (*cdkl-1::mNeonGreen::APX*) and APX-control strains (*cdkl-1::mNeonGreen*) have been generated using CRISPR/CAS9 and the proteins correctly localize to ciliary compartments including the TZ (**Figures 3.1B** and **4.1**). A large number of synchronized adult *C. elegans* nematodes, expressing APX-tagged CDKL-1::mNeonGreen and its control (CDKL-1::mNeonGreen) will be prepared and incubated with biotin-phenol for 1 hour. H_2O_2 will be added for 1 minute to biotinylate proteins in close spatial proximity to CDKL-1. Biotinylated proteins including potential interaction partners will be isolated with streptavidin beads and identified by mass spectrometry.

Depending on the binding partners identified—for example, IFT kinesin(s), other IFT subunits, kinases or other proteins previously implicated in ciliary functions—they may provide mechanistic insights into how their functional interactions could influence cilium length control. Identifying potential phosphorylation site(s) on binding partners would provide further molecular insights into the activities of CDKL-1. Phospho-dead, or phosphor-mimetic variants of the substrates could demonstrate direct effects of the proteins on, for example, IFT dynamics, and consequently, cilium length control.

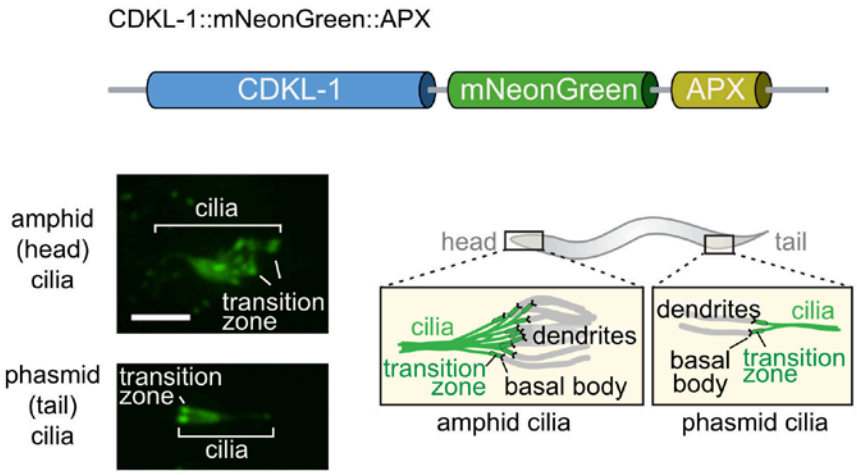

Figure 4.1 CDKL-1 localization pattern in a *cdkl-1::mNeonGreen::APX* knock-in strain mirrors that seen in CDKL-1::mNeonGreen protein. Both mNeonGreen and ascorbate peroxidase (APX) were tagged at the C-terminus of endogenous CDKL-1. The fusion proteins collectively localize to ciliary compartments except for the basal body in amphid (head) and phasmid (tail)neurons (see schematic). Scale bar, 4 μm.

4.2 Protein kinases work cooperatively for the precise cilium length regulation

DYF-18 is essential for correct cilium localization of DYF-5 in AWA cilia (Maurya et al., 2019). We also find that CDKL-1A localizes to the TZ in a DYF-18-dependent manner (**Figure 3.12**). These data suggest that DYF-18 is an upstream regulator of ciliary localization of DYF-5 and CDKL-1A. However, although three protein kinases (DYF-5, DYF-18, and CDKL-1) negatively control cilium length, the ciliary phenotypes of each mutant suggest that the length regulation mechanism of the individual kinases is different (Yi et al., 2018) (**Figures 2.3A**, **3.5B** and **3.12**). Furthermore, our genetic interaction analysis also supports this possibility.

First, the IFT-B complex protein, IFT-20, accumulates at ciliary tips, and cilia do not properly enter into the amphid channel of the *dyf-5* mutant (Burghoorn et al., 2007) (**Figure 3.5B**). These phenotypes are not observed in either *dyf-18* or *cdkl-1* mutants (Canning et al., 2018) (**Figures 2.3A**). However, in the *dyf-5;cdkl-1* double mutant, IFT-20 accumulates to a larger extent at the ciliary tip compared to the *dyf-5* single mutant

(there is no accumulation in the *cdkl-1* mutant), and the length of cilia shortens, owing to failure of recycling of functional IFT particles to the cilium base. These findings indicate that DYF-5 and CDKL-1 control different aspects of IFT functions to negatively regulates ciliary length. However, when both kinases are absent, IFT functions are greatly compromised and this results in failure of the negative regulation of ciliary length.

Moreover, cilia are longer in the *dyf-18;cdkl-1* double mutant compared to the *dyf-18* single mutant (**Figure 3.5F**). In *dyf-18* mutants, the flux and speed of IFT reduce and anterograde kinesin-2 motor abnormally enters into the distal segment (Yi et al., 2018). However, in *cdkl-1* mutants, the IFT entry into the cilia increases and velocity of IFT reduces only in the more distal region of the middle segment, resulted from slow exchange process of anterograde IFT motors (from slower-moving kinesin-2 to faster-moving OSM-3) along the elongated middle segment (**Figures 3.4E** and **F**). Unlike *dyf-18* mutants, IFT speed in the distal segment of *cdkl-1* mutant cilia is similar to that of wild-type cilia, indicating that the IFT machinery is completely handed over to OSM-3 motor before entering to the distal segment. These suggest that the two kinases work in different pathways for cilium length regulation.

We also find that NIMA-related kinase NEKL-1 (ortholog of mammalian NEK8/9) functions to negatively regulate cilium length in *C. elegans*. Our genetic interaction study further shows that NEKL-1 and CDKL-1 work in separate regulatory pathway (**Figures 3.6D and 3.12**). It still remains to be explored whether NEKL-1 modulates the activities of IFT and/or depolymerizing kinesins, or controls the stability of microtubules to maintain correct cilium length. Similar to the CMGC kinases mentioned above, NEKL-1 may influence the function of the IFT machinery. Alternatively, NEKL-1 could be an upstream regulator for depolymerizing kinesins another like the NIMA-related kinase NEK2, which promotes the activity of the depolymerizing kinesin KIF24 by phosphorylation during cilium disassembly. We also cannot rule out the possibility that NEKL-1 modifies microtubule associated proteins which regulate the stability of microtubules.

In summary, identifying the binding partners and substrates of these kinases will be required to ascertain the molecular mechanisms important for cilium length regulation. Our finding that CDKL-1 specifically influences the length of the middle segment is of great interest. Many if not all mammalian cilia have such a ‘proximal’

segment which contains doublet microtubules and the protein Inversin (NPHP2), and is followed by a distal segment containing singlet microtubules. For example, olfactory cilia have a long proximal segment followed by an even longer distal segment (Falk et al., 2015). The sequestration of certain proteins to the proximal region (*e.g.*, Inversin) may be important for the signaling functions of the cilia. The converse is likely true for the distal segment. While slightly altering the length of the proximal (middle) segment in the *cdkl-1* mutant might not be expected to be consequential, the loss of CDKL-1 affects one cilium-mediated behavior (CO_2 avoidance) and body size development. However, we cannot exclude the possibility that these specific phenotypes are due to another function of CDKL-1, perhaps unrelated to its cilium length control.

4.3 Potential link between cilium length regulation and human disorders

CDKL family members have ciliary functions

Although there is currently limited information regarding the biological functions of CDKL protein family members, our study of *C. elegans* CDKL-1, and other published work suggest a general link among CDKL family members, cilia, neurological disorders and potentially cell proliferation/cancer.

Three studies link CDKL1 to cell proliferation and tumourigenesis (Song et al., 2015; Sun et al., 2012; Tang et al., 2012), although the molecular basis for this is unclear. Interestingly, disruption of zebrafish *cdkl1* leads to several developmental phenotypes (brain and eye malformation, pericardial edema, and body axis curvature defects) that are ascribed to dysregulated sonic hedgehog signaling (Hsu et al., 2011). Such phenotypes are reminiscent of cilia function anomalies (Briscoe and Therond, 2013; Mukhopadhyay and Rohatgi, 2014), but this was not suggested or tested in this study.

CDKL2 is also potentially associated with cancer progression (Bonifaci et al., 2010; Li et al., 2014), albeit with an uncertain molecular etiology. A possible role for CDKL2 in cognition and learning is known from mouse studies (Gomi et al., 2010; Gomi et al., 1999). Aside from the expression of the gene in relevant neurons of the brain

(*e.g.*, cerebral cortex, hippocampus and amygdala), its neuronal function remains obscure.

Further evidence for CDKL family members in brain function has been obtained. CDKL3, widely expressed in the developing brain, is tentatively linked to mild mental retardation (Dubos et al., 2008) and influences the morphogenesis of neurons (dendrites) in cell culture knockdown studies (Liu et al., 2010). Similar to CDKL1 and CDKL2, a role for CDKL3 in cell proliferation is proposed (Jaluria et al., 2007).

No molecular or cellular studies on CDKL4 have been published, although one study suggests a positive correlation between CDKL4 copy number and clinical outcomes of colorectal cancer deaths in patients (Lin et al., 2015b).

Our own study suggests that a CDKL1-4-related protein from *C. elegans* functions in sensory neurons to regulate cilium length, sensory perception, and development. Investigating the roles of mammalian CDKL1, 2, 3 and 4 proteins in vertebrate systems should provide further evidence for a more general role for CDKL proteins in cilium length control. One possibility is that expansion of the CDKL protein family in vertebrates coincides with the evolution of cell type-specific functions.

Compared to CDKL1-4, CDKL5 is more extensively studied. CDKL5 plays roles in the development of dendritic spines, dendritic branching, synaptic activity, learning, and gene expression (Fuchs et al., 2014; Migaud et al., 1998; Ricciardi et al., 2012; Zhu et al., 2013). In particular, *cdkl5* mutations are linked to neurological disorders. The disorders include epileptic encephalopathy, atypical Rett syndrome, and autism (Castren et al., 2011; Scala et al., 2005; Tao et al., 2004; Weaving et al., 2004). However, although *Chlamydomonas* CDKL5 is implicated in ciliary length regulation, a ciliary role for mammalian CDKL5 has not been reported. In this study, we show that human CDKL5 localizes to primary cilia and its overexpression influences cilium formation in RPE-1 cells. How the effect on ciliogenesis may influence various aspects of dendritic development, and activity of the neuron itself, is unclear.

C. elegans KLP-7 (kinesin-13 family) positively regulates cilium length

The evolutionarily conserved kinesin-13 protein family functions as microtubule depolymerases which remove tubulins from the microtubules. This family is also involved in cilium disassembly through the depolymerizing activity (Kim et al., 2015; Kobayashi et al., 2011; Miyamoto et al., 2015). For example, mammalian kinesin-13 family KIF2A, whose mutations are associated with brain development disorders (cortical dysplasia and microcephaly), plays a role in cilium resorption at the base of cilia. In *C. elegans*, we show that KLP-7 promotes cilium assembly in sensory neurons, indicating that it controls the cilium length using an unconventional function of a microtubule depolymerizing kinesin. Our genetic interaction data suggest that KLP-7 and CDKL-1 play roles in separate regulatory pathways of cilium length control. KLP-7 is phosphorylated by Aurora A and Aurora B kinases *in vitro* and the putative phosphorylation site, S546, in KLP-7 is crucial for its function at the centrosome (Han et al., 2015). Therefore, it is possible that KLP-7 and Aurora kinases might operate together to influence ciliary length in *C. elegans* sensory neurons.

Modeling of CDKL5 and KIF2A human patient mutations

Two of the proteins implicated in cilium length control that we studied are associated with human disorders in humans, namely CDKL5 and KIF2A. As the biological effects of the patient mutations have not specifically been studied, we decided to model them in the *C. elegans* orthologs, CDKL-1 and KLP-7, respectively. Our findings revealed two potential pathogenic mechanisms that are not mutually exclusive. The first is disruption of function; *cdkl-1* null and *klp-7* null mutants have long and short cilia, respectively. CDKL-1 and KLP-7 variants carrying human patient mutations exhibit cilium length defects similar to their null mutants, when expressed in the worm. The second mechanism is protein mislocalization. For example, all tested three CDKL5 mutations cluster in its kinase domain, and two mutations results in mislocalization of CDKL-1 in *C. elegans*. Similarly, KIF2A mutations, located near the ATP-binding pocket in the kinesin motor domain, also interfere with the correct TZ-localization of KLP-7. Dissecting the relationship between protein activity and localization for ciliary length regulation will necessitate further studies.

Closing thoughts

Based largely on the phylogenetic consideration that CDKL protein family members cluster amongst a group of kinases involved in cilium length regulation, we undertook a detailed analysis of *C. elegans* CDKL-1, the sole CDKL-type kinase in this nematode. After uncovering an association between CDKL-1 and the IFT system, we expanded our analysis of other kinases, and depolymerizing kinesins, to understand how they function collectively to regulate the length of cilia. Our major finding is that *C. elegans* CDKL-1 and microtubule depolymerizing kinesin KLP-7 negatively and positively regulate ciliary length, respectively, as part of separate pathways. While other kinases, namely DYF-5 and DYF-18 also influence cilium length in an IFT-dependent manner, they appear to also act independently of CDKL-1, although loss of DYF-18 affects the localization of CDKL-1. Finally, our studies hint at an expanded role of cilium length dysregulation as the potential pathomechanism for the mammalian CDKL family and KIF2A proteins. More work on the mammalian orthologs of these proteins will be needed to reveal how their dysfunction may be relevant to human brain development and neurological disorders, including epilepsy, and potentially other cilium-associated disorders.

References

Adhiambo, C., Blisnick, T., Toutirais, G., Delannoy, E., and Bastin, P. (2009). A novel function for the atypical small G protein Rab-like 5 in the assembly of the trypanosome flagellum. J Cell Sci *122*, 834-841.

Altschul, S.F., Madden, T.L., Schaffer, A.A., Zhang, J., Zhang, Z., Miller, W., and Lipman, D.J. (1997). Gapped BLAST and PSI-BLAST: a new generation of protein database search programs. Nucleic Acids Res *25*, 3389-3402.

Ansley, S.J., Badano, J.L., Blacque, O.E., Hill, J., Hoskins, B.E., Leitch, C.C., Kim, J.C., Ross, A.J., Eichers, E.R., Teslovich, T.M*., et al.* (2003). Basal body dysfunction is a likely cause of pleiotropic Bardet-Biedl syndrome. Nature *425*, 628-633.

Archer, H.L., Evans, J., Edwards, S., Colley, J., Newbury-Ecob, R., O'Callaghan, F., Huyton, M., O'Regan, M., Tolmie, J., Sampson, J*., et al.* (2006). CDKL5 mutations cause infantile spasms, early onset seizures, and severe mental retardation in female patients. J Med Genet *43*, 729-734.

Arts, H.H., Doherty, D., van Beersum, S.E., Parisi, M.A., Letteboer, S.J., Gorden, N.T., Peters, T.A., Marker, T., Voesenek, K., Kartono, A*., et al.* (2007). Mutations in the gene encoding the basal body protein RPGRIP1L, a nephrocystin-4 interactor, cause Joubert syndrome. Nat Genet *39*, 882-888.

Asleson, C.M., and Lefebvre, P.A. (1998). Genetic analysis of flagellar length control in Chlamydomonas reinhardtii: a new long-flagella locus and extragenic suppressor mutations. Genetics *148*, 693-702.

Avasthi, P., and Marshall, W.F. (2012). Stages of ciliogenesis and regulation of ciliary length. Differentiation *83*, S30-42.

Awata, J., Takada, S., Standley, C., Lechtreck, K.F., Bellve, K.D., Pazour, G.J., Fogarty, K.E., and Witman, G.B. (2014). NPHP4 controls ciliary trafficking of membrane proteins and large soluble proteins at the transition zone. J Cell Sci *127*, 4714-4727.

Bae, Y.K., Qin, H., Knobel, K.M., Hu, J., Rosenbaum, J.L., and Barr, M.M. (2006). General and cell-type specific mechanisms target TRPP2/PKD-2 to cilia. Development *133*, 3859-3870.

Baker, S.A., Freeman, K., Luby-Phelps, K., Pazour, G.J., and Besharse, J.C. (2003). IFT20 links kinesin II with a mammalian intraflagellar transport complex that is conserved in motile flagella and sensory cilia. J Biol Chem *278*, 34211-34218.

Barr, M.M., and Sternberg, P.W. (1999). A polycystic kidney-disease gene homologue required for male mating behaviour in C. elegans. Nature *401*, 386-389.

Bengs, F., Scholz, A., Kuhn, D., and Wiese, M. (2005). LmxMPK9, a mitogen-activated protein kinase homologue affects flagellar length in Leishmania mexicana. Mol Microbiol *55*, 1606-1615.

Berbari, N.F., Lewis, J.S., Bishop, G.A., Askwith, C.C., and Mykytyn, K. (2008). Bardet-Biedl syndrome proteins are required for the localization of G protein-coupled receptors to primary cilia. Proc Natl Acad Sci U S A *105*, 4242-4246.

Berman, S.A., Wilson, N.F., Haas, N.A., and Lefebvre, P.A. (2003). A novel MAP kinase regulates flagellar length in Chlamydomonas. Curr Biol *13*, 1145-1149.

Bhogaraju, S., Cajanek, L., Fort, C., Blisnick, T., Weber, K., Taschner, M., Mizuno, N., Lamla, S., Bastin, P., Nigg, E.A*., et al.* (2013). Molecular basis of tubulin transport within the cilium by IFT74 and IFT81. Science *341*, 1009-1012.

Biasini, M., Bienert, S., Waterhouse, A., Arnold, K., Studer, G., Schmidt, T., Kiefer, F., Gallo Cassarino, T., Bertoni, M., Bordoli, L*., et al.* (2014). SWISS-MODEL: modelling protein tertiary and quaternary structure using evolutionary information. Nucleic Acids Res *42*, W252-258.

Blacque, O.E., Li, C., Inglis, P.N., Esmail, M.A., Ou, G., Mah, A.K., Baillie, D.L., Scholey, J.M., and Leroux, M.R. (2006). The WD repeat-containing protein IFTA-1 is required for retrograde intraflagellar transport. Mol Biol Cell *17*, 5053-5062.

Blacque, O.E., Perens, E.A., Boroevich, K.A., Inglis, P.N., Li, C., Warner, A., Khattra, J., Holt, R.A., Ou, G., Mah, A.K*., et al.* (2005). Functional genomics of the cilium, a sensory organelle. Curr Biol *15*, 935-941.

Blacque, O.E., Reardon, M.J., Li, C., McCarthy, J., Mahjoub, M.R., Ansley, S.J., Badano, J.L., Mah, A.K., Beales, P.L., Davidson, W.S*., et al.* (2004). Loss of C. elegans BBS-7 and BBS-8 protein function results in cilia defects and compromised intraflagellar transport. Genes Dev *18*, 1630-1642.

Blaineau, C., Tessier, M., Dubessay, P., Tasse, L., Crobu, L., Pages, M., and Bastien, P. (2007). A novel microtubule-depolymerizing kinesin involved in length control of a eukaryotic flagellum. Curr Biol *17*, 778-782.

Bonifaci, N., Gorski, B., Masojc, B., Wokolorczyk, D., Jakubowska, A., Debniak, T., Berenguer, A., Serra Musach, J., Brunet, J., Dopazo, J*., et al.* (2010). Exploring the link between germline and somatic genetic alterations in breast carcinogenesis. PLoS One *5*, e14078.

Bradley, B.A., and Quarmby, L.M. (2005). A NIMA-related kinase, Cnk2p, regulates both flagellar length and cell size in Chlamydomonas. J Cell Sci *118*, 3317-3326.

Brazelton, W.J., Amundsen, C.D., Silflow, C.D., and Lefebvre, P.A. (2001). The bld1 mutation identifies the Chlamydomonas osm-6 homolog as a gene required for flagellar assembly. Curr Biol *11*, 1591-1594.

Brenner, S. (1974). The genetics of Caenorhabditis elegans. Genetics *77*, 71-94.

Breslow, D.K., Koslover, E.F., Seydel, F., Spakowitz, A.J., and Nachury, M.V. (2013). An in vitro assay for entry into cilia reveals unique properties of the soluble diffusion barrier. J Cell Biol *203*, 129-147.

Bretscher, A.J., Kodama-Namba, E., Busch, K.E., Murphy, R.J., Soltesz, Z., Laurent, P., and de Bono, M. (2011). Temperature, oxygen, and salt-sensing neurons in C. elegans are carbon dioxide sensors that control avoidance behavior. Neuron *69*, 1099-1113.

Briscoe, J., and Therond, P.P. (2013). The mechanisms of Hedgehog signalling and its roles in development and disease. Nat Rev Mol Cell Biol *14*, 416-429.

Broekhuis, J.R., Leong, W.Y., and Jansen, G. (2013). Regulation of cilium length and intraflagellar transport. Int Rev Cell Mol Biol *303*, 101-138.

Broekhuis, J.R., Verhey, K.J., and Jansen, G. (2014). Regulation of cilium length and intraflagellar transport by the RCK-kinases ICK and MOK in renal epithelial cells. PLoS One *9*, e108470.

Burghoorn, J., Dekkers, M.P., Rademakers, S., de Jong, T., Willemsen, R., and Jansen, G. (2007). Mutation of the MAP kinase DYF-5 affects docking and undocking of kinesin-2 motors and reduces their speed in the cilia of Caenorhabditis elegans. Proc Natl Acad Sci U S A *104*, 7157-7162.

Cai, Q., Wang, W., Gao, Y., Yang, Y., Zhu, Z., and Fan, Q. (2009). Ce-wts-1 plays important roles in Caenorhabditis elegans development. FEBS Lett *583*, 3158-3164.

Canning, P., Park, K., Goncalves, J., Li, C., Howard, C.J., Sharpe, T.D., Holt, L.J., Pelletier, L., Bullock, A.N., and Leroux, M.R. (2018). CDKL Family Kinases Have Evolved Distinct Structural Features and Ciliary Function. Cell Rep *22*, 885-894.

Cao, M., Meng, D., Wang, L., Bei, S., Snell, W.J., and Pan, J. (2013). Activation loop phosphorylation of a protein kinase is a molecular marker of organelle size that dynamically reports flagellar length. Proc Natl Acad Sci U S A *110*, 12337-12342.

Carvalho-Santos, Z., Azimzadeh, J., Pereira-Leal, J.B., and Bettencourt-Dias, M. (2011). Evolution: Tracing the origins of centrioles, cilia, and flagella. J Cell Biol *194*, 165-175.

Casey, J.P., Brennan, K., Scheidel, N., McGettigan, P., Lavin, P.T., Carter, S., Ennis, S., Dorkins, H., Ghali, N., Blacque, O.E.*, et al.* (2016). Recessive NEK9 mutation causes a lethal skeletal dysplasia with evidence of cell cycle and ciliary defects. Hum Mol Genet *25*, 1824-1835.

Castren, M., Gaily, E., Tengstrom, C., Lahdetie, J., Archer, H., and Ala-Mello, S. (2011). Epilepsy caused by CDKL5 mutations. Eur J Paediatr Neurol *15*, 65-69.

Cevik, S., Sanders, A.A., Van Wijk, E., Boldt, K., Clarke, L., van Reeuwijk, J., Hori, Y., Horn, N., Hetterschijt, L., Wdowicz, A.*, et al.* (2013). Active transport and diffusion barriers restrict Joubert Syndrome-associated ARL13B/ARL-13 to an Inv-like ciliary membrane subdomain. PLoS Genet *9*, e1003977.

Chaya, T., Omori, Y., Kuwahara, R., and Furukawa, T. (2014). ICK is essential for cell type-specific ciliogenesis and the regulation of ciliary transport. EMBO J *33*, 1227-1242.

Chevenet, F., Brun, C., Banuls, A.L., Jacq, B., and Christen, R. (2006). TreeDyn: towards dynamic graphics and annotations for analyses of trees. BMC Bioinformatics *7*, 439.

Chien, A., Shih, S.M., Bower, R., Tritschler, D., Porter, M.E., and Yildiz, A. (2017). Dynamics of the IFT machinery at the ciliary tip. Elife *6*.

Chih, B., Liu, P., Chinn, Y., Chalouni, C., Komuves, L.G., Hass, P.E., Sandoval, W., and Peterson, A.S. (2011). A ciliopathy complex at the transition zone protects the cilia as a privileged membrane domain. Nat Cell Biol *14*, 61-72.

Clark, J.F., Meade, M., Ranepura, G., Hall, D.H., and Savage-Dunn, C. (2018). Caenorhabditis elegans DBL-1/BMP Regulates Lipid Accumulation via Interaction with Insulin Signaling. G3 (Bethesda) *8*, 343-351.

Coene, K.L., Mans, D.A., Boldt, K., Gloeckner, C.J., van Reeuwijk, J., Bolat, E., Roosing, S., Letteboer, S.J., Peters, T.A., Cremers, F.P.*, et al.* (2011). The ciliopathy-associated protein homologs RPGRIP1 and RPGRIP1L are linked to cilium integrity through interaction with Nek4 serine/threonine kinase. Hum Mol Genet *20*, 3592-3605.

Craige, B., Tsao, C.C., Diener, D.R., Hou, Y., Lechtreck, K.F., Rosenbaum, J.L., and Witman, G.B. (2010). CEP290 tethers flagellar transition zone microtubules to the membrane and regulates flagellar protein content. J Cell Biol *190*, 927-940.

Culotti, J.G., and Russell, R.L. (1978). Osmotic avoidance defective mutants of the nematode Caenorhabditis elegans. Genetics *90*, 243-256.

Dang, H.Q., Zhou, Q., Rowlett, V.W., Hu, H., Lee, K.J., Margolin, W., and Li, Z. (2017). Proximity Interactions among Basal Body Components in Trypanosoma brucei Identify Novel Regulators of Basal Body Biogenesis and Inheritance. MBio *8*.

Dawson, S.C., Sagolla, M.S., Mancuso, J.J., Woessner, D.J., House, S.A., Fritz-Laylin, L., and Cande, W.Z. (2007). Kinesin-13 regulates flagellar, interphase, and mitotic microtubule dynamics in Giardia intestinalis. Eukaryot Cell *6*, 2354-2364.

Delous, M., Baala, L., Salomon, R., Laclef, C., Vierkotten, J., Tory, K., Golzio, C., Lacoste, T., Besse, L., Ozilou, C.*, et al.* (2007). The ciliary gene RPGRIP1L is mutated in cerebello-oculo-renal syndrome (Joubert syndrome type B) and Meckel syndrome. Nat Genet *39*, 875-881.

Dentler, W. (2005). Intraflagellar transport (IFT) during assembly and disassembly of Chlamydomonas flagella. J Cell Biol *170*, 649-659.

Dereeper, A., Audic, S., Claverie, J.M., and Blanc, G. (2010). BLAST-EXPLORER helps you building datasets for phylogenetic analysis. BMC Evol Biol *10*, 8.

Dereeper, A., Guignon, V., Blanc, G., Audic, S., Buffet, S., Chevenet, F., Dufayard, J.F., Guindon, S., Lefort, V., Lescot, M.*, et al.* (2008). Phylogeny.fr: robust phylogenetic analysis for the non-specialist. Nucleic Acids Res *36*, W465-469.

Desai, A., Maddox, P.S., Mitchison, T.J., and Salmon, E.D. (1998). Anaphase A chromosome movement and poleward spindle microtubule flux occur At similar rates in Xenopus extract spindles. J Cell Biol *141*, 703-713.

DiBella, L.M., Park, A., and Sun, Z. (2009). Zebrafish Tsc1 reveals functional interactions between the cilium and the TOR pathway. Hum Mol Genet *18*, 595-606.

Dickinson, D.J., Pani, A.M., Heppert, J.K., Higgins, C.D., and Goldstein, B. (2015). Streamlined Genome Engineering with a Self-Excising Drug Selection Cassette. Genetics *200*, 1035-1049.

Diener, D.R., Lupetti, P., and Rosenbaum, J.L. (2015). Proteomic analysis of isolated ciliary transition zones reveals the presence of ESCRT proteins. Curr Biol *25*, 379-384.

Doroquez, D.B., Berciu, C., Anderson, J.R., Sengupta, P., and Nicastro, D. (2014). A high-resolution morphological and ultrastructural map of anterior sensory cilia and glia in Caenorhabditis elegans. Elife *3*, e01948.

Dowdle, W.E., Robinson, J.F., Kneist, A., Sirerol-Piquer, M.S., Frints, S.G., Corbit, K.C., Zaghloul, N.A., van Lijnschoten, G., Mulders, L., Verver, D.E.*, et al.* (2011). Disruption of a ciliary B9 protein complex causes Meckel syndrome. Am J Hum Genet *89*, 94-110.

Dubos, A., Pannetier, S., and Hanauer, A. (2008). Inactivation of the CDKL3 gene at 5q31.1 by a balanced t(X;5) translocation associated with nonspecific mild mental retardation. Am J Med Genet A *146A*, 1267-1279.

Edgar, R.C. (2004). MUSCLE: multiple sequence alignment with high accuracy and high throughput. Nucleic Acids Res *32*, 1792-1797.

Efimenko, E., Blacque, O.E., Ou, G., Haycraft, C.J., Yoder, B.K., Scholey, J.M., Leroux, M.R., and Swoboda, P. (2006). Caenorhabditis elegans DYF-2, an orthologue of human WDR19, is a component of the intraflagellar transport machinery in sensory cilia. Mol Biol Cell *17*, 4801-4811.

Efimenko, E., Bubb, K., Mak, H.Y., Holzman, T., Leroux, M.R., Ruvkun, G., Thomas, J.H., and Swoboda, P. (2005). Analysis of xbx genes in C. elegans. Development *132*, 1923-1934.

Endicott, S.J., and Brueckner, M. (2018). NUP98 Sets the Size-Exclusion Diffusion Limit through the Ciliary Base. Curr Biol *28*, 1643-1650 e1643.

Engel, B.D., Ishikawa, H., Wemmer, K.A., Geimer, S., Wakabayashi, K., Hirono, M., Craige, B., Pazour, G.J., Witman, G.B., Kamiya, R.*, et al.* (2012). The role of retrograde intraflagellar transport in flagellar assembly, maintenance, and function. J Cell Biol *199*, 151-167.

Falk, N., Losl, M., Schroder, N., and Giessl, A. (2015). Specialized Cilia in Mammalian Sensory Systems. Cells *4*, 500-519.

Fan, Z.C., Behal, R.H., Geimer, S., Wang, Z., Williamson, S.M., Zhang, H., Cole, D.G., and Qin, H. (2010). Chlamydomonas IFT70/CrDYF-1 is a core component of IFT particle complex B and is required for flagellar assembly. Mol Biol Cell *21*, 2696-2706.

Follit, J.A., Tuft, R.A., Fogarty, K.E., and Pazour, G.J. (2006). The intraflagellar transport protein IFT20 is associated with the Golgi complex and is required for cilia assembly. Mol Biol Cell *17*, 3781-3792.

Friedland, A.E., Tzur, Y.B., Esvelt, K.M., Colaiacovo, M.P., Church, G.M., and Calarco, J.A. (2013). Heritable genome editing in C. elegans via a CRISPR-Cas9 system. Nat Methods *10*, 741-743.

Fuchs, C., Trazzi, S., Torricella, R., Viggiano, R., De Franceschi, M., Amendola, E., Gross, C., Calza, L., Bartesaghi, R., and Ciani, E. (2014). Loss of CDKL5 impairs survival and dendritic growth of newborn neurons by altering AKT/GSK-3beta signaling. Neurobiol Dis *70*, 53-68.

Fujiwara, M., Hino, T., Miyamoto, R., Inada, H., Mori, I., Koga, M., Miyahara, K., Ohshima, Y., and Ishihara, T. (2015). The Importance of cGMP Signaling in Sensory Cilia for Body Size Regulation in Caenorhabditis elegans. Genetics *201*, 1497-1510.

Fujiwara, M., Sengupta, P., and McIntire, S.L. (2002). Regulation of body size and behavioral state of C. elegans by sensory perception and the EGL-4 cGMP-dependent protein kinase. Neuron *36*, 1091-1102.

Garcia-Gonzalo, F.R., Corbit, K.C., Sirerol-Piquer, M.S., Ramaswami, G., Otto, E.A., Noriega, T.R., Seol, A.D., Robinson, J.F., Bennett, C.L., Josifova, D.J.*, et al.* (2011). A transition zone complex regulates mammalian ciliogenesis and ciliary membrane composition. Nat Genet *43*, 776-784.

Garcia-Gonzalo, F.R., and Reiter, J.F. (2012). Scoring a backstage pass: mechanisms of ciliogenesis and ciliary access. J Cell Biol *197*, 697-709.

Garcia-Gonzalo, F.R., and Reiter, J.F. (2017). Open Sesame: How Transition Fibers and the Transition Zone Control Ciliary Composition. Cold Spring Harb Perspect Biol *9*.

Goetz, S.C., and Anderson, K.V. (2010). The primary cilium: a signalling centre during vertebrate development. Nat Rev Genet *11*, 331-344.

Gomi, H., Sassa, T., Thompson, R.F., and Itohara, S. (2010). Involvement of cyclin-dependent kinase-like 2 in cognitive function required for contextual and spatial learning in mice. Front Behav Neurosci *4*, 17.

Gomi, H., Sun, W., Finch, C.E., Itohara, S., Yoshimi, K., and Thompson, R.F. (1999). Learning induces a CDC2-related protein kinase, KKIAMRE. J Neurosci *19*, 9530-9537.

Grissom, P.M., Vaisberg, E.A., and McIntosh, J.R. (2002). Identification of a novel light intermediate chain (D2LIC) for mammalian cytoplasmic dynein 2. Mol Biol Cell *13*, 817-829.

Guindon, S., Dufayard, J.F., Lefort, V., Anisimova, M., Hordijk, W., and Gascuel, O. (2010). New algorithms and methods to estimate maximum-likelihood phylogenies: assessing the performance of PhyML 3.0. Syst Biol *59*, 307-321.

Gupta, M.L., Jr., Carvalho, P., Roof, D.M., and Pellman, D. (2006). Plus end-specific depolymerase activity of Kip3, a kinesin-8 protein, explains its role in positioning the yeast mitotic spindle. Nat Cell Biol *8*, 913-923.

Hall, D.H., and Russell, R.L. (1991). The posterior nervous system of the nematode Caenorhabditis elegans: serial reconstruction of identified neurons and complete pattern of synaptic interactions. J Neurosci *11*, 1-22.

Hallem, E.A., Spencer, W.C., McWhirter, R.D., Zeller, G., Henz, S.R., Ratsch, G., Miller, D.M., 3rd, Horvitz, H.R., Sternberg, P.W., and Ringstad, N. (2011). Receptor-type guanylate cyclase is required for carbon dioxide sensation by Caenorhabditis elegans. Proc Natl Acad Sci U S A *108*, 254-259.

Hallem, E.A., and Sternberg, P.W. (2008). Acute carbon dioxide avoidance in Caenorhabditis elegans. Proc Natl Acad Sci U S A *105*, 8038-8043.

Han, X., Adames, K., Sykes, E.M., and Srayko, M. (2015). The KLP-7 Residue S546 Is a Putative Aurora Kinase Site Required for Microtubule Regulation at the Centrosome in C. elegans. PLoS One *10*, e0132593.

Hao, L., Efimenko, E., Swoboda, P., and Scholey, J.M. (2011a). The retrograde IFT machinery of C. elegans cilia: two IFT dynein complexes? PLoS One *6*, e20995.

Hao, L., Thein, M., Brust-Mascher, I., Civelekoglu-Scholey, G., Lu, Y., Acar, S., Prevo, B., Shaham, S., and Scholey, J.M. (2011b). Intraflagellar transport delivers tubulin isotypes to sensory cilium middle and distal segments. Nat Cell Biol *13*, 790-798.

Haycraft, C.J., Banizs, B., Aydin-Son, Y., Zhang, Q., Michaud, E.J., and Yoder, B.K. (2005). Gli2 and Gli3 localize to cilia and require the intraflagellar transport protein polaris for processing and function. PLoS Genet *1*, e53.

Haycraft, C.J., Schafer, J.C., Zhang, Q., Taulman, P.D., and Yoder, B.K. (2003). Identification of CHE-13, a novel intraflagellar transport protein required for cilia formation. Exp Cell Res *284*, 251-263.

He, M., Subramanian, R., Bangs, F., Omelchenko, T., Liem, K.F., Jr., Kapoor, T.M., and Anderson, K.V. (2014). The kinesin-4 protein Kif7 regulates mammalian Hedgehog signalling by organizing the cilium tip compartment. Nat Cell Biol *16*, 663-672.

Heller, R.F., and Gordon, R.E. (1986). Chronic effects of nitrogen dioxide on cilia in hamster bronchioles. Exp Lung Res *10*, 137-152.

Hilton, L.K., Gunawardane, K., Kim, J.W., Schwarz, M.C., and Quarmby, L.M. (2013). The kinases LF4 and CNK2 control ciliary length by feedback regulation of assembly and disassembly rates. Curr Biol *23*, 2208-2214.

Hou, Y., Pazour, G.J., and Witman, G.B. (2004). A dynein light intermediate chain, D1bLIC, is required for retrograde intraflagellar transport. Mol Biol Cell *15*, 4382-4394.

Howard, P.W., Jue, S.F., and Maurer, R.A. (2013). Interaction of mouse TTC30/DYF-1 with multiple intraflagellar transport complex B proteins and KIF17. Exp Cell Res *319*, 2275-2281.

Hsu, L.S., Liang, C.J., Tseng, C.Y., Yeh, C.W., and Tsai, J.N. (2011). Zebrafish cyclin-dependent protein kinase-like 1 (zcdkl1): identification and functional characterization. Int J Mol Sci *12*, 3606-3617.

Hu, Z., Liang, Y., He, W., and Pan, J. (2015a). Cilia disassembly with two distinct phases of regulation. Cell Rep *10*, 1803-1810.

Hu, Z., Liang, Y., Meng, D., Wang, L., and Pan, J. (2015b). Microtubule-depolymerizing kinesins in the regulation of assembly, disassembly, and length of cilia and flagella. Int Rev Cell Mol Biol *317*, 241-265.

Huang, L., and Lipschutz, J.H. (2014). Cilia and polycystic kidney disease, kith and kin. Birth Defects Res C Embryo Today *102*, 174-185.

Huang, L., Szymanska, K., Jensen, V.L., Janecke, A.R., Innes, A.M., Davis, E.E., Frosk, P., Li, C., Willer, J.R., Chodirker, B.N.*, et al.* (2011). TMEM237 is mutated in individuals with a Joubert syndrome related disorder and expands the role of the TMEM family at the ciliary transition zone. Am J Hum Genet *89*, 713-730.

Huber, C., and Cormier-Daire, V. (2012). Ciliary disorder of the skeleton. Am J Med Genet C Semin Med Genet *160C*, 165-174.

Hunt-Newbury, R., Viveiros, R., Johnsen, R., Mah, A., Anastas, D., Fang, L., Halfnight, E., Lee, D., Lin, J., Lorch, A.*, et al.* (2007). High-throughput in vivo analysis of gene expression in Caenorhabditis elegans. PLoS Biol *5*, e237.

Hurd, T.W., and Hildebrandt, F. (2011). Mechanisms of nephronophthisis and related ciliopathies. Nephron Exp Nephrol *118*, e9-14.

Husson, H., Moreno, S., Smith, L.A., Smith, M.M., Russo, R.J., Pitstick, R., Sergeev, M., Ledbetter, S.R., Bukanov, N.O., Lane, M.*, et al.* (2016). Reduction of ciliary length through pharmacologic or genetic inhibition of CDK5 attenuates polycystic kidney disease in a model of nephronophthisis. Hum Mol Genet.

Hwang, J., and Espenshade, P.J. (2016). Proximity-dependent biotin labelling in yeast using the engineered ascorbate peroxidase APEX2. Biochem J *473*, 2463-2469.

Inglis, P.N., Ou, G., Leroux, M.R., and Scholey, J.M. (2007). The sensory cilia of Caenorhabditis elegans. WormBook, 1-22.

Insinna, C., Pathak, N., Perkins, B., Drummond, I., and Besharse, J.C. (2008). The homodimeric kinesin, Kif17, is essential for vertebrate photoreceptor sensory outer segment development. Dev Biol *316*, 160-170.

Iomini, C., Babaev-Khaimov, V., Sassaroli, M., and Piperno, G. (2001). Protein particles in Chlamydomonas flagella undergo a transport cycle consisting of four phases. J Cell Biol *153*, 13-24.

Iomini, C., Li, L., Esparza, J.M., and Dutcher, S.K. (2009). Retrograde intraflagellar transport mutants identify complex A proteins with multiple genetic interactions in Chlamydomonas reinhardtii. Genetics *183*, 885-896.

Ishijima, S. (2013). Regulations of microtubule sliding by Ca2+ and cAMP and their roles in forming flagellar waveforms. Cell Struct Funct *38*, 89-95.

Ishikawa, H., Ide, T., Yagi, T., Jiang, X., Hirono, M., Sasaki, H., Yanagisawa, H., Wemmer, K.A., Stainier, D.Y., Qin, H.*, et al.* (2014). TTC26/DYF13 is an intraflagellar transport protein required for transport of motility-related proteins into flagella. Elife *3*, e01566.

Ishikawa, H., and Marshall, W.F. (2017). Intraflagellar Transport and Ciliary Dynamics. Cold Spring Harb Perspect Biol *9*.

Jaluria, P., Betenbaugh, M., Konstantopoulos, K., and Shiloach, J. (2007). Enhancement of cell proliferation in various mammalian cell lines by gene insertion of a cyclin-dependent kinase homolog. BMC Biotechnol *7*, 71.

Jauregui, A.R., and Barr, M.M. (2005). Functional characterization of the C. elegans nephrocystins NPHP-1 and NPHP-4 and their role in cilia and male sensory behaviors. Exp Cell Res *305*, 333-342.

Jensen, V.L., Lambacher, N.J., Li, C., Mohan, S., Williams, C.L., Inglis, P.N., Yoder, B.K., Blacque, O.E., and Leroux, M.R. (2018). Role for intraflagellar transport in building a functional transition zone. EMBO Rep *19*.

Jensen, V.L., and Leroux, M.R. (2017). Gates for soluble and membrane proteins, and two trafficking systems (IFT and LIFT), establish a dynamic ciliary signaling compartment. Curr Opin Cell Biol *47*, 83-91.

Jensen, V.L., Li, C., Bowie, R.V., Clarke, L., Mohan, S., Blacque, O.E., and Leroux, M.R. (2015). Formation of the transition zone by Mks5/Rpgrip1L establishes a ciliary zone of exclusion (CIZE) that compartmentalises ciliary signalling proteins and controls PIP2 ciliary abundance. EMBO J *34*, 2537-2556.

Jiang, S.T., Chiou, Y.Y., Wang, E., Lin, H.K., Lee, S.P., Lu, H.Y., Wang, C.K., Tang, M.J., and Li, H. (2008). Targeted disruption of Nphp1 causes male infertility due to defects in the later steps of sperm morphogenesis in mice. Hum Mol Genet *17*, 3368-3379.

Jin, H., White, S.R., Shida, T., Schulz, S., Aguiar, M., Gygi, S.P., Bazan, J.F., and Nachury, M.V. (2010). The conserved Bardet-Biedl syndrome proteins assemble a coat that traffics membrane proteins to cilia. Cell *141*, 1208-1219.

Johnson, K.A., and Rosenbaum, J.L. (1992). Polarity of flagellar assembly in Chlamydomonas. J Cell Biol *119*, 1605-1611.

Jones, K.T., Greer, E.R., Pearce, D., and Ashrafi, K. (2009). Rictor/TORC2 regulates Caenorhabditis elegans fat storage, body size, and development through sgk-1. PLoS Biol *7*, e60.

Keady, B.T., Samtani, R., Tobita, K., Tsuchya, M., San Agustin, J.T., Follit, J.A., Jonassen, J.A., Subramanian, R., Lo, C.W., and Pazour, G.J. (2012). IFT25 links the signal-dependent movement of Hedgehog components to intraflagellar transport. Dev Cell *22*, 940-951.

Kee, H.L., Dishinger, J.F., Blasius, T.L., Liu, C.J., Margolis, B., and Verhey, K.J. (2012). A size-exclusion permeability barrier and nucleoporins characterize a ciliary pore complex that regulates transport into cilia. Nat Cell Biol *14*, 431-437.

Keeling, J., Tsiokas, L., and Maskey, D. (2016). Cellular Mechanisms of Ciliary Length Control. Cells *5*.

Kilstrup-Nielsen, C., Rusconi, L., La Montanara, P., Ciceri, D., Bergo, A., Bedogni, F., and Landsberger, N. (2012). What we know and would like to know about CDKL5 and its involvement in epileptic encephalopathy. Neural Plast *2012*, 728267.

Kim, H., Ishidate, T., Ghanta, K.S., Seth, M., Conte, D., Jr., Shirayama, M., and Mello, C.C. (2014). A co-CRISPR strategy for efficient genome editing in Caenorhabditis elegans. Genetics *197*, 1069-1080.

Kim, S., Lee, K., Choi, J.H., Ringstad, N., and Dynlacht, B.D. (2015). Nek2 activation of Kif24 ensures cilium disassembly during the cell cycle. Nat Commun *6*, 8087.

King, N., Westbrook, M.J., Young, S.L., Kuo, A., Abedin, M., Chapman, J., Fairclough, S., Hellsten, U., Isogai, Y., Letunic, I.*, et al.* (2008). The genome of the choanoflagellate Monosiga brevicollis and the origin of metazoans. Nature *451*, 783-788.

Kobayashi, T., Tsang, W.Y., Li, J., Lane, W., and Dynlacht, B.D. (2011). Centriolar kinesin Kif24 interacts with CP110 to remodel microtubules and regulate ciliogenesis. Cell *145*, 914-925.

Kozminski, K.G., Beech, P.L., and Rosenbaum, J.L. (1995). The Chlamydomonas kinesin-like protein FLA10 is involved in motility associated with the flagellar membrane. J Cell Biol *131*, 1517-1527.

Kozminski, K.G., Johnson, K.A., Forscher, P., and Rosenbaum, J.L. (1993). A motility in the eukaryotic flagellum unrelated to flagellar beating. Proc Natl Acad Sci U S A *90*, 5519-5523.

Kubo, T., Brown, J.M., Bellve, K., Craige, B., Craft, J.M., Fogarty, K., Lechtreck, K.F., and Witman, G.B. (2016). Together, the IFT81 and IFT74 N-termini form the main module for intraflagellar transport of tubulin. J Cell Sci *129*, 2106-2119.

Kulaga, H.M., Leitch, C.C., Eichers, E.R., Badano, J.L., Lesemann, A., Hoskins, B.E., Lupski, J.R., Beales, P.L., Reed, R.R., and Katsanis, N. (2004). Loss of BBS proteins causes anosmia in humans and defects in olfactory cilia structure and function in the mouse. Nat Genet *36*, 994-998.

Lambacher, N.J., Bruel, A.L., van Dam, T.J., Szymanska, K., Slaats, G.G., Kuhns, S., McManus, G.J., Kennedy, J.E., Gaff, K., Wu, K.M.*, et al.* (2016). TMEM107 recruits ciliopathy proteins to subdomains of the ciliary transition zone and causes Joubert syndrome. Nat Cell Biol *18*, 122-131.

Lechtreck, K.F., Johnson, E.C., Sakai, T., Cochran, D., Ballif, B.A., Rush, J., Pazour, G.J., Ikebe, M., and Witman, G.B. (2009). The Chlamydomonas reinhardtii BBSome is an IFT cargo required for export of specific signaling proteins from flagella. J Cell Biol *187*, 1117-1132.

Lee, J., and Chung, Y.D. (2015). Ciliary subcompartments: how are they established and what are their functions? BMB Rep *48*, 380-387.

Li, C., Jensen, V.L., Park, K., Kennedy, J., Garcia-Gonzalo, F.R., Romani, M., De Mori, R., Bruel, A.L., Gaillard, D., Doray, B.*, et al.* (2016). MKS5 and CEP290 Dependent Assembly Pathway of the Ciliary Transition Zone. PLoS Biol *14*, e1002416.

Li, L., Liu, C., Amato, R.J., Chang, J.T., Du, G., and Li, W. (2014). CDKL2 promotes epithelial-mesenchymal transition and breast cancer progression. Oncotarget *5*, 10840-10853.

Li, Y., Wei, Q., Zhang, Y., Ling, K., and Hu, J. (2010). The small GTPases ARL-13 and ARL-3 coordinate intraflagellar transport and ciliogenesis. J Cell Biol *189*, 1039-1051.

Liang, Y., Pang, Y., Wu, Q., Hu, Z., Han, X., Xu, Y., Deng, H., and Pan, J. (2014). FLA8/KIF3B phosphorylation regulates kinesin-II interaction with IFT-B to control IFT entry and turnaround. Dev Cell *30*, 585-597.

Lin, H., Nauman, N.P., Albee, A.J., Hsu, S., and Dutcher, S.K. (2013a). New mutations in flagellar motors identified by whole genome sequencing in Chlamydomonas. Cilia *2*, 14.

Lin, H., Zhang, Z., Guo, S., Chen, F., Kessler, J.M., Wang, Y.M., and Dutcher, S.K. (2015a). A NIMA-Related Kinase Suppresses the Flagellar Instability Associated with the Loss of Multiple Axonemal Structures. PLoS Genet *11*, e1005508.

Lin, M., Zhang, Y., Li, A., Tang, E., Peng, J., Tang, W., Zhang, Y., Lu, L., Xiao, Y., Wei, Q.*, et al.* (2015b). High-throughput RNAi screening of human kinases identifies predictors of clinical outcome in colorectal cancer patients treated with oxaliplatin. Oncotarget *6*, 16774-16785.

Lin, Y.C., Niewiadomski, P., Lin, B., Nakamura, H., Phua, S.C., Jiao, J., Levchenko, A., Inoue, T., Rohatgi, R., and Inoue, T. (2013b). Chemically inducible diffusion trap at cilia reveals molecular sieve-like barrier. Nat Chem Biol *9*, 437-443.

Liu, Z., Xu, D., Zhao, Y., and Zheng, J. (2010). Non-syndromic mild mental retardation candidate gene CDKL3 regulates neuronal morphogenesis. Neurobiol Dis *39*, 242-251.

Ludington, W.B., Wemmer, K.A., Lechtreck, K.F., Witman, G.B., and Marshall, W.F. (2013). Avalanche-like behavior in ciliary import. Proc Natl Acad Sci U S A *110*, 3925-3930.

Mahjoub, M.R., Montpetit, B., Zhao, L., Finst, R.J., Goh, B., Kim, A.C., and Quarmby, L.M. (2002). The FA2 gene of Chlamydomonas encodes a NIMA family kinase with roles in cell cycle progression and microtubule severing during deflagellation. J Cell Sci *115*, 1759-1768.

Mahjoub, M.R., Qasim Rasi, M., and Quarmby, L.M. (2004). A NIMA-related kinase, Fa2p, localizes to a novel site in the proximal cilia of Chlamydomonas and mouse kidney cells. Mol Biol Cell *15*, 5172-5186.

Mahjoub, M.R., Trapp, M.L., and Quarmby, L.M. (2005). NIMA-related kinases defective in murine models of polycystic kidney diseases localize to primary cilia and centrosomes. J Am Soc Nephrol *16*, 3485-3489.

Marshall, W.F., and Rosenbaum, J.L. (2001). Intraflagellar transport balances continuous turnover of outer doublet microtubules: implications for flagellar length control. J Cell Biol *155*, 405-414.

Martell, J.D., Deerinck, T.J., Sancak, Y., Poulos, T.L., Mootha, V.K., Sosinsky, G.E., Ellisman, M.H., and Ting, A.Y. (2012). Engineered ascorbate peroxidase as a genetically encoded reporter for electron microscopy. Nat Biotechnol *30*, 1143-1148.

Martinez-Velazquez, L.A., and Ringstad, N. (2018). Antagonistic regulation of trafficking to Caenorhabditis elegans sensory cilia by a Retinal Degeneration 3 homolog and retromer. Proc Natl Acad Sci U S A *115*, E438-E447.

Maskey, D., Marlin, M.C., Kim, S., Kim, S., Ong, E.C., Li, G., and Tsiokas, L. (2015). Cell cycle-dependent ubiquitylation and destruction of NDE1 by CDK5-FBW7 regulates ciliary length. EMBO J *34*, 2424-2440.

Massinen, S., Hokkanen, M.E., Matsson, H., Tammimies, K., Tapia-Paez, I., Dahlstrom-Heuser, V., Kuja-Panula, J., Burghoorn, J., Jeppsson, K.E., Swoboda, P.*, et al.* (2011). Increased expression of the dyslexia candidate gene DCDC2 affects length and signaling of primary cilia in neurons. PLoS One *6*, e20580.

Maurya, A.K., Rogers, T., and Sengupta, P. (2019). A CCRK and a MAK Kinase Modulate Cilia Branching and Length via Regulation of Axonemal Microtubule Dynamics in Caenorhabditis elegans. Curr Biol *29*, 1286-1300 e1284.

May-Simera, H.L., and Kelley, M.W. (2012). Cilia, Wnt signaling, and the cytoskeleton. Cilia *1*, 7.

May, S.R., Ashique, A.M., Karlen, M., Wang, B., Shen, Y., Zarbalis, K., Reiter, J., Ericson, J., and Peterson, A.S. (2005). Loss of the retrograde motor for IFT disrupts localization of Smo to cilia and prevents the expression of both activator and repressor functions of Gli. Dev Biol *287*, 378-389.

McCulloch, D., and Gems, D. (2003). Body size, insulin/IGF signaling and aging in the nematode Caenorhabditis elegans. Exp Gerontol *38*, 129-136.

McKay, S.J., Johnsen, R., Khattra, J., Asano, J., Baillie, D.L., Chan, S., Dube, N., Fang, L., Goszczynski, B., Ha, E.*, et al.* (2003). Gene expression profiling of cells, tissues, and developmental stages of the nematode C. elegans. Cold Spring Harb Symp Quant Biol *68*, 159-169.

Meng, D., and Pan, J. (2016). A NIMA-related kinase, CNK4, regulates ciliary stability and length. Mol Biol Cell *27*, 838-847.

Mick, D.U., Rodrigues, R.B., Leib, R.D., Adams, C.M., Chien, A.S., Gygi, S.P., and Nachury, M.V. (2015). Proteomics of Primary Cilia by Proximity Labeling. Dev Cell *35*, 497-512.

Migaud, M., Charlesworth, P., Dempster, M., Webster, L.C., Watabe, A.M., Makhinson, M., He, Y., Ramsay, M.F., Morris, R.G., Morrison, J.H.*, et al.* (1998). Enhanced long-term potentiation and impaired learning in mice with mutant postsynaptic density-95 protein. Nature *396*, 433-439.

Miki, H., Okada, Y., and Hirokawa, N. (2005). Analysis of the kinesin superfamily: insights into structure and function. Trends Cell Biol *15*, 467-476.

Mitchison, H.M., and Valente, E.M. (2017). Motile and non-motile cilia in human pathology: from function to phenotypes. J Pathol *241*, 294-309.

Miyamoto, T., Hosoba, K., Ochiai, H., Royba, E., Izumi, H., Sakuma, T., Yamamoto, T., Dynlacht, B.D., and Matsuura, S. (2015). The Microtubule-Depolymerizing Activity of a Mitotic Kinesin Protein KIF2A Drives Primary Cilia Disassembly Coupled with Cell Proliferation. Cell Rep *10*, 664-673.

Mohan, S., Timbers, T.A., Kennedy, J., Blacque, O.E., and Leroux, M.R. (2013). Striated rootlet and nonfilamentous forms of rootletin maintain ciliary function. Curr Biol *23*, 2016-2022.

Moon, H., Song, J., Shin, J.O., Lee, H., Kim, H.K., Eggenschwiller, J.T., Bok, J., and Ko, H.W. (2014). Intestinal cell kinase, a protein associated with endocrine-cerebro-osteodysplasia syndrome, is a key regulator of cilia length and Hedgehog signaling. Proc Natl Acad Sci U S A *111*, 8541-8546.

Morita, K., Chow, K.L., and Ueno, N. (1999). Regulation of body length and male tail ray pattern formation of Caenorhabditis elegans by a member of TGF-beta family. Development *126*, 1337-1347.

Mukhopadhyay, S., and Rohatgi, R. (2014). G-protein-coupled receptors, Hedgehog signaling and primary cilia. Semin Cell Dev Biol *33*, 63-72.

Mukhopadhyay, S., Wen, X., Chih, B., Nelson, C.D., Lane, W.S., Scales, S.J., and Jackson, P.K. (2010). TULP3 bridges the IFT-A complex and membrane phosphoinositides to promote trafficking of G protein-coupled receptors into primary cilia. Genes Dev *24*, 2180-2193.

Nachury, M.V., Loktev, A.V., Zhang, Q., Westlake, C.J., Peranen, J., Merdes, A., Slusarski, D.C., Scheller, R.H., Bazan, J.F., Sheffield, V.C*., et al.* (2007). A core complex of BBS proteins cooperates with the GTPase Rab8 to promote ciliary membrane biogenesis. Cell *129*, 1201-1213.

Najafi, M., Maza, N.A., and Calvert, P.D. (2012). Steric volume exclusion sets soluble protein concentrations in photoreceptor sensory cilia. Proc Natl Acad Sci U S A *109*, 203-208.

Nakata, K., Shiba, D., Kobayashi, D., and Yokoyama, T. (2012). Targeting of Nphp3 to the primary cilia is controlled by an N-terminal myristoylation site and coiled-coil domains. Cytoskeleton (Hoboken) *69*, 221-234.

Nguyen, P.A., Liou, W., Hall, D.H., and Leroux, M.R. (2014). Ciliopathy proteins establish a bipartite signaling compartment in a C. elegans thermosensory neuron. J Cell Sci *127*, 5317-5330.

Nguyen, R.L., Tam, L.W., and Lefebvre, P.A. (2005). The LF1 gene of Chlamydomonas reinhardtii encodes a novel protein required for flagellar length control. Genetics *169*, 1415-1424.

Nikopoulos, K., Farinelli, P., Giangreco, B., Tsika, C., Royer-Bertrand, B., Mbefo, M.K., Bedoni, N., Kjellstrom, U., El Zaoui, I., Di Gioia, S.A*., et al.* (2016). Mutations in CEP78 Cause Cone-Rod Dystrophy and Hearing Loss Associated with Primary-Cilia Defects. Am J Hum Genet *99*, 770-776.

Niwa, S., Nakajima, K., Miki, H., Minato, Y., Wang, D., and Hirokawa, N. (2012). KIF19A is a microtubule-depolymerizing kinesin for ciliary length control. Dev Cell *23*, 1167-1175.

Nonaka, S., Tanaka, Y., Okada, Y., Takeda, S., Harada, A., Kanai, Y., Kido, M., and Hirokawa, N. (1998). Randomization of left-right asymmetry due to loss of nodal cilia generating leftward flow of extraembryonic fluid in mice lacking KIF3B motor protein. Cell *95*, 829-837.

Oh, E.C., and Katsanis, N. (2012). Cilia in vertebrate development and disease. Development *139*, 443-448.

Omori, Y., Chaya, T., Katoh, K., Kajimura, N., Sato, S., Muraoka, K., Ueno, S., Koyasu, T., Kondo, M., and Furukawa, T. (2010). Negative regulation of ciliary length by ciliary male germ cell-associated kinase (Mak) is required for retinal photoreceptor survival. Proc Natl Acad Sci U S A *107*, 22671-22676.

Paige Taylor, S., Kunova Bosakova, M., Varecha, M., Balek, L., Barta, T., Trantirek, L., Jelinkova, I., Duran, I., Vesela, I., Forlenza, K.N*., et al.* (2016). An inactivating mutation in intestinal cell kinase, ICK, impairs hedgehog signalling and causes short rib-polydactyly syndrome. Hum Mol Genet *25*, 3998-4011.

Pan, J., and Snell, W.J. (2005). Chlamydomonas shortens its flagella by activating axonemal disassembly, stimulating IFT particle trafficking, and blocking anterograde cargo loading. Dev Cell *9*, 431-438.

Pan, J., Wang, Q., and Snell, W.J. (2004). An aurora kinase is essential for flagellar disassembly in Chlamydomonas. Dev Cell *6*, 445-451.

Pan, X., Ou, G., Civelekoglu-Scholey, G., Blacque, O.E., Endres, N.F., Tao, L., Mogilner, A., Leroux, M.R., Vale, R.D., and Scholey, J.M. (2006). Mechanism of transport of IFT particles in C. elegans cilia by the concerted action of kinesin-II and OSM-3 motors. J Cell Biol *174*, 1035-1045.

Parker, J.D., Bradley, B.A., Mooers, A.O., and Quarmby, L.M. (2007). Phylogenetic analysis of the Neks reveals early diversification of ciliary-cell cycle kinases. PLoS One *2*, e1076.

Patel-King, R.S., Gilberti, R.M., Hom, E.F., and King, S.M. (2013). WD60/FAP163 is a dynein intermediate chain required for retrograde intraflagellar transport in cilia. Mol Biol Cell *24*, 2668-2677.

Pazour, G.J., Dickert, B.L., Vucica, Y., Seeley, E.S., Rosenbaum, J.L., Witman, G.B., and Cole, D.G. (2000). Chlamydomonas IFT88 and its mouse homologue, polycystic kidney disease gene tg737, are required for assembly of cilia and flagella. J Cell Biol *151*, 709-718.

Pazour, G.J., Dickert, B.L., and Witman, G.B. (1999). The DHC1b (DHC2) isoform of cytoplasmic dynein is required for flagellar assembly. J Cell Biol *144*, 473-481.

Pazour, G.J., Wilkerson, C.G., and Witman, G.B. (1998). A dynein light chain is essential for the retrograde particle movement of intraflagellar transport (IFT). J Cell Biol *141*, 979-992.

Perkins, L.A., Hedgecock, E.M., Thomson, J.N., and Culotti, J.G. (1986). Mutant sensory cilia in the nematode Caenorhabditis elegans. Dev Biol *117*, 456-487.

Perrault, I., Saunier, S., Hanein, S., Filhol, E., Bizet, A.A., Collins, F., Salih, M.A., Gerber, S., Delphin, N., Bigot, K.*, et al.* (2012). Mainzer-Saldino syndrome is a ciliopathy caused by IFT140 mutations. Am J Hum Genet *90*, 864-870.

Perrone, C.A., Tritschler, D., Taulman, P., Bower, R., Yoder, B.K., and Porter, M.E. (2003). A novel dynein light intermediate chain colocalizes with the retrograde motor for intraflagellar transport at sites of axoneme assembly in chlamydomonas and Mammalian cells. Mol Biol Cell *14*, 2041-2056.

Phirke, P., Efimenko, E., Mohan, S., Burghoorn, J., Crona, F., Bakhoum, M.W., Trieb, M., Schuske, K., Jorgensen, E.M., Piasecki, B.P.*, et al.* (2011). Transcriptional profiling of C. elegans DAF-19 uncovers a ciliary base-associated protein and a CDK/CCRK/LF2p-related kinase required for intraflagellar transport. Dev Biol *357*, 235-247.

Piao, T., Luo, M., Wang, L., Guo, Y., Li, D., Li, P., Snell, W.J., and Pan, J. (2009). A microtubule depolymerizing kinesin functions during both flagellar disassembly and flagellar assembly in Chlamydomonas. Proc Natl Acad Sci U S A *106*, 4713-4718.

Pigino, G., Geimer, S., Lanzavecchia, S., Paccagnini, E., Cantele, F., Diener, D.R., Rosenbaum, J.L., and Lupetti, P. (2009). Electron-tomographic analysis of intraflagellar transport particle trains in situ. J Cell Biol *187*, 135-148.

Piperno, G., Siuda, E., Henderson, S., Segil, M., Vaananen, H., and Sassaroli, M. (1998). Distinct mutants of retrograde intraflagellar transport (IFT) share similar morphological and molecular defects. J Cell Biol *143*, 1591-1601.

Pires, D.E., Ascher, D.B., and Blundell, T.L. (2014). DUET: a server for predicting effects of mutations on protein stability using an integrated computational approach. Nucleic Acids Res *42*, W314-319.

Poirier, K., Lebrun, N., Broix, L., Tian, G., Saillour, Y., Boscheron, C., Parrini, E., Valence, S., Pierre, B.S., Oger, M.*, et al.* (2013). Mutations in TUBG1, DYNC1H1, KIF5C and KIF2A cause malformations of cortical development and microcephaly. Nat Genet *45*, 639-647.

Porter, M.E., Bower, R., Knott, J.A., Byrd, P., and Dentler, W. (1999). Cytoplasmic dynein heavy chain 1b is required for flagellar assembly in Chlamydomonas. Mol Biol Cell *10*, 693-712.

Prevo, B., Mangeol, P., Oswald, F., Scholey, J.M., and Peterman, E.J. (2015). Functional differentiation of cooperating kinesin-2 motors orchestrates cargo import and transport in C. elegans cilia. Nat Cell Biol *17*, 1536-1545.

Pugacheva, E.N., Jablonski, S.A., Hartman, T.R., Henske, E.P., and Golemis, E.A. (2007). HEF1-dependent Aurora A activation induces disassembly of the primary cilium. Cell *129*, 1351-1363.

Reikofski, J., and Tao, B.Y. (1992). Polymerase chain reaction (PCR) techniques for site-directed mutagenesis. Biotechnol Adv *10*, 535-547.

Reinke, A.W., Mak, R., Troemel, E.R., and Bennett, E.J. (2017). In vivo mapping of tissue- and subcellular-specific proteomes in Caenorhabditis elegans. Sci Adv *3*, e1602426.

Reiter, J.F., Blacque, O.E., and Leroux, M.R. (2012). The base of the cilium: roles for transition fibres and the transition zone in ciliary formation, maintenance and compartmentalization. EMBO Rep *13*, 608-618.

Reiter, J.F., and Leroux, M.R. (2017). Genes and molecular pathways underpinning ciliopathies. Nat Rev Mol Cell Biol *18*, 533-547.

Rhee, H.W., Zou, P., Udeshi, N.D., Martell, J.D., Mootha, V.K., Carr, S.A., and Ting, A.Y. (2013). Proteomic mapping of mitochondria in living cells via spatially restricted enzymatic tagging. Science *339*, 1328-1331.

Ricciardi, S., Ungaro, F., Hambrock, M., Rademacher, N., Stefanelli, G., Brambilla, D., Sessa, A., Magagnotti, C., Bachi, A., Giarda, E.*, et al.* (2012). CDKL5 ensures excitatory synapse stability by reinforcing NGL-1-PSD95 interaction in the postsynaptic compartment and is impaired in patient iPSC-derived neurons. Nat Cell Biol *14*, 911-923.

Ringo, D.L. (1967). Flagellar motion and fine structure of the flagellar apparatus in Chlamydomonas. J Cell Biol *33*, 543-571.

Roberson, E.C., Dowdle, W.E., Ozanturk, A., Garcia-Gonzalo, F.R., Li, C., Halbritter, J., Elkhartoufi, N., Porath, J.D., Cope, H., Ashley-Koch, A.*, et al.* (2015). TMEM231, mutated in orofaciodigital and Meckel syndromes, organizes the ciliary transition zone. J Cell Biol *209*, 129-142.

Roepman, R., Letteboer, S.J., Arts, H.H., van Beersum, S.E., Lu, X., Krieger, E., Ferreira, P.A., and Cremers, F.P. (2005). Interaction of nephrocystin-4 and RPGRIP1 is disrupted by nephronophthisis or Leber congenital amaurosis-associated mutations. Proc Natl Acad Sci U S A *102*, 18520-18525.

Rompolas, P., Pedersen, L.B., Patel-King, R.S., and King, S.M. (2007). Chlamydomonas FAP133 is a dynein intermediate chain associated with the retrograde intraflagellar transport motor. J Cell Sci *120*, 3653-3665.

Rosas-Vargas, H., Bahi-Buisson, N., Philippe, C., Nectoux, J., Girard, B., N'Guyen Morel, M.A., Gitiaux, C., Lazaro, L., Odent, S., Jonveaux, P.*, et al.* (2008). Impairment of CDKL5 nuclear localisation as a cause for severe infantile encephalopathy. J Med Genet *45*, 172-178.

Rosenbaum, J.L., and Witman, G.B. (2002). Intraflagellar transport. Nat Rev Mol Cell Biol *3*, 813-825.

Sang, L., Miller, J.J., Corbit, K.C., Giles, R.H., Brauer, M.J., Otto, E.A., Baye, L.M., Wen, X., Scales, S.J., Kwong, M.*, et al.* (2011). Mapping the NPHP-JBTS-MKS protein network reveals ciliopathy disease genes and pathways. Cell *145*, 513-528.

Savage-Dunn, C. (2005). TGF-beta signaling. WormBook, 1-12.

Scala, E., Ariani, F., Mari, F., Caselli, R., Pescucci, C., Longo, I., Meloni, I., Giachino, D., Bruttini, M., Hayek, G.*, et al.* (2005). CDKL5/STK9 is mutated in Rett syndrome variant with infantile spasms. J Med Genet *42*, 103-107.

Schafer, J.C., Haycraft, C.J., Thomas, J.H., Yoder, B.K., and Swoboda, P. (2003). XBX-1 encodes a dynein light intermediate chain required for retrograde intraflagellar transport and cilia assembly in Caenorhabditis elegans. Mol Biol Cell *14*, 2057-2070.

Schouteden, C., Serwas, D., Palfy, M., and Dammermann, A. (2015). The ciliary transition zone functions in cell adhesion but is dispensable for axoneme assembly in C. elegans. J Cell Biol *210*, 35-44.

Shaheen, R., Faqeih, E., Shamseldin, H.E., Noche, R.R., Sunker, A., Alshammari, M.J., Al-Sheddi, T., Adly, N., Al-Dosari, M.S., Megason, S.G.*, et al.* (2012). POC1A truncation mutation causes a ciliopathy in humans characterized by primordial dwarfism. Am J Hum Genet *91*, 330-336.

Shalom, O., Shalva, N., Altschuler, Y., and Motro, B. (2008). The mammalian Nek1 kinase is involved in primary cilium formation. FEBS Lett *582*, 1465-1470.

Shiba, D., Yamaoka, Y., Hagiwara, H., Takamatsu, T., Hamada, H., and Yokoyama, T. (2009). Localization of Inv in a distinctive intraciliary compartment requires the C-terminal ninein-homolog-containing region. J Cell Sci *122*, 44-54.

Signor, D., Wedaman, K.P., Orozco, J.T., Dwyer, N.D., Bargmann, C.I., Rose, L.S., and Scholey, J.M. (1999). Role of a class DHC1b dynein in retrograde transport of IFT motors and IFT raft particles along cilia, but not dendrites, in chemosensory neurons of living Caenorhabditis elegans. J Cell Biol *147*, 519-530.

Smith, L.A., Bukanov, N.O., Husson, H., Russo, R.J., Barry, T.C., Taylor, A.L., Beier, D.R., and Ibraghimov-Beskrovnaya, O. (2006). Development of polycystic kidney disease in juvenile cystic kidney mice: insights into pathogenesis, ciliary abnormalities, and common features with human disease. J Am Soc Nephrol *17*, 2821-2831.

Snouffer, A., Brown, D., Lee, H., Walsh, J., Lupu, F., Norman, R., Lechtreck, K., Ko, H.W., and Eggenschwiler, J. (2017). Cell Cycle-Related Kinase (CCRK) regulates ciliogenesis and Hedgehog signaling in mice. PLoS Genet *13*, e1006912.

Snow, J.J., Ou, G., Gunnarson, A.L., Walker, M.R., Zhou, H.M., Brust-Mascher, I., and Scholey, J.M. (2004). Two anterograde intraflagellar transport motors cooperate to build sensory cilia on C. elegans neurons. Nat Cell Biol *6*, 1109-1113.

Sohara, E., Luo, Y., Zhang, J., Manning, D.K., Beier, D.R., and Zhou, J. (2008). Nek8 regulates the expression and localization of polycystin-1 and polycystin-2. J Am Soc Nephrol *19*, 469-476.

Song, Z., Lin, J., Sun, Z., Ni, J., and Sha, Y. (2015). RNAi-mediated downregulation of CDKL1 inhibits growth and colony-formation ability, promotes apoptosis of human melanoma cells. J Dermatol Sci *79*, 57-63.

Spalluto, C., Wilson, D.I., and Hearn, T. (2012). Nek2 localises to the distal portion of the mother centriole/basal body and is required for timely cilium disassembly at the G2/M transition. Eur J Cell Biol *91*, 675-686.

Srinivasan, J., Durak, O., and Sternberg, P.W. (2008). Evolution of a polymodal sensory response network. BMC Biol *6*, 52.

Sun, S., Fisher, R.L., Bowser, S.S., Pentecost, B.T., and Sui, H. (2019). Three-dimensional architecture of epithelial primary cilia. Proc Natl Acad Sci U S A *116*, 9370-9379.

Sun, W., Yao, L., Jiang, B., Shao, H., Zhao, Y., and Wang, Q. (2012). A role for Cdkl1 in the development of gastric cancer. Acta Oncol *51*, 790-796.

Sun, Z., Amsterdam, A., Pazour, G.J., Cole, D.G., Miller, M.S., and Hopkins, N. (2004). A genetic screen in zebrafish identifies cilia genes as a principal cause of cystic kidney. Development *131*, 4085-4093.

Sung, C.H., and Leroux, M.R. (2013). The roles of evolutionarily conserved functional modules in cilia-related trafficking. Nat Cell Biol *15*, 1387-1397.

Suzuki, Y., Yandell, M.D., Roy, P.J., Krishna, S., Savage-Dunn, C., Ross, R.M., Padgett, R.W., and Wood, W.B. (1999). A BMP homolog acts as a dose-dependent regulator of body size and male tail patterning in Caenorhabditis elegans. Development *126*, 241-250.

Tam, L.W., Dentler, W.L., and Lefebvre, P.A. (2003). Defective flagellar assembly and length regulation in LF3 null mutants in Chlamydomonas. J Cell Biol *163*, 597-607.

Tam, L.W., Ranum, P.T., and Lefebvre, P.A. (2013). CDKL5 regulates flagellar length and localizes to the base of the flagella in Chlamydomonas. Mol Biol Cell *24*, 588-600.

Tam, L.W., Wilson, N.F., and Lefebvre, P.A. (2007). A CDK-related kinase regulates the length and assembly of flagella in Chlamydomonas. J Cell Biol *176*, 819-829.

Tammachote, R., Hommerding, C.J., Sinders, R.M., Miller, C.A., Czarnecki, P.G., Leightner, A.C., Salisbury, J.L., Ward, C.J., Torres, V.E., Gattone, V.H., 2nd*, et al.* (2009). Ciliary and centrosomal defects associated with mutation and depletion of the Meckel syndrome genes MKS1 and MKS3. Hum Mol Genet *18*, 3311-3323.

Tang, L., Gao, Y., Yan, F., and Tang, J. (2012). Evaluation of cyclin-dependent kinase-like 1 expression in breast cancer tissues and its regulation in cancer cell growth. Cancer Biother Radiopharm *27*, 392-398.

Tao, J., Van Esch, H., Hagedorn-Greiwe, M., Hoffmann, K., Moser, B., Raynaud, M., Sperner, J., Fryns, J.P., Schwinger, E., Gecz, J.*, et al.* (2004). Mutations in the X-linked cyclin-dependent kinase-like 5 (CDKL5/STK9) gene are associated with severe neurodevelopmental retardation. Am J Hum Genet *75*, 1149-1154.

Thiel, C., Kessler, K., Giessl, A., Dimmler, A., Shalev, S.A., von der Haar, S., Zenker, M., Zahnleiter, D., Stoss, H., Beinder, E.*, et al.* (2011). NEK1 mutations cause short-rib polydactyly syndrome type majewski. Am J Hum Genet *88*, 106-114.

Thompson, O., Edgley, M., Strasbourger, P., Flibotte, S., Ewing, B., Adair, R., Au, V., Chaudhry, I., Fernando, L., Hutter, H.*, et al.* (2013). The million mutation project: a new approach to genetics in Caenorhabditis elegans. Genome Res *23*, 1749-1762.

Tran, P.V., Haycraft, C.J., Besschetnova, T.Y., Turbe-Doan, A., Stottmann, R.W., Herron, B.J., Chesebro, A.L., Qiu, H., Scherz, P.J., Shah, J.V.*, et al.* (2008). THM1 negatively modulates mouse sonic hedgehog signal transduction and affects retrograde intraflagellar transport in cilia. Nat Genet *40*, 403-410.

Tsao, C.C., and Gorovsky, M.A. (2008). Tetrahymena IFT122A is not essential for cilia assembly but plays a role in returning IFT proteins from the ciliary tip to the cell body. J Cell Sci *121*, 428-436.

Valente, E.M., Dallapiccola, B., and Bertini, E. (2013). Joubert syndrome and related disorders. Handb Clin Neurol *113*, 1879-1888.

Varga, V., Helenius, J., Tanaka, K., Hyman, A.A., Tanaka, T.U., and Howard, J. (2006). Yeast kinesin-8 depolymerizes microtubules in a length-dependent manner. Nat Cell Biol *8*, 957-962.

Vasudevan, K.K., Jiang, Y.Y., Lechtreck, K.F., Kushida, Y., Alford, L.M., Sale, W.S., Hennessey, T., and Gaertig, J. (2015). Kinesin-13 regulates the quantity and quality of tubulin inside cilia. Mol Biol Cell *26*, 478-494.

Verhey, K.J., and Yang, W. (2016). Permeability barriers for generating a unique ciliary protein and lipid composition. Curr Opin Cell Biol *41*, 109-116.

Walczak, C.E., Gayek, S., and Ohi, R. (2013). Microtubule-depolymerizing kinesins. Annu Rev Cell Dev Biol *29*, 417-441.

Walther, Z., Vashishtha, M., and Hall, J.L. (1994). The Chlamydomonas FLA10 gene encodes a novel kinesin-homologous protein. J Cell Biol *126*, 175-188.

Wang, L., Piao, T., Cao, M., Qin, T., Huang, L., Deng, H., Mao, T., and Pan, J. (2013). Flagellar regeneration requires cytoplasmic microtubule depolymerization and kinesin-13. J Cell Sci *126*, 1531-1540.

Wang, W., Wu, T., and Kirschner, M.W. (2014). The master cell cycle regulator APC-Cdc20 regulates ciliary length and disassembly of the primary cilium. Elife *3*, e03083.

Wang, Y., Ren, Y., and Pan, J. (2019). Regulation of flagellar assembly and length in Chlamydomonas by LF4, a MAPK-related kinase. FASEB J *33*, 6431-6441.

Wang, Z., Fan, Z.C., Williamson, S.M., and Qin, H. (2009). Intraflagellar transport (IFT) protein IFT25 is a phosphoprotein component of IFT complex B and physically interacts with IFT27 in Chlamydomonas. PLoS One *4*, e5384.

Warburton-Pitt, S.R., Silva, M., Nguyen, K.C., Hall, D.H., and Barr, M.M. (2014). The nphp-2 and arl-13 genetic modules interact to regulate ciliogenesis and ciliary microtubule patterning in C. elegans. PLoS Genet *10*, e1004866.

Watanabe, N., Ishihara, T., and Ohshima, Y. (2007). Mutants carrying two sma mutations are super small in the nematode C. elegans. Genes Cells *12*, 603-609.

Waters, A.M., and Beales, P.L. (2011). Ciliopathies: an expanding disease spectrum. Pediatr Nephrol *26*, 1039-1056.

Weatherbee, S.D., Niswander, L.A., and Anderson, K.V. (2009). A mouse model for Meckel syndrome reveals Mks1 is required for ciliogenesis and Hedgehog signaling. Hum Mol Genet *18*, 4565-4575.

Weaving, L.S., Christodoulou, J., Williamson, S.L., Friend, K.L., McKenzie, O.L., Archer, H., Evans, J., Clarke, A., Pelka, G.J., Tam, P.P.*, et al.* (2004). Mutations of CDKL5 cause a severe neurodevelopmental disorder with infantile spasms and mental retardation. Am J Hum Genet *75*, 1079-1093.

Wei, Q., Ling, K., and Hu, J. (2015). The essential roles of transition fibers in the context of cilia. Curr Opin Cell Biol *35*, 98-105.

White, R., Ho, G., Schmidt, S., Scheffer, I.E., Fischer, A., Yendle, S.C., Bienvenu, T., Nectoux, J., Ellaway, C.J., Darmanian, A.*, et al.* (2010). Cyclin-dependent kinase-like 5 (CDKL5) mutation screening in Rett syndrome and related disorders. Twin Res Hum Genet *13*, 168-178.

Williams, C.L., Li, C., Kida, K., Inglis, P.N., Mohan, S., Semenec, L., Bialas, N.J., Stupay, R.M., Chen, N., Blacque, O.E.*, et al.* (2011). MKS and NPHP modules cooperate to establish basal body/transition zone membrane associations and ciliary gate function during ciliogenesis. J Cell Biol *192*, 1023-1041.

Wilson, N.F., and Lefebvre, P.A. (2004). Regulation of flagellar assembly by glycogen synthase kinase 3 in Chlamydomonas reinhardtii. Eukaryot Cell *3*, 1307-1319.

Winkelbauer, M.E., Schafer, J.C., Haycraft, C.J., Swoboda, P., and Yoder, B.K. (2005). The C. elegans homologs of nephrocystin-1 and nephrocystin-4 are cilia transition zone proteins involved in chemosensory perception. J Cell Sci *118*, 5575-5587.

Wloga, D., Camba, A., Rogowski, K., Manning, G., Jerka-Dziadosz, M., and Gaertig, J. (2006). Members of the NIMA-related kinase family promote disassembly of cilia by multiple mechanisms. Mol Biol Cell *17*, 2799-2810.

Wloga, D., and Gaertig, J. (2010). Post-translational modifications of microtubules. J Cell Sci *123*, 3447-3455.

Wojtyniak, M., Brear, A.G., O'Halloran, D.M., and Sengupta, P. (2013). Cell- and subunit-specific mechanisms of CNG channel ciliary trafficking and localization in C. elegans. J Cell Sci *126*, 4381-4395.

Wolf, M.T., Saunier, S., O'Toole, J.F., Wanner, N., Groshong, T., Attanasio, M., Salomon, R., Stallmach, T., Sayer, J.A., Waldherr, R.*, et al.* (2007). Mutational analysis of the RPGRIP1L gene in patients with Joubert syndrome and nephronophthisis. Kidney Int *72*, 1520-1526.

Wren, K.N., Craft, J.M., Tritschler, D., Schauer, A., Patel, D.K., Smith, E.F., Porter, M.E., Kner, P., and Lechtreck, K.F. (2013). A differential cargo-loading model of ciliary length regulation by IFT. Curr Biol *23*, 2463-2471.

Yang, N., Li, L., Eguether, T., Sundberg, J.P., Pazour, G.J., and Chen, J. (2015a). Intraflagellar transport 27 is essential for hedgehog signaling but dispensable for ciliogenesis during hair follicle morphogenesis. Development *142*, 2860.

Yang, T.T., Su, J., Wang, W.J., Craige, B., Witman, G.B., Tsou, M.F., and Liao, J.C. (2015b). Superresolution Pattern Recognition Reveals the Architectural Map of the Ciliary Transition Zone. Sci Rep *5*, 14096.

Yang, Y., Roine, N., and Makela, T.P. (2013). CCRK depletion inhibits glioblastoma cell proliferation in a cilium-dependent manner. EMBO Rep *14*, 741-747.

Ye, S., Dhillon, S., Ke, X., Collins, A.R., and Day, I.N. (2001). An efficient procedure for genotyping single nucleotide polymorphisms. Nucleic Acids Res *29*, E88-88.

Yee, K.W., Moore, S.J., Midmer, M., Zanke, B.W., Tong, F., Hedley, D., and Minden, M.D. (2003). NKIAMRE, a novel conserved CDC2-related kinase with features of both mitogen-activated protein kinases and cyclin-dependent kinases. Biochem Biophys Res Commun *308*, 784-792.

Yee, L.E., Garcia-Gonzalo, F.R., Bowie, R.V., Li, C., Kennedy, J.K., Ashrafi, K., Blacque, O.E., Leroux, M.R., and Reiter, J.F. (2015). Conserved Genetic Interactions between Ciliopathy Complexes Cooperatively Support Ciliogenesis and Ciliary Signaling. PLoS Genet *11*, e1005627.

Yi, P., Xie, C., and Ou, G. (2018). The kinases male germ cell-associated kinase and cell cycle-related kinase regulate kinesin-2 motility in Caenorhabditis elegans neuronal cilia. Traffic *19*, 522-535.

Yuan, S., Li, J., Diener, D.R., Choma, M.A., Rosenbaum, J.L., and Sun, Z. (2012). Target-of-rapamycin complex 1 (Torc1) signaling modulates cilia size and function through protein synthesis regulation. Proc Natl Acad Sci U S A *109*, 2021-2026.

Zalli, D., Bayliss, R., and Fry, A.M. (2012). The Nek8 protein kinase, mutated in the human cystic kidney disease nephronophthisis, is both activated and degraded during ciliogenesis. Hum Mol Genet *21*, 1155-1171.

Zhang, D., and Aravind, L. (2012). Novel transglutaminase-like peptidase and C2 domains elucidate the structure, biogenesis and evolution of the ciliary compartment. Cell Cycle *11*, 3861-3875.

Zhao, C., and Malicki, J. (2011). Nephrocystins and MKS proteins interact with IFT particle and facilitate transport of selected ciliary cargos. EMBO J *30*, 2532-2544.

Zhou, F.Q., and Snider, W.D. (2005). Cell biology. GSK-3beta and microtubule assembly in axons. Science *308*, 211-214.

Zhu, Y.C., Li, D., Wang, L., Lu, B., Zheng, J., Zhao, S.L., Zeng, R., and Xiong, Z.Q. (2013). Palmitoylation-dependent CDKL5-PSD-95 interaction regulates synaptic targeting of CDKL5 and dendritic spine development. Proc Natl Acad Sci U S A *110*, 9118-9123.

Zoller, M.J. (1991). New molecular biology methods for protein engineering. Curr Opin Biotechnol *2*, 526-531.

Appendix A.

Strains used in Chapter 2.

Strain	Genotype
N2	*Bristol wild-type*
MX1420	*nxEx172[Pbbs-8::tram-1::tdtomato; Pbbs-8::mks-2::gfp; rol-6(su1006)]*
MX1388	*nxEx231[arl-13::gfp; Posm-5::xbx-1::tdtomato; rol-6(su1006)]*
MX1813	*tmem-231*(*tm5963*); *nxEx172[Pbbs-8::tram-1::tdtomato; Pbbs-8::mks-2::gfp; rol-6(su1006)]*
MX1924	*raIs12964[Pgrd-15::gfp]; nxEx256[Psrh-220::ift-20::tdtomato; rol-6(su1006)]*
MX1929	*nxEx969[cdkl-1A::gfp; xbx-1::tdtomato; rol-6(su1006)]*
MX1932	*nxEx250[rpi-2::gfp; mksr-1::tdtomato; rol-6(su1006)]*
MX1938	*cdkl-1(tm4182); nxEx250[rpi-2::gfp; mksr-1::tdtomato; rol-6(su1006)]*
MX1940	*tmem-231*(*tm5963*); *nxEx250[rpi-2::gfp; mksr-1::tdtomato; rol-6(su1006)]*
MX1943	*cdkl-1(tm4182); nxEx231[arl-13::gfp; Posm-5::xbx-1::tdtomato; rol-6(su1006)]*
MX1965	*cep-290*(*gk415029*); *nxEx231[arl-13::gfp; Posm-5::xbx-1::tdtomato; rol-6(su1006)]*
MX2100	*cdkl-1(tm4182); nxEx172[Pbbs-8::tram-1::tdtomato; Pbbs-8::mks-2::gfp; rol-6(su1006)]*
MX2102	*cdkl-1(tm4182)*
MX2246	*cdkl-1(nx132); nxEx172[Pbbs-8::tram-1::tdtomato; Pbbs-8::mks-2::gfp; rol-6(su1006)]*
MX2247	*cdkl-1(nx132); nxEx231[arl-13::gfp; Posm-5::xbx-1::tdtomato; rol-6(su1006)]*
MX2277	*cdkl-1(nx131) (c. G90T, A98G)(p.K33R)*
MX2278	*cdkl-1(nx132) (c. 85ATTGT89del)*
MX2293	*nxEx258[cdkl-1A(K33R)::tdtomato; Pbbs-8::mks-2::gfp; rol-6(su1006)]*
MX2301	*nxEx1193[cdkl-1A(G11R)::tdtomato; Pbbs-8::mks-2::gfp; rol-6(su1006)]*

MX2303 *nxEx1195[cdkl-1A(L210P)::tdtomato; Pbbs-8::mks-2::gfp; rol-6(su1006)]*

MX2304 *nxEx1329[cdkl-1A::tdtomato; Pbbs-8::mks-2::gfp; rol-6(su1006)]*

MX2362 *nxEx1232[cdkl-1A(P169L)::tdtomato; Pbbs-8::mks-2::gfp; rol-6(su1006)]*

MX2397 *cdkl-1(nx132); nxEx250[rpi-2::gfp; mksr-1::tdtomato; rol-6(su1006)]*

MX2415 *cdkl-1(tm4182); raIs12964[Pgrd-15::gfp]; nxEx256[Psrh-220::ift-20::tdtomato; rol-6(su1006)]*

MX2426 *nxIs30[Psrh-220::IFT-20::gfp; cc::gfp]*

MX2427 *cdkl-1(nx132); nxIs30[Psrh-220::ift-20::gfp; cc::gfp]*

MX2428 *cdkl-1(nx131); nxIs30[Psrh-220::ift-20::gfp; cc::gfp]*

MX2429 *cdkl-1(tm4182); nxIs30[Psrh-220::ift-20::gfp; cc::gfp]*

MX2447 *cdkl-1(tm4182); nxIs30[Psrh-220::ift-20::gfp; cc::gfp]; nxEx261[cdkl-1A; coel::rfp]*

MX2471 *nxEx1282[Pcdkl-1A::gfp; rol-6(su1006)]*

MX2527 *nxIs30[Psrh-220::ift-20::gfp; cc::gfp]; nxEx261[cdkl-1A; coel::rfp]*

MX2538 *cdkl-1(tm4182); nxIs30[Psrh-220::ift-20::gfp; cc::gfp]; nxEx1344[cdkl-1A(G11R); coel::rfp] line1*

MX2539 *cdkl-1(tm4182); nxIs30[Psrh-220::ift-20::gfp; cc::gfp]; nxEx1345[cdkl-1A(G11R); coel::rfp] line2*

MX2540 *cdkl-1(tm4182); nxIs30[Psrh-220::ift-20::gfp; cc::gfp]; nxEx1346[cdkl-1A(P169L); coel::rfp] line1*

MX2541 *cdkl-1(tm4182); nxIs30[Psrh-220::ift-20::gfp; cc::gfp]; nxEx1347[cdkl-1A(L210P); coel::rfp] line1*

MX2542 *cdkl-1(tm4182); nxIs30[Psrh-220::ift-20::gfp; cc::gfp]; nxEx1348[cdkl-1A(L210P); coel::rfp] line2*

MX2544 *cdkl-1(tm4182); nxIs30[Psrh-220::ift-20::gfp; cc::gfp]; nxEx2544[cdkl-1A(P169L); coel::rfp] line3*

MX2546 *cdkl-1(tm4182); nxIs30[Psrh-220::ift-20::gfp; cc::gfp]; nxEx2546[cdkl-1A(P169L); coel::rfp] line2*

MX2560 *cdkl-1(tm4182); nxIs30[Psrh-220::ift-20::gfp; cc::gfp]; nxEx2560[cdkl-1A; coel::rfp] line1*

MX2561 *cdkl-1(tm4182); nxIs30[Psrh-220::ift-20::gfp; cc::gfp]; nxEx2561[cdkl-1A; coel::rfp] line2*

MX2642 *cdkl-1(tm4182); nxIs30[Psrh-220::ift-20::gfp; cc::gfp]; nxEx2642[cdkl-1A; coel::rfp] line3*

MX2761 *nxEx2761[cdkl-1A(ΔαJ)::mNeonGreen; Posm-5::xbx-1::tdTomato; rol-6(su1006)]*

MX2764	*cdkl-1(tm4182); nxIs30[Psrh-220::ift-20::gfp; cc::gfp]; nxEx2764[cdkl-1A(ΔαJ); coel::rfp] line1*
MX2765	*cdkl-1(tm4182); nxIs30[Psrh-220::ift-20::gfp; cc::gfp]; nxEx2765[cdkl-1A(ΔαJ); coel::rfp] line2*
MX2766	*cdkl-1(tm4182); nxIs30[Psrh-220::ift-20::gfp; cc::gfp]; nxEx2766[cdkl-1A(ΔαJ); coel::rfp] line3*

Appendix B.

Strains used in Chapter 3.

Strain	Genotype
N2	*Bristol wild-type*
BW1940	*ctIs40[dbl-1(+); sur-5::gfp]*
EJP13	*kap-1(ok676) III; vuaSi1 [pBP20; Pkap-1::kap-1::eGFP; cb-unc-119(+)] IV*
EJP76	*osm-6(p811) V; unc-119(ed3) III; vuaSi15 [pBP36; Posm-6::osm-6::eGFP; cb-unc-119(+)] I*
EJP81	*che-11(tm3433) V; unc-119(ed3) III; vuaSi24 [pBP43; Pche-11::che-11::mCherry; cb-unc-119(+)] II*
EJP206	*xbx-1(ok279) V; vuaSi26 [pJM6; Pxbx-1::xbx-1::EGFP; cb-unc-119(+)] I*
ET100	*dyf-18 (ok200)*
MAS7	*klp-7 (tm2143)*
MX135	*osm-3 (p802)*
MX1071	*yhwEx[Posm-5::mks-5::tdTomato + Posm-5::dyf-11::gfp + rol-6(su1006)]*
MX1444	*cdkl-1(tm4182); osm-6(p811) V; vuaSi15 [pBP36; Posm-6::osm-6::eGFP; cb-unc-119(+)] I*
MX1445	*cdkl-1(tm4182); che-11(tm3433) V; vuaSi24 [pBP43; Pche-11::che-11::mCherry; cb-unc-119(+)] II*
MX1929	*nxEx969[cdkl-1a::gfp + xbx-1::tdTomato + rol-6(su1006)]*
MX1980	*nxEx255[Pbbs-8::cep-290(cDNA)::gfp+ Posm-5::xbx-1::tdTomato + rol-6(su1006)]*
MX2012	*nxEx1017[(Pbbs8::klp-13(cDNA)::gfp + Posm-5::xbx-1::tdTomato + rol-6(su1006)])*
MX2102	*cdkl-1(tm4182)*
MX2242	*cdkl-1a(nx132) (c. 85ATTGT89del)*
MX2277	*cdkl-1(nx131)*

MX2426 *nxIs30[Psrh220::IFT-20:: gfp + cc::gfp]*

MX2429 *cdkl-1(tm4182); nxIs30[Psrh220::IFT-20::gfp + cc::gfp]*

MX2586 *dyf-18(ok200); nxIs30[srh220P::IFT-20::GFP + cc::GFP]*

MX2587 *dyf-18(ok200); cdkl-1(tm4182); nxIs30[srh220P::IFT-20::GFP + cc::GFP]*

MX2598 *nxEx2598[nekl-4:gfp + Posm-5::xbx-1::tdTomato + rol-6(su1006)] strain 1*

MX2632 *nekl-4 (tm4910)*

MX2633 *dyf-5 (ok1177)*

MX2634 *dyf-18(ok200); nxEx969[cdkl-1a::gfp + xbx-1::tdTomato + rol-6(su1006)]*

MX2636 *dyf-5(ok1177); nxEx969[cdkl-1a::gfp + xbx-1::tdTomato + rol-6(su1006)]*

MX2638 *dyf-5(ok1177); nxIs30[srh220P::IFT-20::GFP + cc::GFP]*

MX2639 *dyf-5(ok1177); cdkl-1(tm4182); nxIs30[srh220P::IFT-20::GFP + cc::GFP]*

MX2640 *nekl-4(tm4910); nxIs30[srh220P::IFT-20::GFP + cc::GFP]*

MX2641 *nekl-4(tm4910); cdkl-1(tm4182); nxIs30[srh220P::IFT-20::GFP + cc::GFP]*

MX2645 *nekl-1 (gk516661)*

MX2731 *nekl-1(gk516661); nxIs30[srh-220P::IFT-20::GFP + cc::GFP]*

MX2732 *nekl-1(gk516661); cdkl-1(tm4182); nxIs30[srh-220P::IFT-20::GFP + cc::GFP]*

MX2758 *cdkl-1(tm4182);klp-13(tm3737);nxIs30[srh220P::IFT-20::GFP + cc::GFP]*

MX2759 *klp-13(tm3737);nxIs30[srh220P::IFT-20::GFP + cc::GFP]*

MX2767 *cdkl-1(tm4182);nxEx1017[(Pbbs8::klp-13(cDNA)::gfp + Posm-5::xbx-1::tdTomato + rol-6(su1006)]*

MX2778 *klp-13(gk951285); nxIs30[srh220P::IFT-20::GFP + cc::GFP]*

MX2779 *klp-13(gk951285); cdkl-1(tm4182); nxIs30[srh220P::IFT-20::GFP + cc::GFP]*

MX2787 *nxEx2787[Pbbs-8:gfp::klp-7a + Posm-5::xbx-1::tdTomato + rol-6(su1006)]*

MX2788 *nxEx2788[Pnekl-1::gfp::nekl-1(cDNA)::nekl-1-3-UTR + Posm-5::xbx-1::tdTomato + rol-6(su1006)]*

MX2813 *klp-7(tm2143); nxIs30[srh220P::IFT-20::GFP + cc::GFP]*

MX2814 *klp-7(tm2143); tm4182; nxIs30[srh220P::IFT-20::GFP + cc::GFP]*

MX2819 *cdkl-1(tm4182); nxEx2787[Pbbs-8:gfp::klp-7a + Posm-5::xbx-1::tdTomato + rol-6(su1006)]*

MX2834 *cep-290; nxEx2787[Pbbs-8:gfp::klp-7a + Posm-5::xbx-1::tdTomato + rol-6(su1006)]*

MX2835 *mks-2(nx111); nxEx2787[Pbbs-8:gfp::klp-7a + Posm-5::xbx-1::tdTomato + rol-6(su1006)]*

MX2836 *klp-7(tm2143); nxEx969[cdkl-1a::gfp + xbx-1::tdTomato + rol-6(su1006)]*

MX2837 *cdkl-1(tm4182) V; kap-1(ok676) III; vuaSi1 [pBP20; Pkap-1::kap-1::eGFP; cb-unc-119(+)] IV*

MX2838 *mks-5(tm3100); nxEx2787[Pbbs-8:gfp::klp-7a + Posm-5::xbx-1::tdTomato + rol-6(su1006)]*

MX2839 *nphp-4(tm925); nxEx2787[Pbbs-8:gfp::klp-7a + Posm-5::xbx-1::tdTomato + rol-6(su1006)]*

MX2851 *osm-3(p802) IV; vuaSi2 [pBP22; Posm-3::osm-3::mCherry; cb-unc-119(+)] II*

MX2852 *cdkl-1(tm4182); osm-3(p802) IV; vuaSi2 [pBP22; Posm-3::osm-3::mCherry; cb-unc-119(+)] II*

MX2853 *cdkl-1(tm4182); xbx-1(ok279) V; vuaSi26 [pJM6; Pxbx-1::xbx-1:: eGFP; cb-unc-119(+)] I*

MX2860 *dyf-18(ok200); nxEx255[Pbbs-8::cep-290(cDNA)::gfp+ Posm-5::xbx-1::tdTomato + rol-6(su1006)]*

MX2861 *dyf-18(ok200); yhwEx[nphp-4::yfp + che-13::cfp + rol-6(su1006)]*

MX2862 *dyf-18(ok200); yhwEx[Posm-5::mks-5::tdTomato + Posm-5::dyf-11::gfp + rol-6(su1006)]*

MX2864 *kap-1(ok676) III; cdkl-1(tm4182); nxIs30[Psrh-220::IFT-20::gfp + cc::gfp]*

MX2865 *kap-1(ok676) III; nxIs30[Psrh-220::IFT-20::gfp + cc::gfp]*

MX2873 *che-3(nx159ts); yhwEx419[Posm-5::mks-6::gfp+ Posm-5::xbx-1::tdTomato + rol-6(su1006)]*

MX2875 *cdkl-1(nx164[Pcdkl-1::gfp::3xFlag::dyp-10])*

MX2877 *cdkl-1(nx165[cdkl-1::mNeongreen::APX])V*

MX2886 *klp-7(syb603); nxIs30[srh-220P::IFT-20::GFP + cc::GFP]*

MX2887 *klp-7(syb603); cdkl-1(tm4182); nxIs30[srh-220P::IFT-20::GFP + cc::GFP]*

MX2888 *osm-3(p802) IV; nxIs30[Psrh-220::IFT-20::gfp + cc::gfp]*

MX2889	*osm-3(p802) IV; cdkl-1(tm4182); nxIs30[Psrh-220::IFT-20::gfp + cc::gfp]*
MX2900	*klp-7(syb613); nxIs30[srh-220P::IFT-20::GFP + cc::GFP]*
MX2901	*klp-7(syb613); cdkl-1(tm4182); nxIs30[srh-220P::IFT-20::GFP + cc::GFP]*
MX2902	*cdkl-1(nx166[cdkl-1::mNeonGreen])V*
MX2903	*osm-3(p802); cdkl-1(nx166[cdkl-1::mNeonGreen])V*
MX2910	*klp-11(tm324); cdkl-1(nx166[cdkl-1::mNeonGreen])V*
MX2911	*bbs-8(nx77); cdkl-1(nx166[cdkl-1::mNeonGreen])V*
MX2919	*cdkl-1(tm4182); nxIs30[Psrh220::IFT-20::gfp + cc::gfp]; nxEx2918[Psrh220::nphp-2::mCherry + rol-6(su1006)]*
MX2920	*nxIs30[Psrh220::IFT-20::gfp + cc::gfp]; nxEx2918[Psrh220::nphp-2::mCherry + rol-6(su1006)]*
MX2925	*che-3(nx159ts);cdkl-1(nx166[cdkl-1::mNeonGreen])V*
MX2929	*ctIs40[dbl-1(+); sur-5::gfp];cdkl-1(tm4182)*
MX2930	*dbl-1(nk3);cdkl-1(tm4182)*
MX2931	*klp-7(tm2143); nxIs30[srh220P::IFT-20::GFP + cc::GFP]; nxIs95[klp-7 + cc::RFP]*
MX2950	*nxEx2950[cdkl-1c(cDNA)::gfp + xbx-1::tdTomato + rol-6(su1006)]*
MX2952	*N2; nxEx2952[Pbbs-8:gfp::klp-7a(S414N) + Posm-5::xbx-1::tdTomato + rol-6(su1006)]*
MX2954	*nxEx2954[cdkl-1b(cDNA)::gfp + xbx-1::tdTomato + rol-6(su1006)]*
MX2964	*N2; nxEx2964[Pbbs-8:gfp::klp-7a(H418D) + Posm-5::xbx-1::tdTomato + rol-6(su1006)]*
NU3	*dbl-1(nk3)*
YH224	*yhwEx[nphp-4::yfp + che-13::cfp + rol-6(su1006)]*